NASA Contractor Report 3101

Rotary Balance Data for a Typical Single-Engine General Aviation Design for an Angle-of-Attack Range of 8° to 90°

II - High-Wing Model A

William Mulcay and Robert Rose

CONTRACT NAS1-14849
SEPTEMBER 1979

NASA

NASA Contractor Report 3101

Rotary Balance Data for a Typical Single-Engine General Aviation Design for an Angle-of-Attack Range of 8° to 90°

II - High-Wing Model A

William Mulcay and Robert Rose
Bihrle Applied Research, Inc.
Jericho, New York

Prepared for
Langley Research Center
under Contract NAS1-14849

NASA
National Aeronautics
and Space Administration

Scientific and Technical
Information Branch

1979

SUMMARY

Aerodynamic characteristics obtained in a rotational flow environment utilizing a rotary balance located in the Langley spin tunnel are presented in plotted form for a 1/5-scale, single-engine, high-wing, general aviation airplane model. The configurations tested included various tail designs and fuselage shapes. Data are presented without analysis for an angle-of-attack range of 8° to 90° and clockwise and counter-clockwise rotations covering an $\frac{\Omega b}{2V}$ range from 0 to 0.85.

INTRODUCTION

The NASA Langley Research Center has initiated a broad general aviation stall/spin research program which includes spin-tunnel and free-flight radio control model tests, as well as full-scale flight tests for a number of configurations typical of light, general aviation airplanes. To support this effort, rotary balance wind tunnel force tests covering these same configurations will be conducted to establish a data base for analysis of model and full-scale flight results, and to develop design charts for desirable stall/spin characteristics.

A 1/5-scale, single-engine, general aviation airplane model, referred to as model A, having a high-wing location was tested in a rotational flow environment utilizing a rotary balance located in the Langley spin tunnel. This report presents the data obtained for various tail designs and fuselage shapes. Data for model A having a low-wing location are presented in reference 1.

SYMBOLS

The units for physical quantities used herein are presented in the International System of Units (SI) and U.S. Customary Units. The measurements were made in the U.S. Customary Units; equivalent dimensions were determined by using the conversion factors given in reference 2.

b wing span, m (ft)

$\bar{c}$ mean aerodynamic chord, cm (in.)

C_L lift-force coefficient, $\frac{\text{Lift force}}{qS}$

C_N normal-force coefficient, $\frac{\text{Normal force}}{qS}$

C_A axial-force coefficient, $\frac{\text{Axial force}}{qS}$

C_Y side-force coefficient, $\frac{\text{Side force}}{qS}$

C_ℓ rolling moment coefficient, $\frac{\text{Rolling moment}}{qSb}$

C_m pitching-moment coefficient, $\frac{\text{Pitching moment}}{qS\bar{c}}$

C_n yawing-moment coefficient, $\frac{\text{Yawing moment}}{qSb}$

q free-stream dynamic pressure, N/m^2 (lb/ft^2)

S wing area, m^2 (ft^2)

V free-stream velocity, m/sec (ft/sec)

α angle of attack, deg

β angle of sideslip, deg

Ω angular velocity about spin axis, rad/sec

$\frac{\Omega b}{2V}$ spin coefficient, positive for clockwise spin

δ_a aileron deflection, positive when right aileron is down

$(\delta_{a_{right}} - \delta_{a_{left}})/2$, deg

δ_e elevator deflection, positive when trailing edge is down, deg

δ_r rudder deflection, positive when trailing edge is to left, deg

Abbreviations:

cg center of gravity

SR spin radius

TE trailing edge

TEST EQUIPMENT

A rotary balance measures the forces and moments acting on an airplane while subjected to rotational flow conditions; the background for this apparatus is discussed in reference 3. A photograph and sketch of the rotary balance apparatus installed in the Langley spin tunnel are shown in figures 1 and 2, respectively. The rotating portion of the balance system, mounted on a horizontal supporting boom which is hinged at the wall, is moved from the wall to the center of the tunnel by cables. The rotary arm of the balance system, which rotates about a vertical axis, is attached to the outer end of the horizontal supporting boom and is driven by a drive shaft through couplings and gears.

A test model is mounted on a strain gauge balance which is affixed to the bottom of the rotary balance apparatus. Controls located outside the tunnel are used to activate motors on the rig which position the model to the desired attitude. The angle-of-attack range of the rig is 8 to 90 degrees and the sideslip angle range is ± 15 degrees. The spin radius and the lateral displacement motors allow the operator to position the moment center of the balance on the spin axis or at a specific distance

from the spin axis. This is done for each combination of angle of attack and sideslip angle. The general practice is to mount the moment center of the balance at the cg location about which the aerodynamic moments are desired. Electrical current from the balance, and to the motors on the rig, is conducted through slip-rings located at the rig head. Examples of how the rig is positioned for different angle of attack and sideslip angles are shown in figures 2a and 2b, respectively.

The model can be rotated up to 90 rpm in either direction. By using different rotational speeds and a specific airflow in the tunnel, the motions of a steady spinning airplane can be simulated. The aerodynamic forces and moments can then be measured for values of $\frac{\Omega b}{2V}$, including the case of $\frac{\Omega b}{2V} = 0$, where static aerodynamic forces and moments can be obtained.

A NASA six-component strain gauge balance is mounted inside the model and measures the normal, lateral and longitudinal forces and the yawing, rolling and pitching moments acting about the model body axis. The interactions that exist between the six components are available from balance calibration tests and are accounted for after the balance voltages are converted to forces and moments.

The data acquisition, reduction and presentation system for the rotary balance set-up is composed of a 12-channel scanner/ voltmeter, a mini-computer and a plotter. With this equipment, on-line digital print-out and/or graphical plots of data are possible.

TEST PROCEDURES

Rotary aerodynamic data are obtained in two steps. The first step is to record the inertial forces and moments (tares) acting on the model at different attitudes and rotational speeds. To accomplish this, a covered bird-cage like structure is mounted to the upper rig which encloses the model without touching it. In this manner, the air immediately surrounding the model is rotated with it. As the rig is rotated at the desired attitude and rate, the inertial forces and moments generated by the model are measured and stored on magnetic tape for later use.

The second step in the data-gathering process is to measure aerodynamic and inertial forces at different attitudes and rotational speeds for a selected tunnel velocity with, of course, the cage structure removed. The tares are subtracted from these values, and the remaining aerodynamic forces and moments are then converted to coefficient form and stored on magnetic tape.

MODEL

A 1/5-scale fiberglass/foam/plywood model of a configuration considered to be a typical high-wing, single-engine, light general aviation airplane was tested in the present study. A three-view drawing of this model is shown in figure 3, dimensional characteristics of the model are presented in Table I, and a photograph of the model installed on the rotary balance located in the Langley spin tunnel is presented in figure 1.

The model was fabricated such that various tail configurations could be tested as well as fuselage modifications. The

two tail configurations tested involved different locations of the horizontal tail as shown in figure 4. The fuselage shape modifications tested are shown in figure 5.

TEST CONDITIONS

The tests were conducted in the spin tunnel at a tunnel velocity of 7.62 m/sec (25 ft/sec) which corresponds to a Reynolds number of 128,000 based on the model mean aerodynamic chord. Unless noted otherwise in Table II, all the configurations were tested through an angle-of-attack range of 8 to 90^{o} at a zero sideslip angle with the spin axis passing through the full-scale airplane cg location of $.255\bar{c}$ for angles of attack above 30^{o}. For angles of attack below 35^{o}, the spin axis was set 76.2cm (30 in.) forward of the cg. Consequently, data was obtained for both a 0 and 76.2cm (30 in.) spin radius at angles of attack of 30 and 35^{o}. At each spin attitude, measurements were obtained for nominal $\frac{\Omega b}{2V}$ values of .1, .2, .3, .4, .45, .55, .65, .75 and .85 in both clockwise and counter-clockwise directions, as well as for $\frac{\Omega b}{2V}$ =0 (static value).

DATA PRESENTATION

Table II identifies the configurations tested and the corresponding appendix figure numbers which present the aerodynamic data. The aerodynamic coefficients vs. $\frac{\Omega b}{2V}$ are presented for each configuration in six sequentially numbered figures in the following order: C_n, C_ℓ, C_m, C_N, C_Y and C_A.

Each figure, in turn, consists of four pages which present the subject aerodynamic coefficient vs. $\frac{\Omega b}{2V}$ for the following angles of attack and spin radii, unless noted otherwise in Table II.

a) α= 8, 10, 12, 14, 16 deg SR= 76cm (30in)

b) α= 18, 20, 25, 30, 35 deg SR= 76cm (30in)

c) α= 30, 35, 40, 45, 50 deg SR= 0

d) α= 55, 60, 70, 80, 90 deg SR= 0

All the moment data are presented for a cg position of $0.255\bar{c}$.

Lift coefficient as a function of angle of attack for zero rotation rate is presented at the end of the Appendix for several configurations cited in Table II.

REFERENCES

1. Hultberg, Randy S.; Mulcay, William J.: Rotary Balance Data for a Typical Single-Engine General Aviation Design for an Angle-of-Attack Range of 8^{o} to 90^{o}. I- Low-Wing Model A. NASA CR 3100, 1979.

2. Mechtly, E.A.: The International System of Units - Physical Constants and Conversion Factors. NASA SP-7012, 1973.

3. Bihrle, William, Jr.; Hultberg, Randy S.; Mulcay, William: Rotary Balance Data for a Typical Single-Engine Low-Wing General Aviation Design for an Angle-of-Attack Range of 30^{o} to 90^{o}. NASA CR 2972, 1978.

TABLE I.- DIMENSIONAL CHARACTERISTICS OF THE BASIC MODEL

Overall length with tail #4, m (ft)	1.23 (4.05)
Wing:	
Span, m (ft)	1.46 (4.80)
Area, m^2 (ft^2)	0.36 (3.87)
Root chord, cm (in.)	24.54 (9.66)
Tip chord, cm (in.)	24.54 (9.66)
Mean aerodynamic chord, cm (in.)	24.54 (9.66)
Leading edge of $\bar{c}$, distance rearward of leading edge of root chord, cm (in.)	0
Aspect ratio	5.9
Dihedral, deg	1.5
Incidence:	
Root, deg	3.5
Tip, deg	3.5
Airfoil section	NACA 64_2-415 modified
Horizontal tail:	
Span, m (ft)	0.47 (1.53)
Incidence, deg	-3.0
Airfoil section	NACA 65_1-012
Vertical tail:	
Airfoil section	NACA 65_1-012

TABLE II.- CONFIGURATIONS TESTED AND FIGURE INDEX

(Unless noted otherwise, all configurations tested through α= 8 to 90° at β= 0°.)

FIGURE NO.	CONFIGURATION	δ_e deg	δ_a deg	δ_r deg	REMARKS
[a]A1-A6	#4 Horizontal tail	0	0	0	
A7-A12	with rounded fuselage bottom aft of wing TE	↓	↓	↓	α= 30-90° only
A13-A18	with rounded fuselage bottom aft of engine cowling	↓	↓	↓	α= 50-90° only
[a]A19-A24	#3 Horizontal tail				
A25-A30	with rounded fuselage bottom aft of wing TE	↓	↓	↓	α= 30-90° only
A31-A36	with rounded fuselage bottom aft of engine cowling	↓	↓	↓	α= 30-90° only

[a] C_L vs α presented in figure A37.

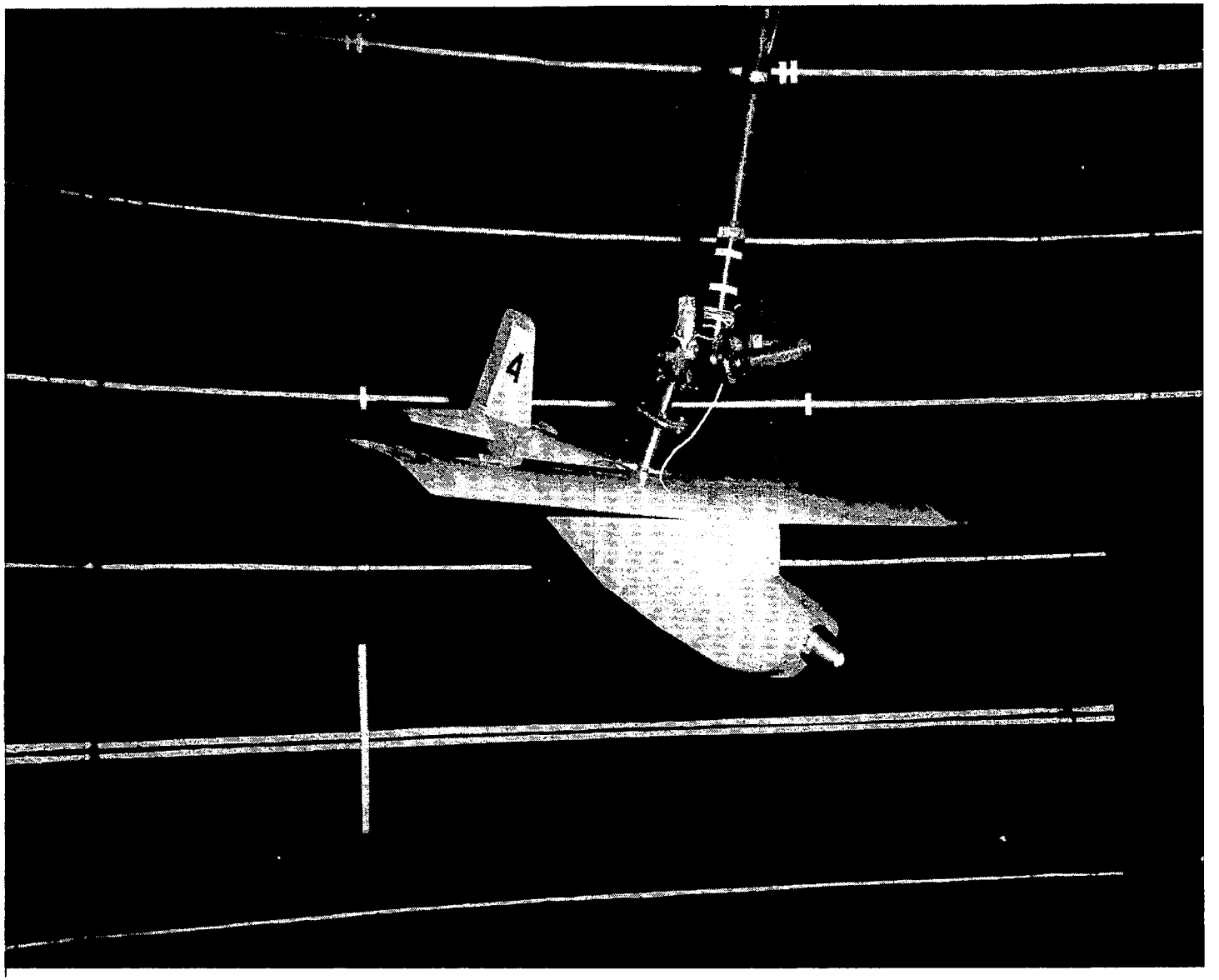

Figure 1.- Photograph of 1/5-scale model installed on rotary balance apparatus.

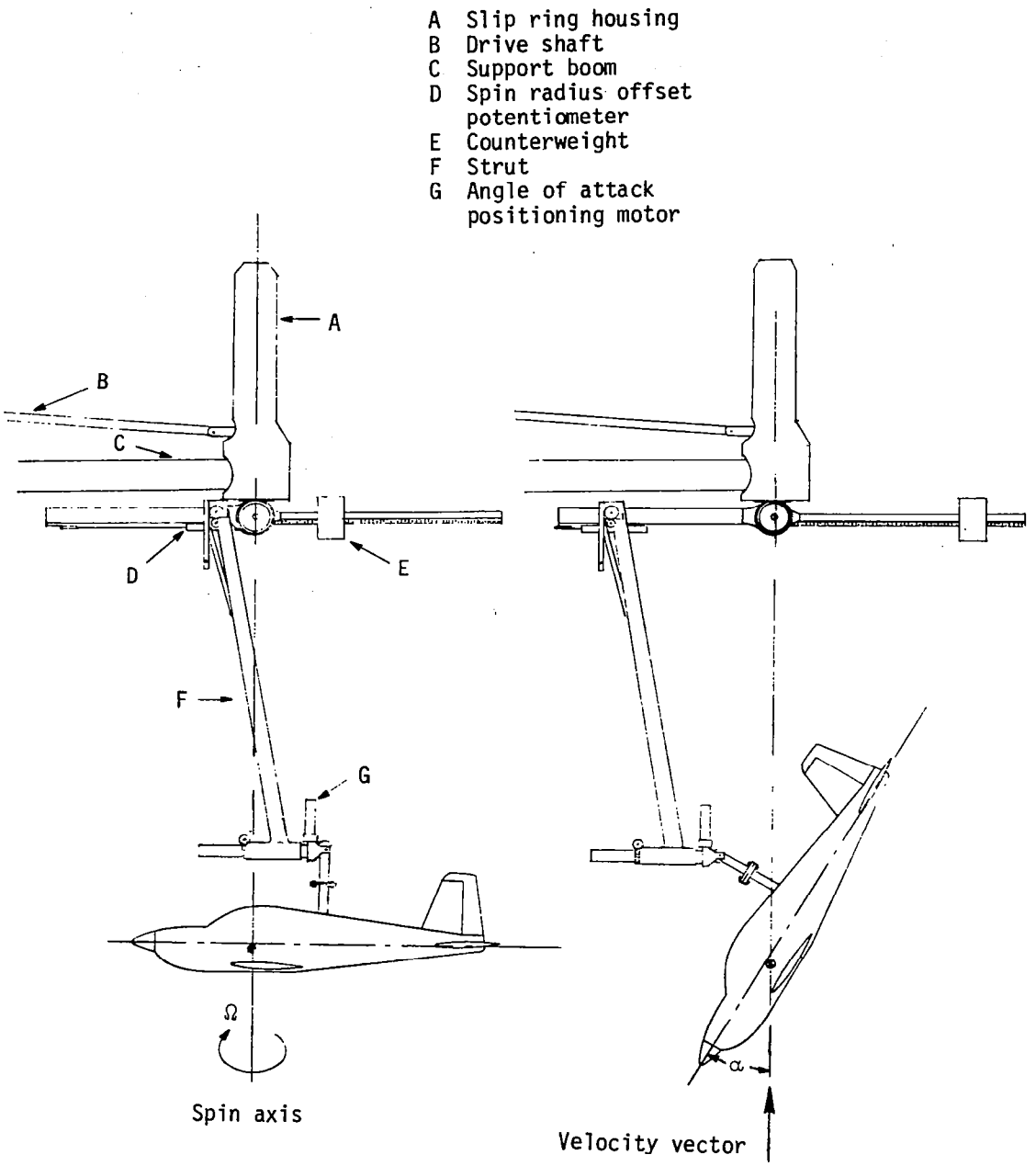

(a) Side view of model.

Figure 2.- Sketch of rotary balance apparatus.

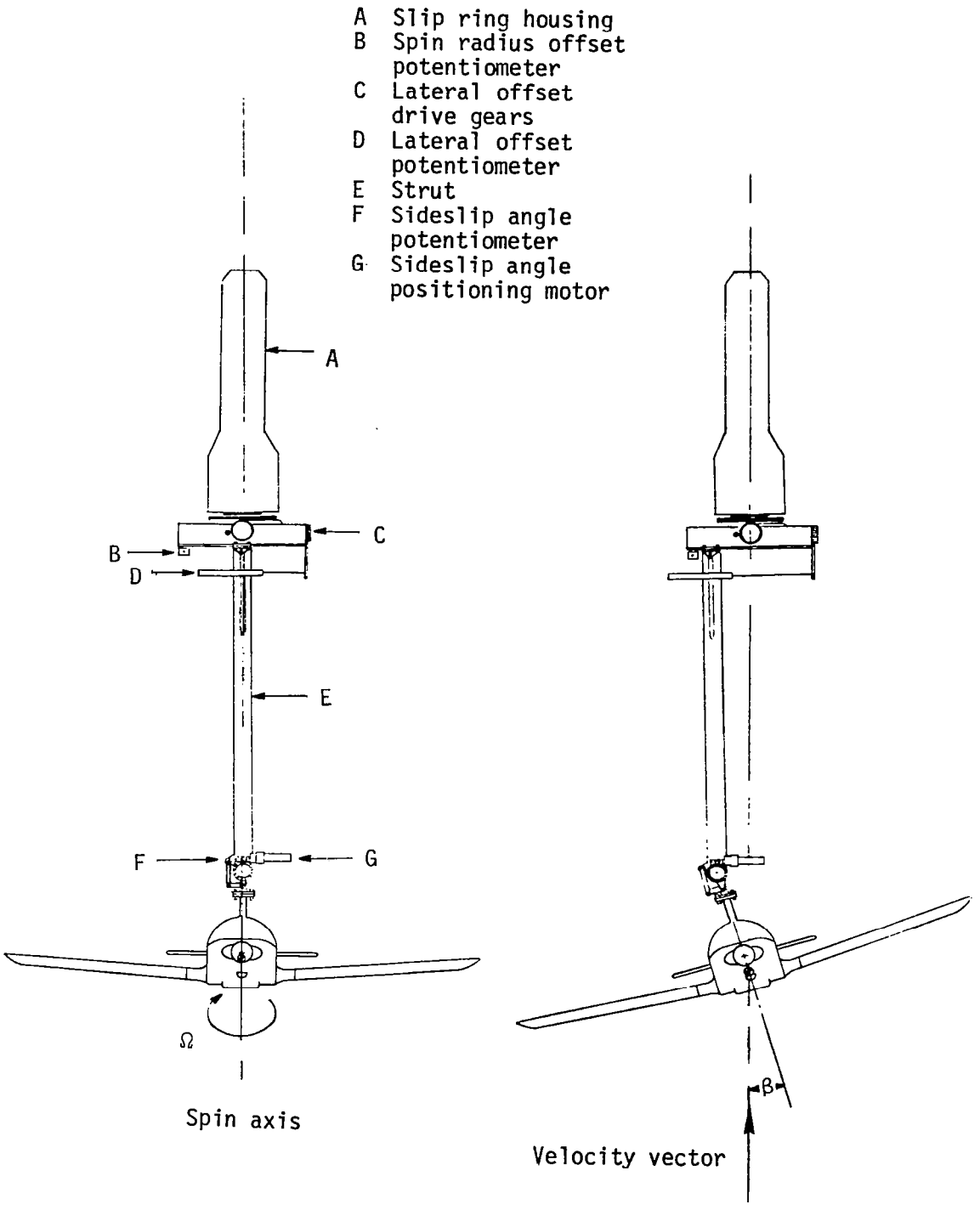

(b) Front view of model.

Figure 2.- Concluded.

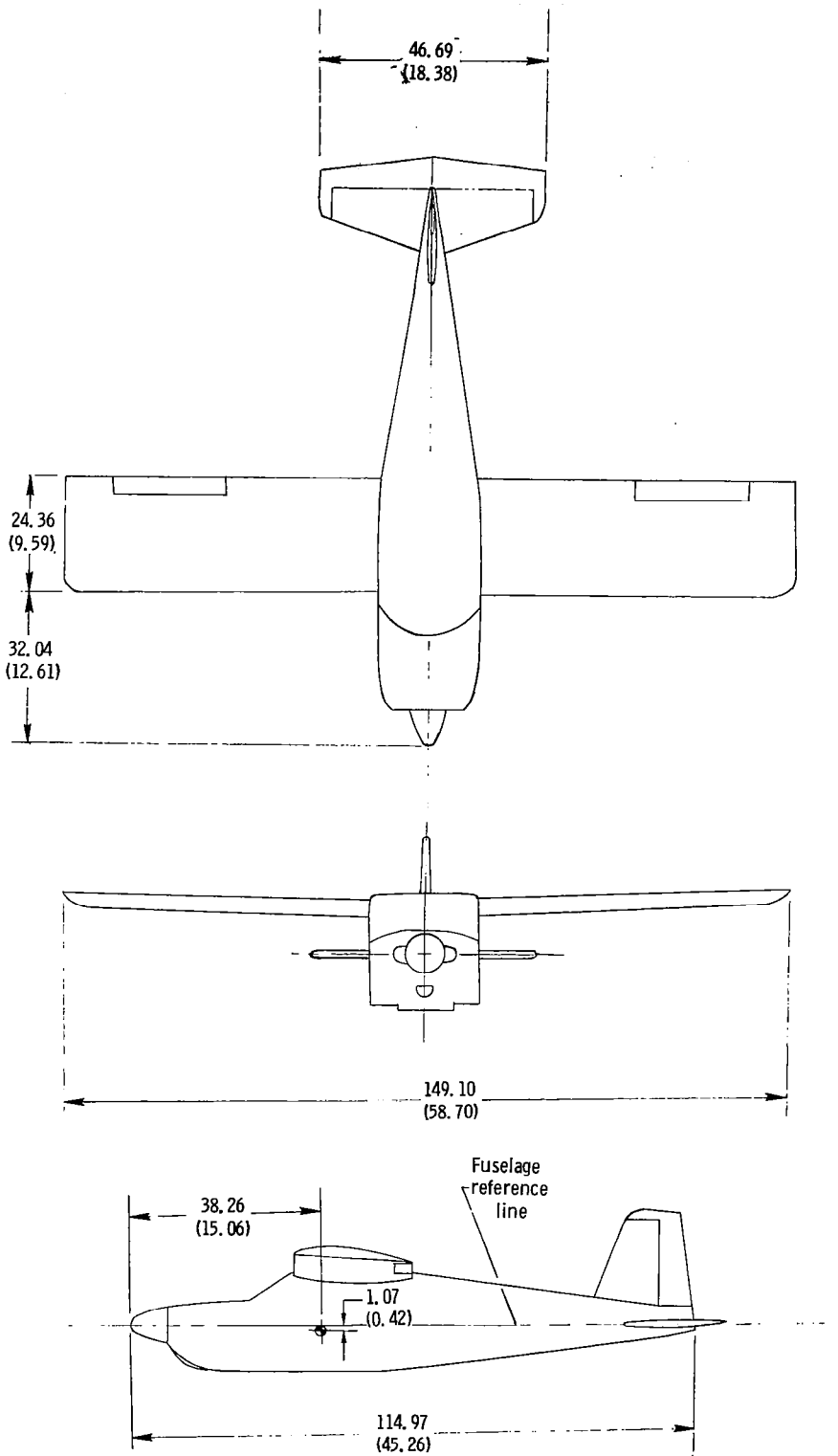

Figure 3. - Three-view drawing of 1/5-scale high-wing general aviation model A. Center-of-gravity positioned at 0.255$\bar{c}$. Dimensions are given in centimeters(inches), model scale.

(b) Tail 4 (Basic)

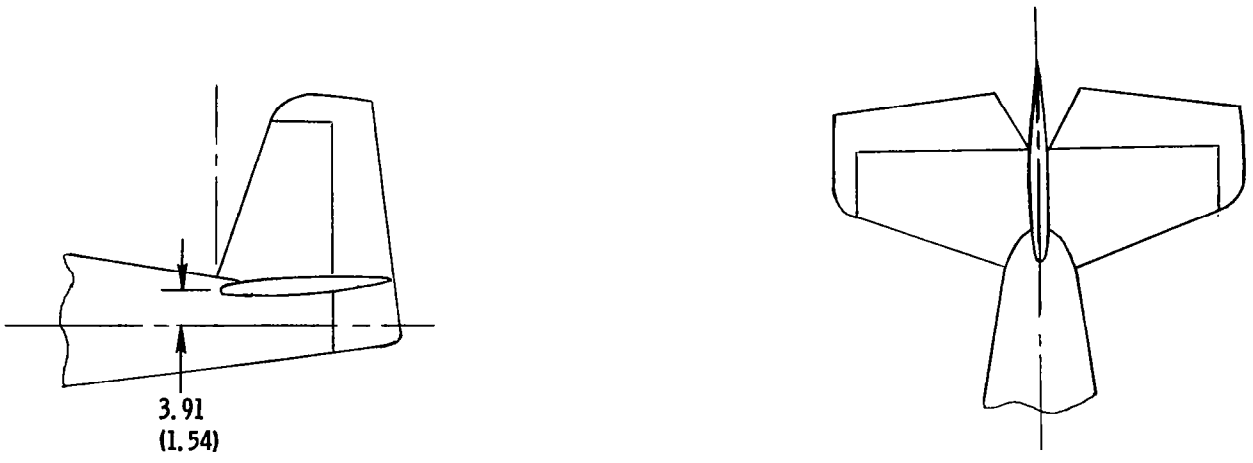

(a) Tail 3

Figure 4.-Tail configurations tested on model. Dimensions are given in centimeters (inches), model scale.

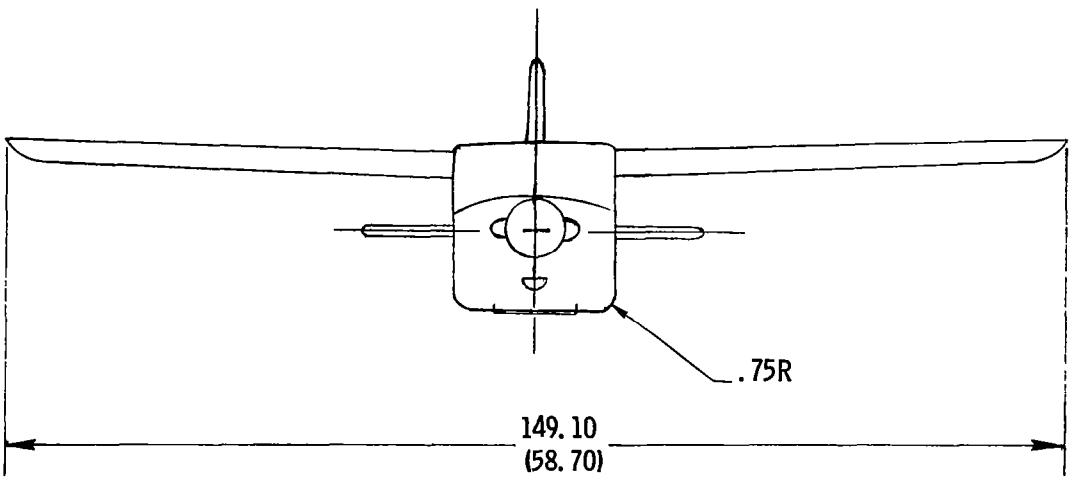

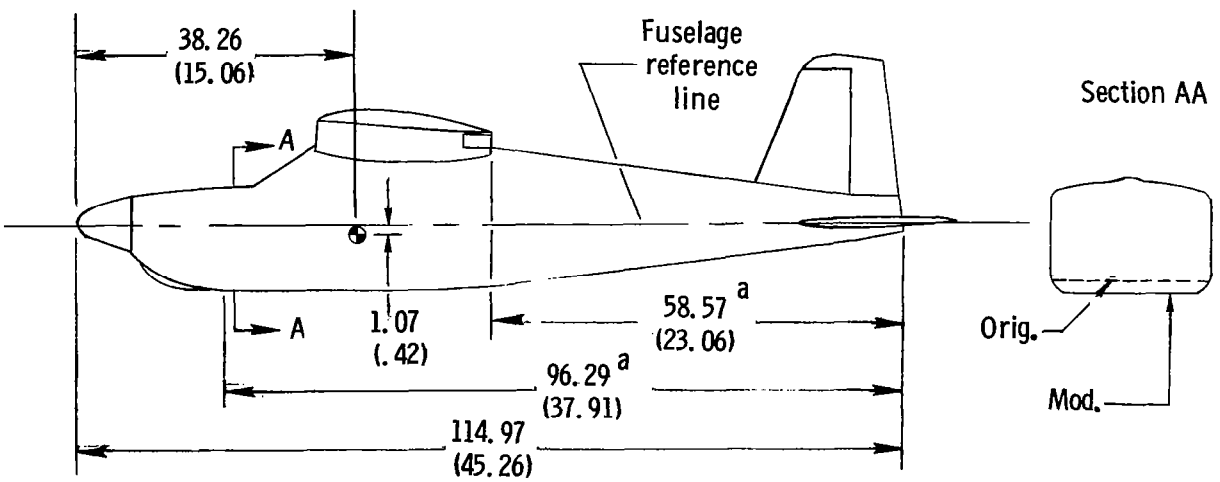

[a]Length of fuselage mod.

Figure 5. - Fuselage shape modifications tested on model. Dimensions are given in centimeters (inches).

APPENDIX

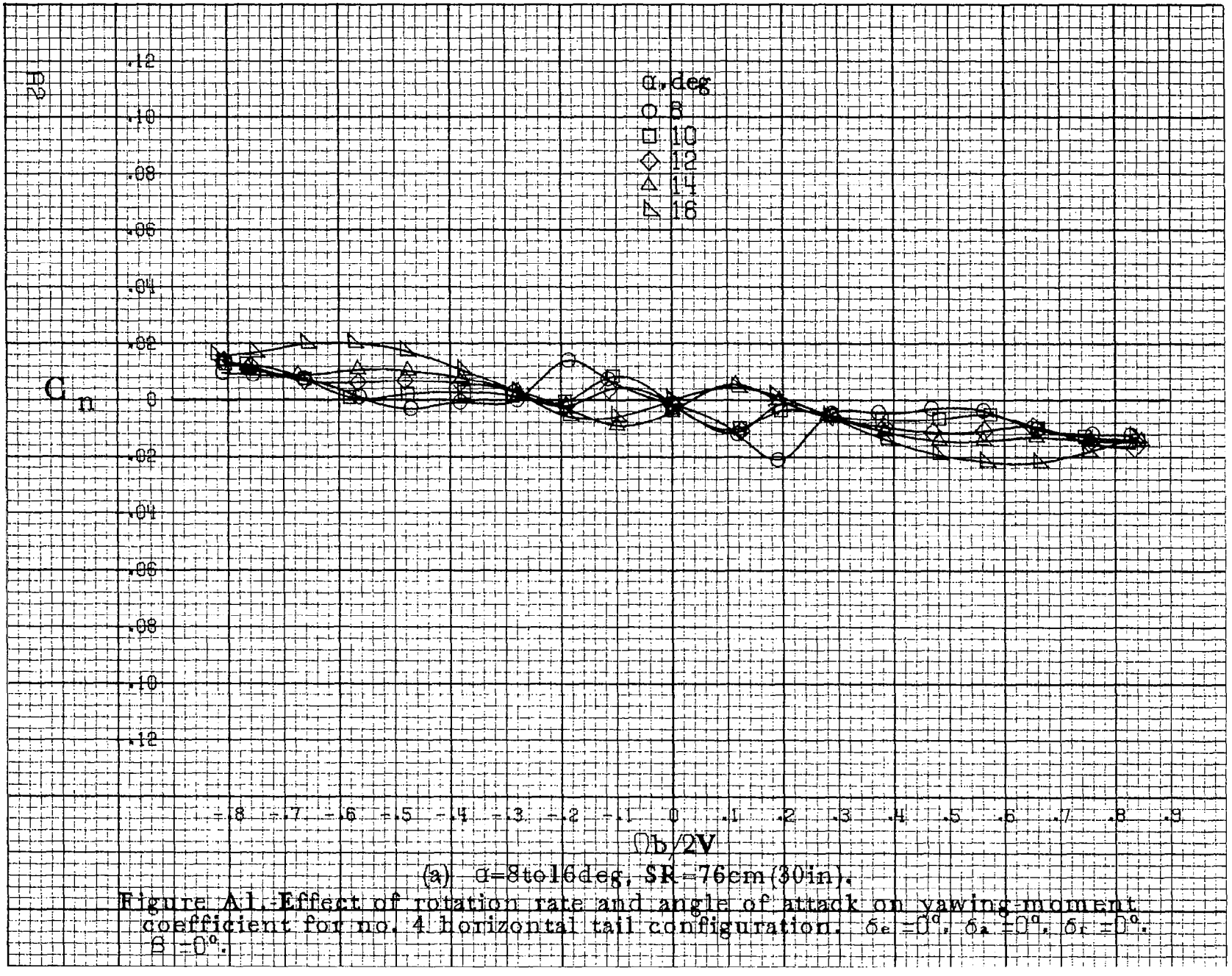

(a) α=8to16deg, $SR=76cm(30in)$.

Figure A1. Effect of rotation rate and angle of attack on yawing-moment coefficient for no. 4 horizontal tail configuration. $\delta_e = 0^o$, $\delta_a = 0^o$, $\delta_r = 0^o$, $\beta = 0^o$.

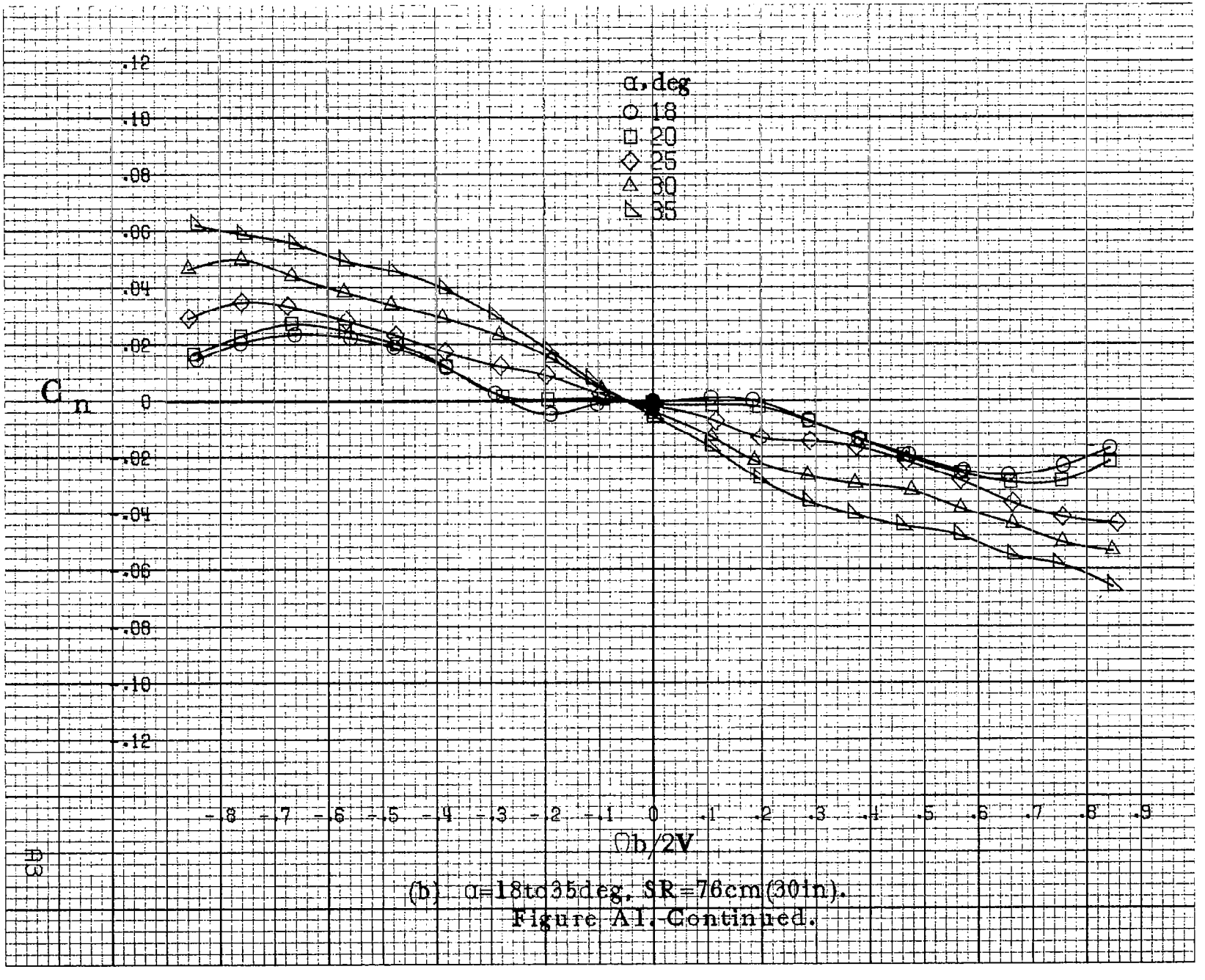

(b) α=18to35deg, SR=76cm(30in).

Figure A1. Continued.

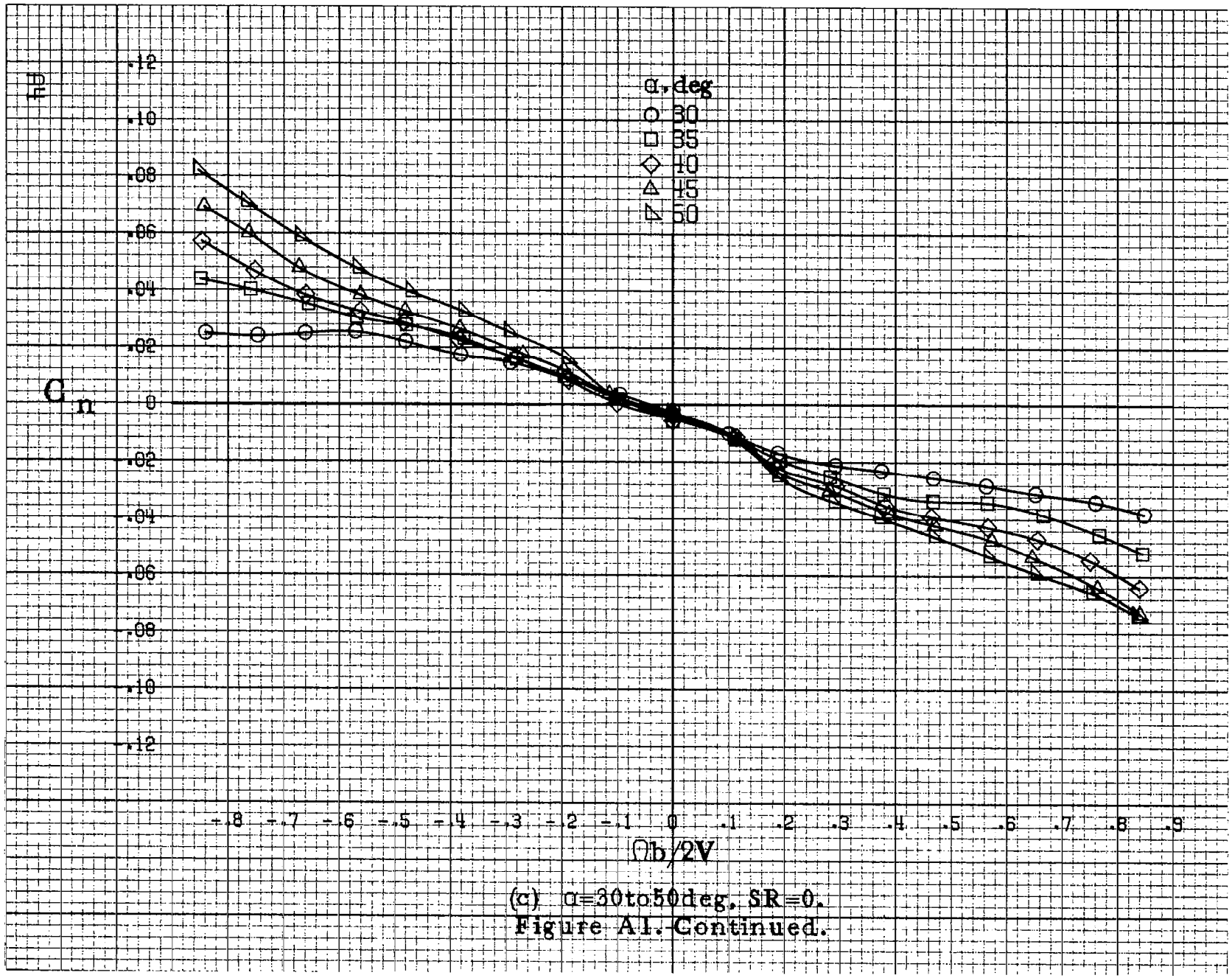

(c) α=30to50deg. SR=0.

Figure A1.-Continued.

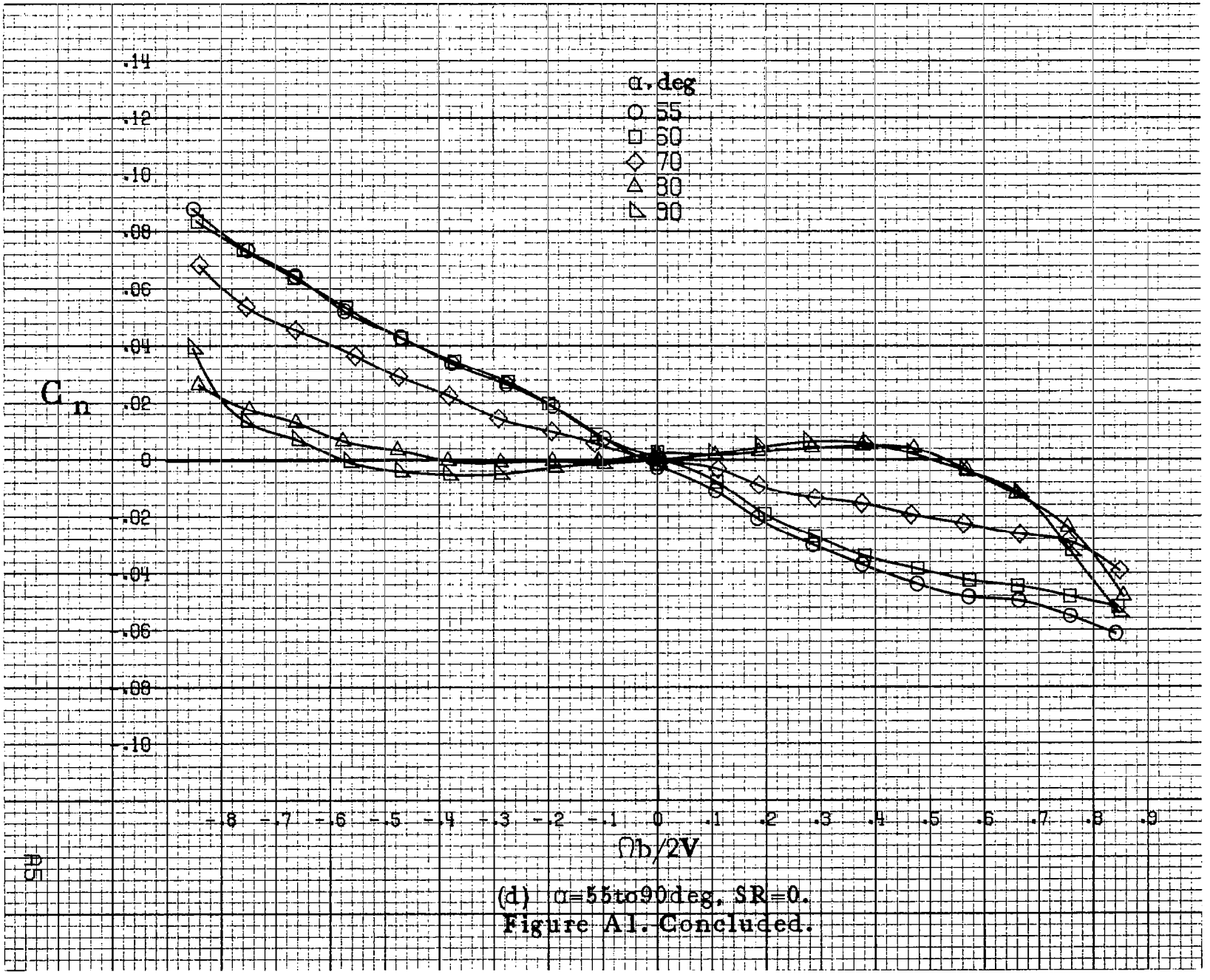

(d) α=55to90deg, SR=0.

Figure A1. Concluded.

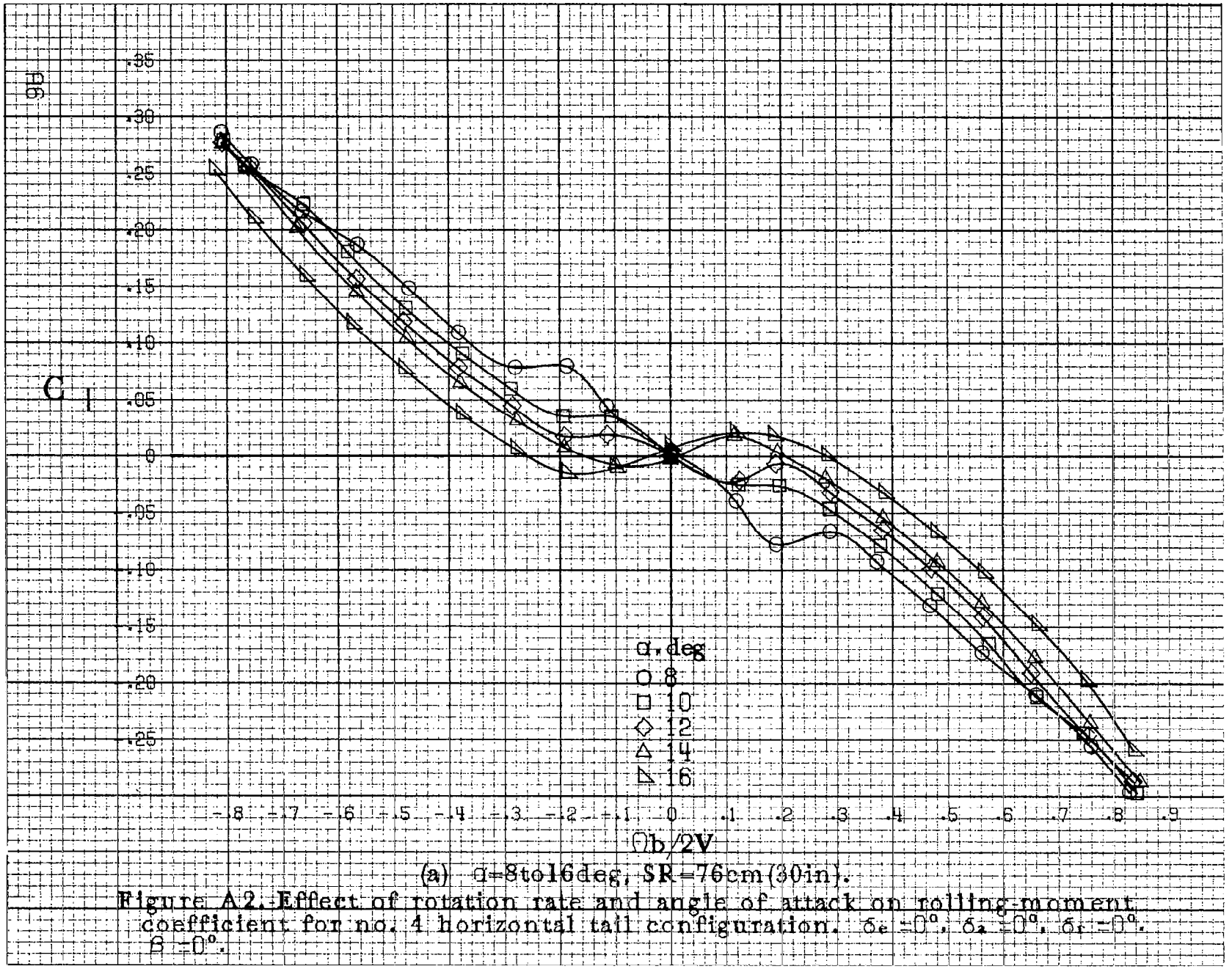

(a) α=8to16deg, $R=76cm(30in).

Figure A2. Effect of rotation rate and angle of attack on rolling-moment coefficient for no. 4 horizontal tail configuration. $\delta_e = 0°$, $\delta_a = 0°$, $\delta_r = 0°$. $\beta = 0°$.

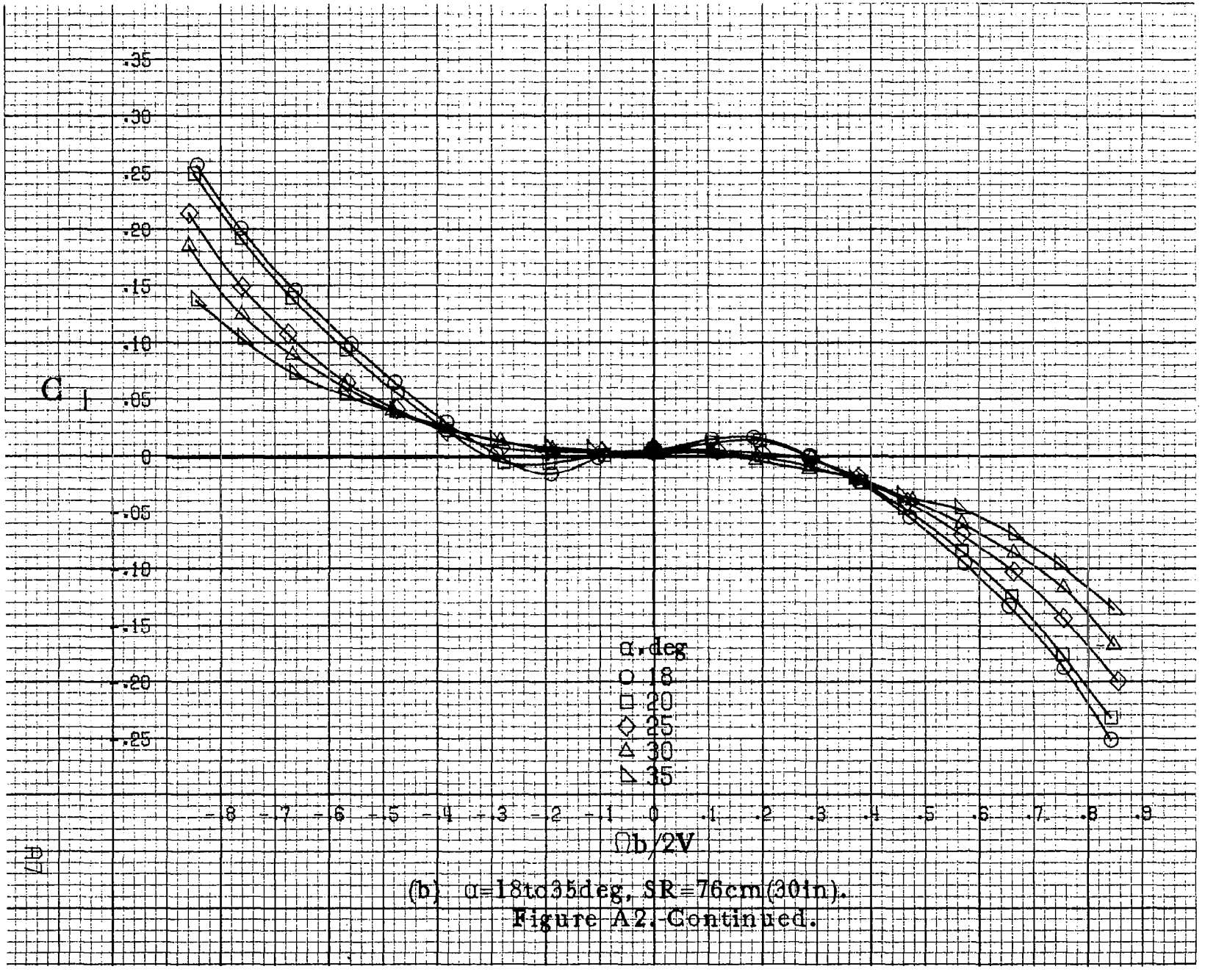

(b) α=18to35deg, SR=76cm(30in).

Figure A2.-Continued.

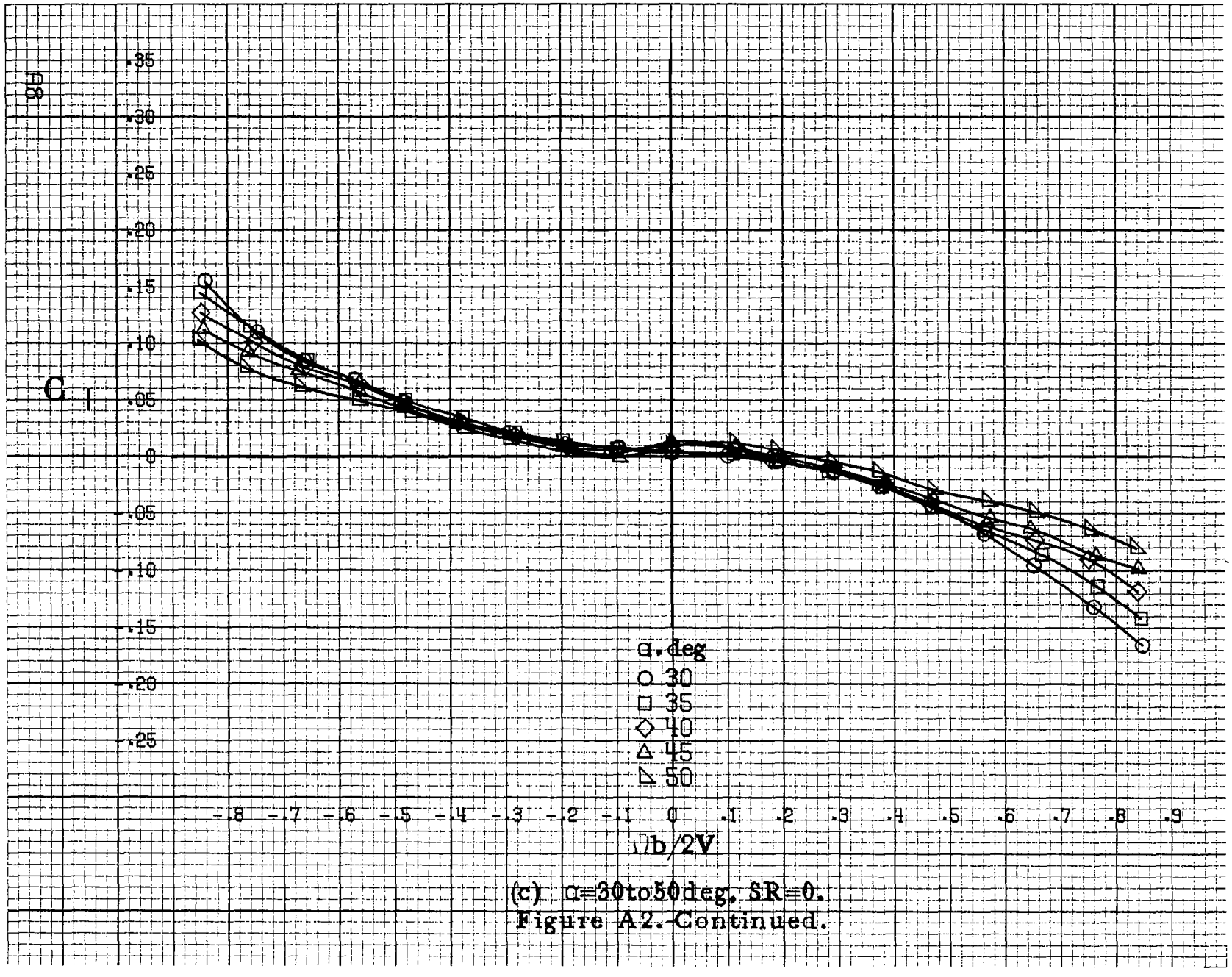

(c) α=30to50deg, SR=0.

Figure A2.-Continued.

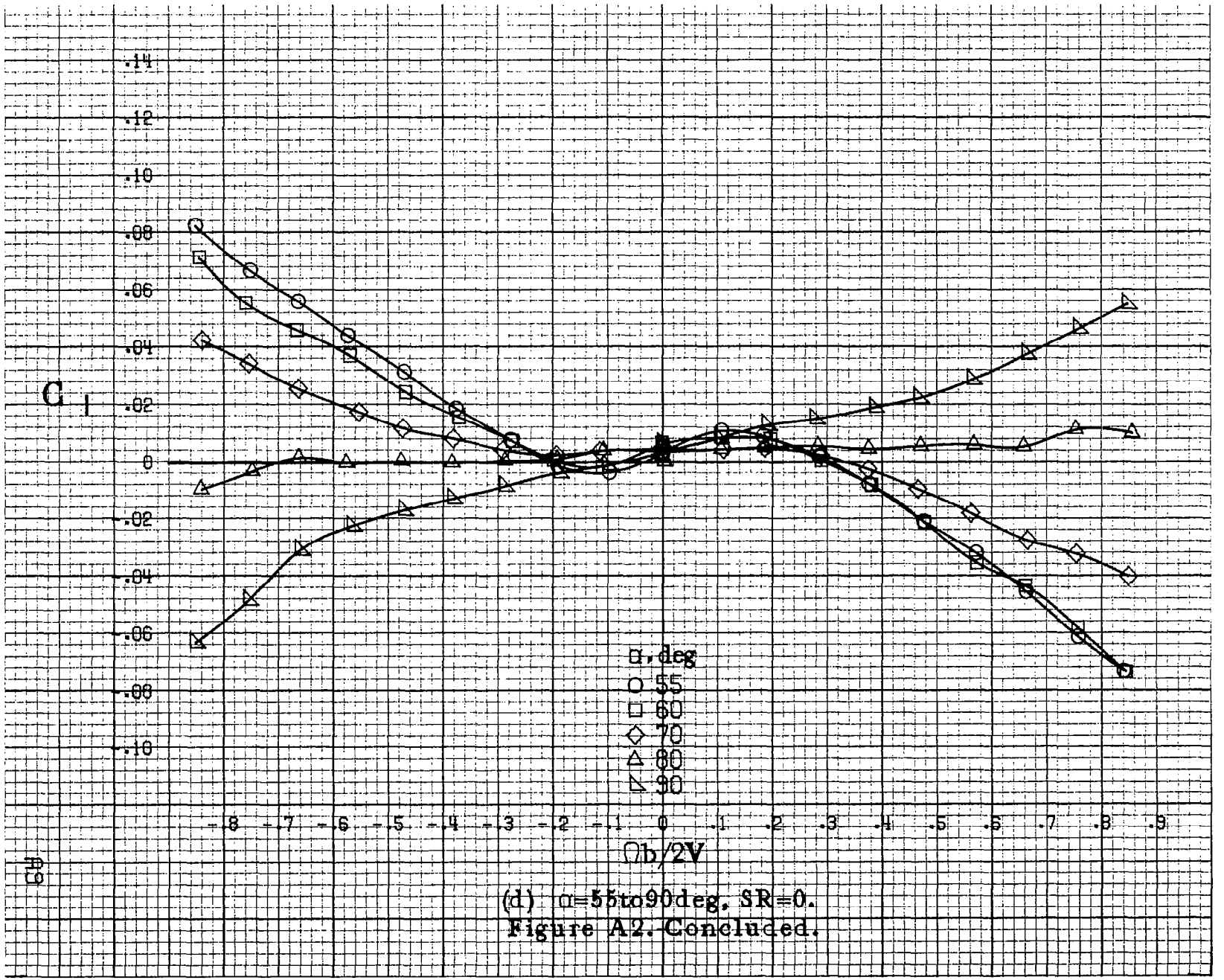

(d) α=55to90deg, SR=0.

Figure A2. Concluded.

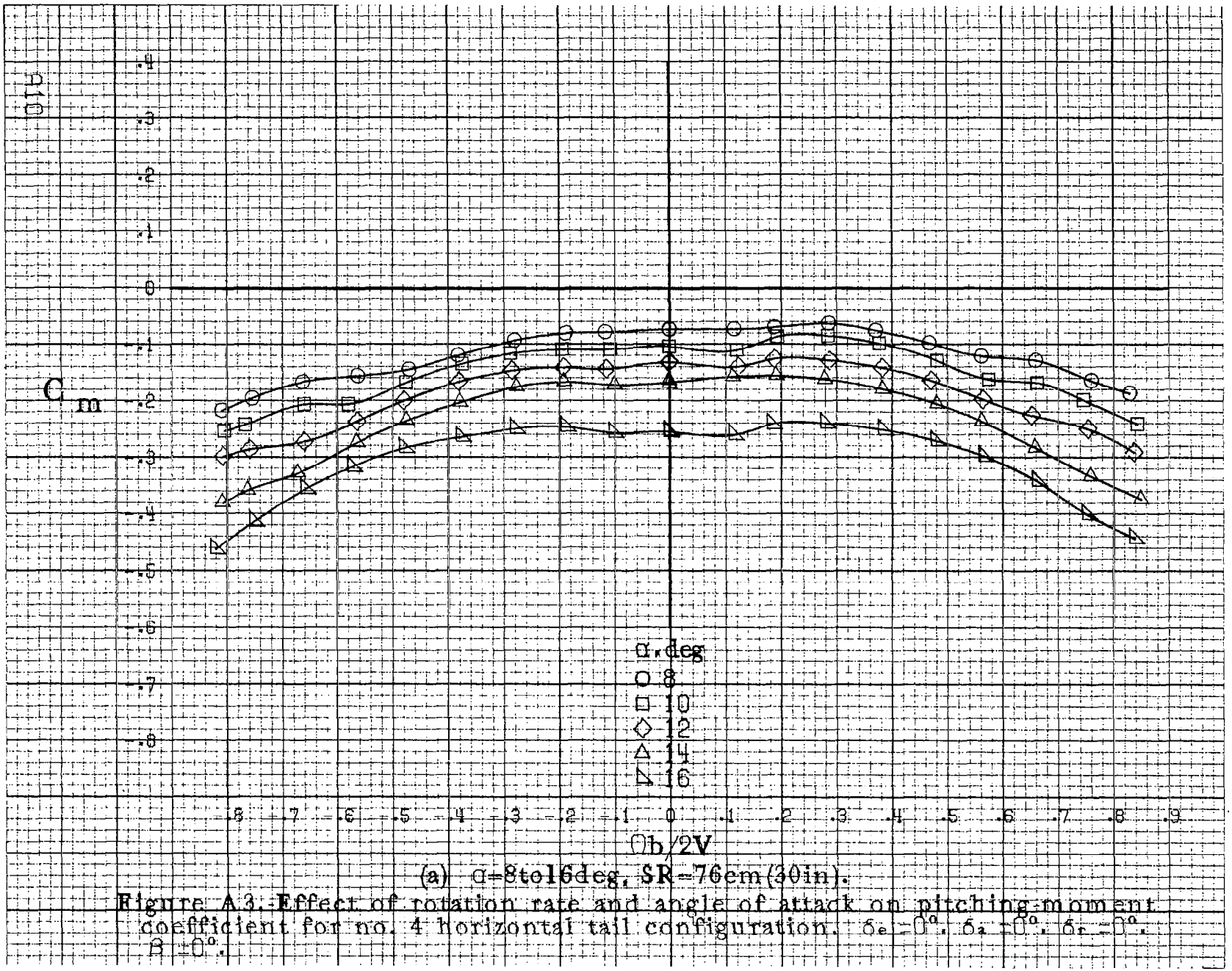

(a) α=8to16deg, SR=76cm(30in).

Figure A.3.-Effect of rotation rate and angle of attack on pitching-moment coefficient for no. 4 horizontal tail configuration. $\delta_e = 0^\circ$, $\delta_a = 0^\circ$, $\delta_r = 0^\circ$, $\beta = 0^\circ$.

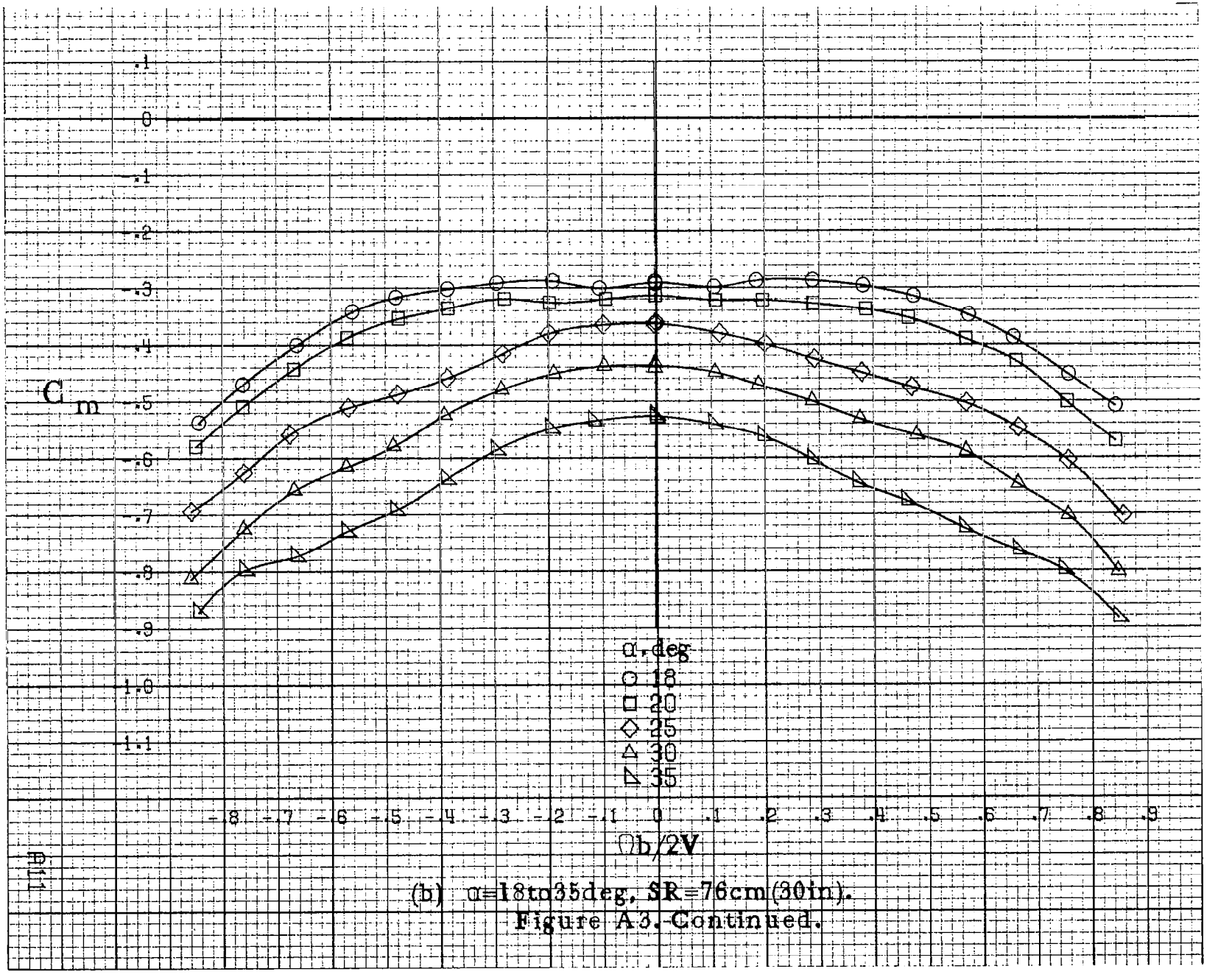

(b) α=18to35deg, SR=76cm(30in).

Figure A3.-Continued.

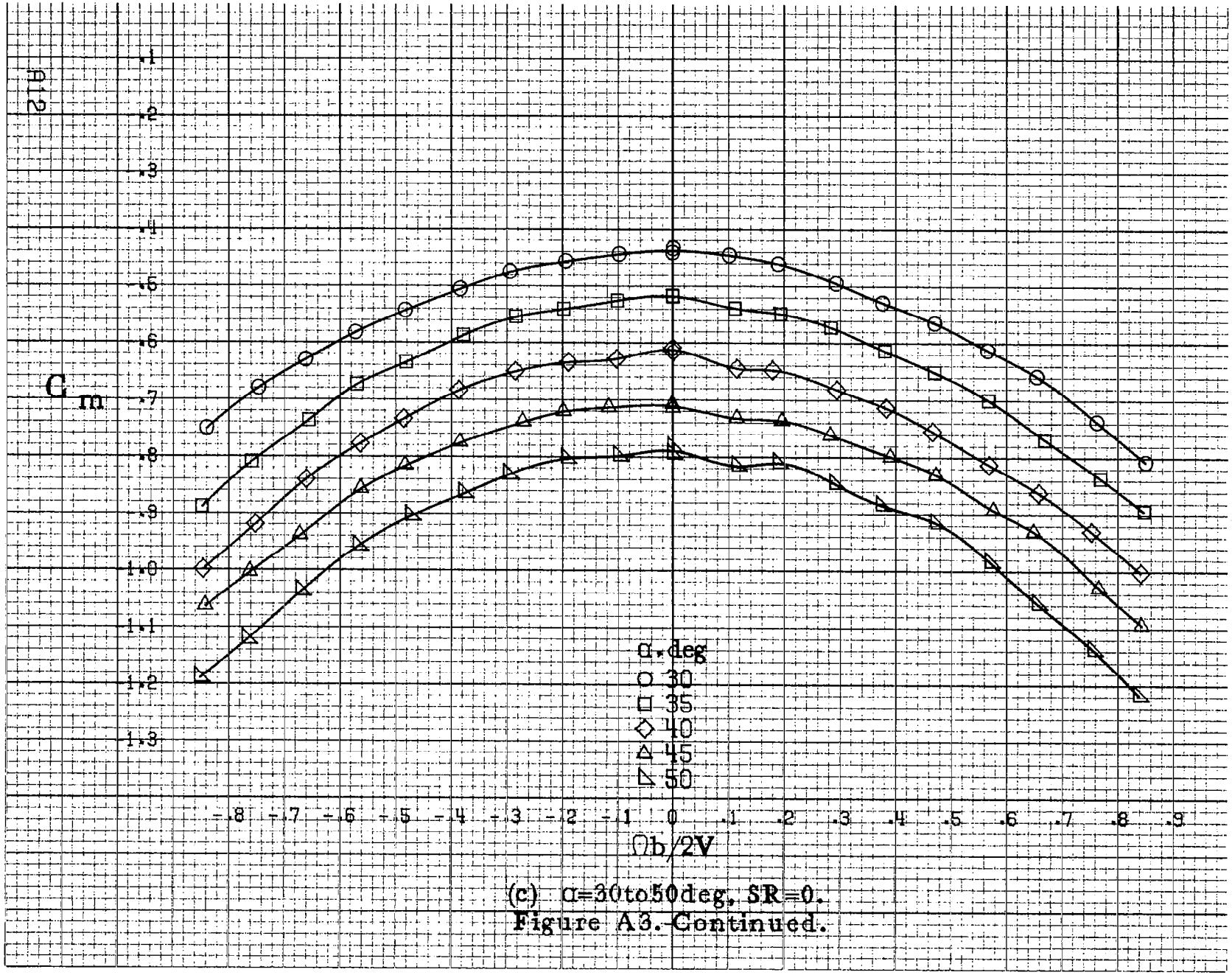

(c) α=30to50deg, SR=0.

Figure A3. Continued.

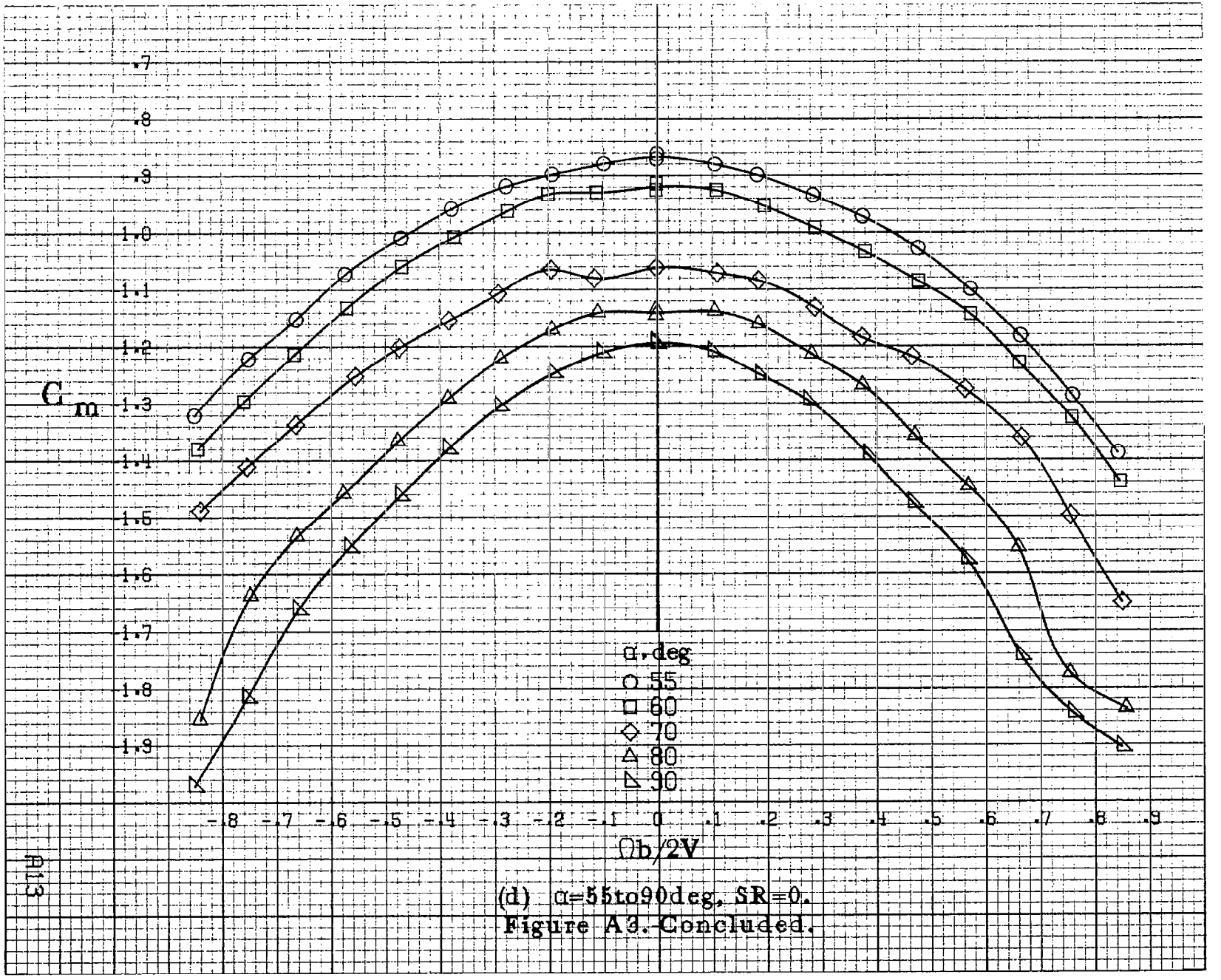

(d) α=55to90deg, SR=0.

Figure A3.-Concluded.

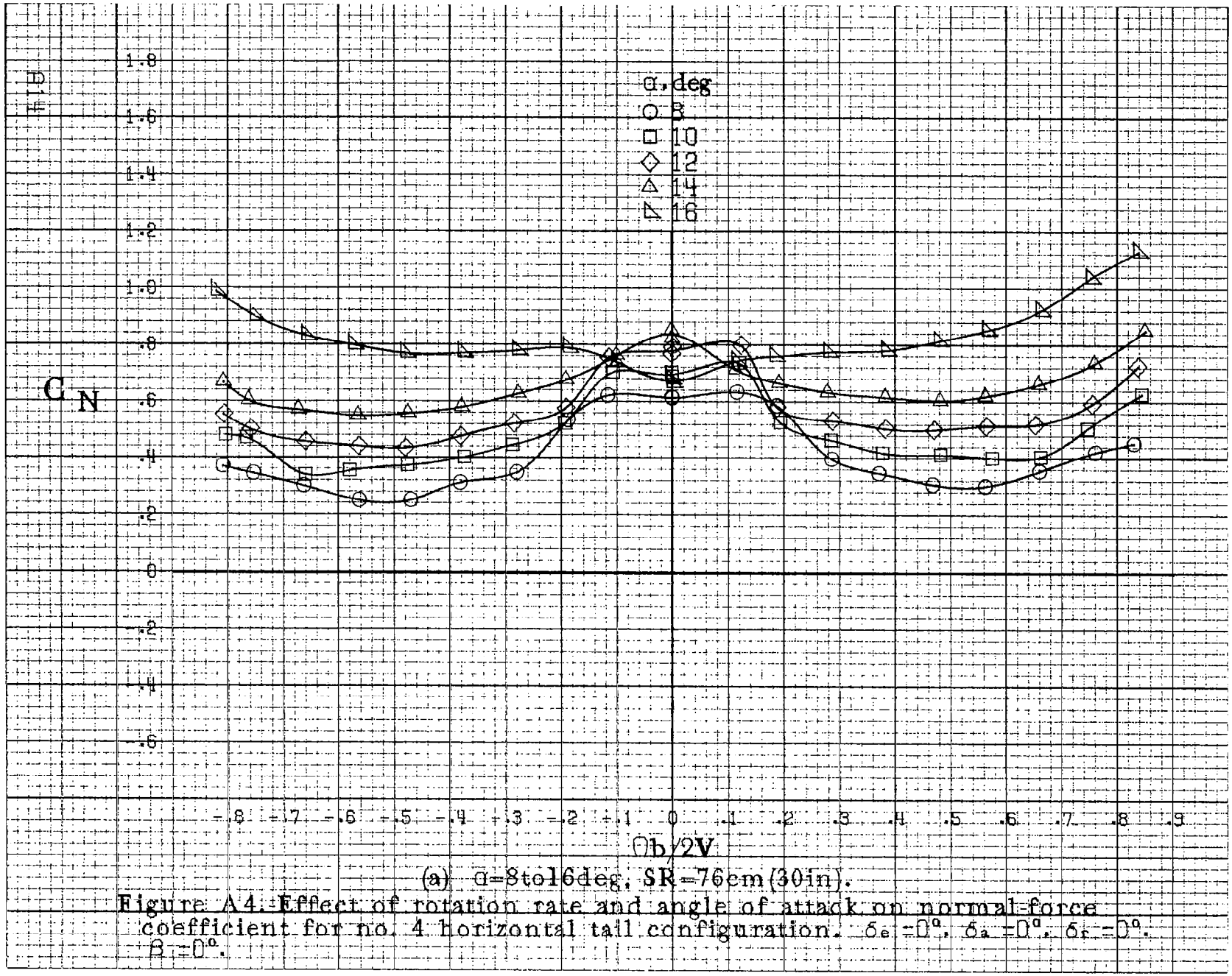

(a) α=8to16deg, SR=76cm(30in).

Figure A4. Effect of rotation rate and angle of attack on normal-force coefficient for no. 4 horizontal tail configuration. $\delta_e = 0°$, $\delta_a = 0°$, $\delta_r = 0°$, $\beta = 0°$.

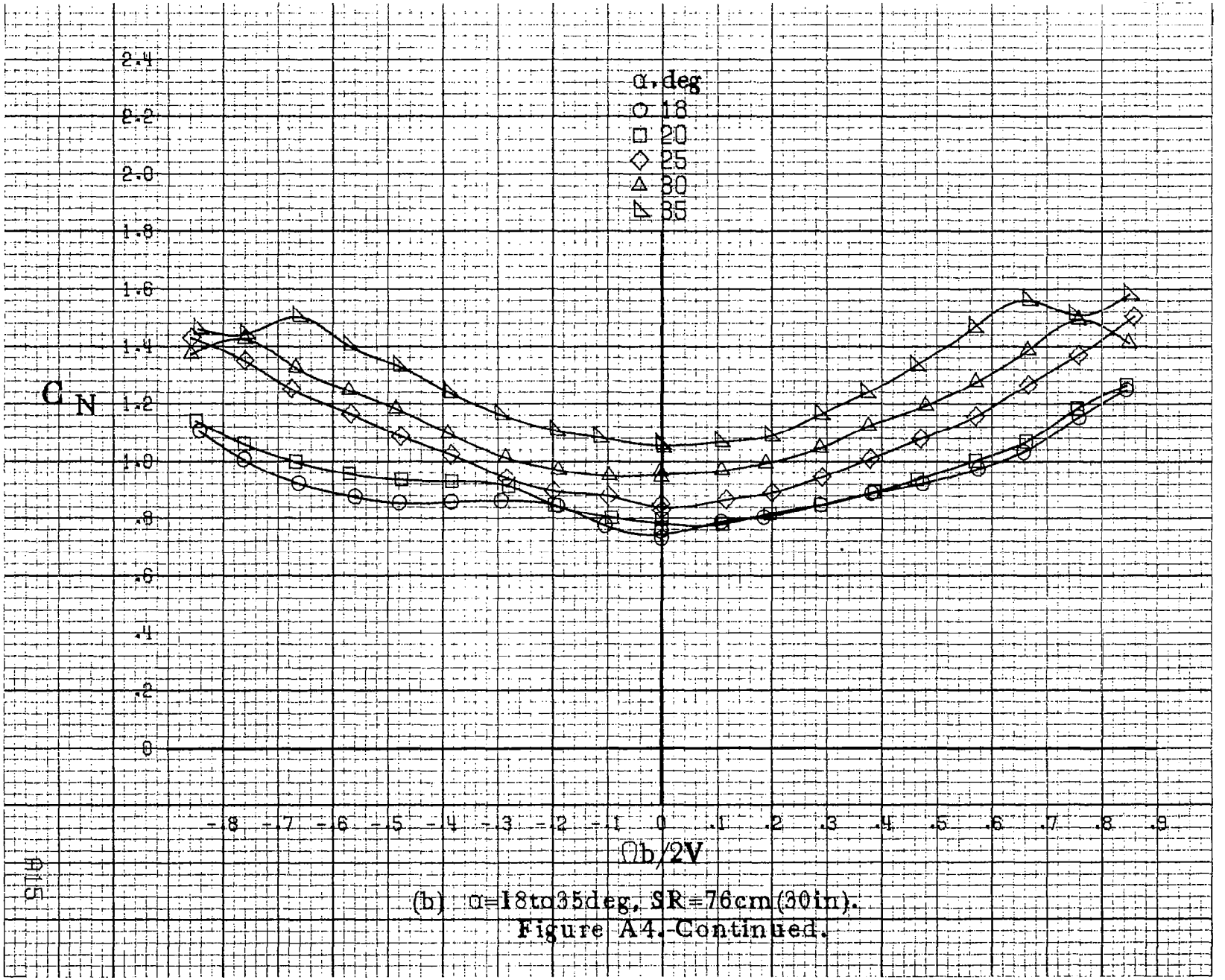

(b) α=18to35deg, SR=76cm(30in).

Figure A4.-Continued.

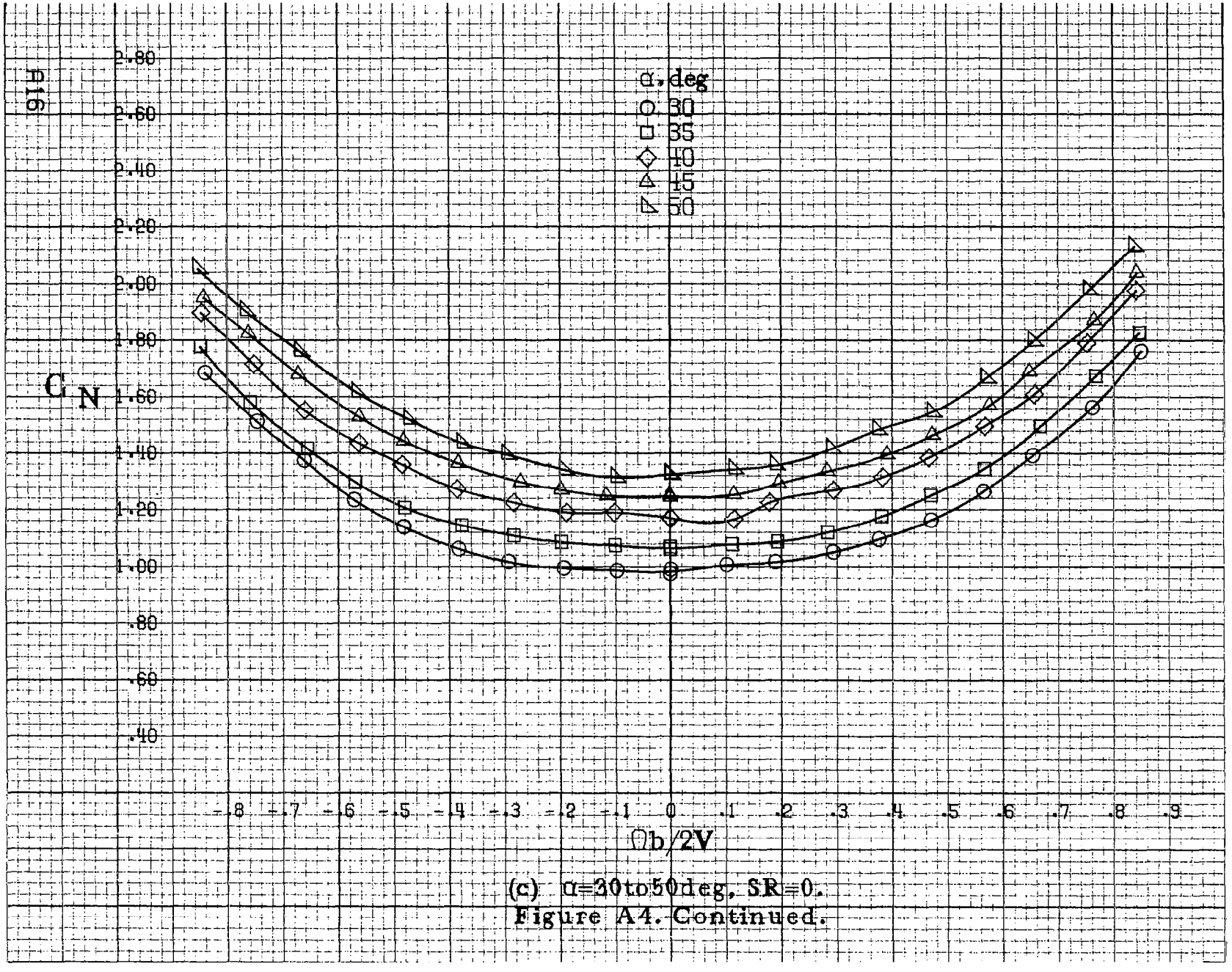

(c) α=30to50deg, SR=0.

Figure A4. Continued.

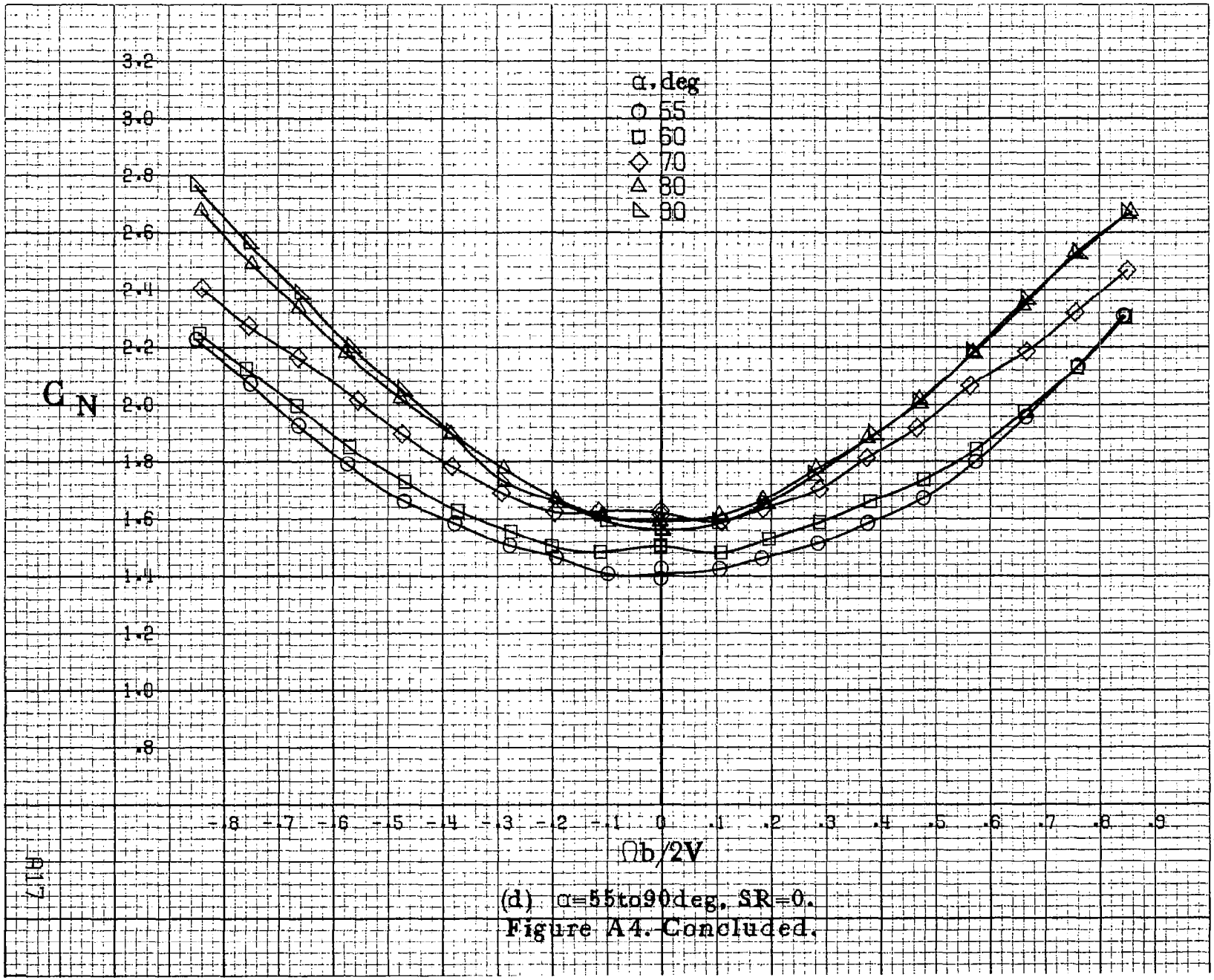

(d) α=55to90deg, SR=0.

Figure A4. Concluded.

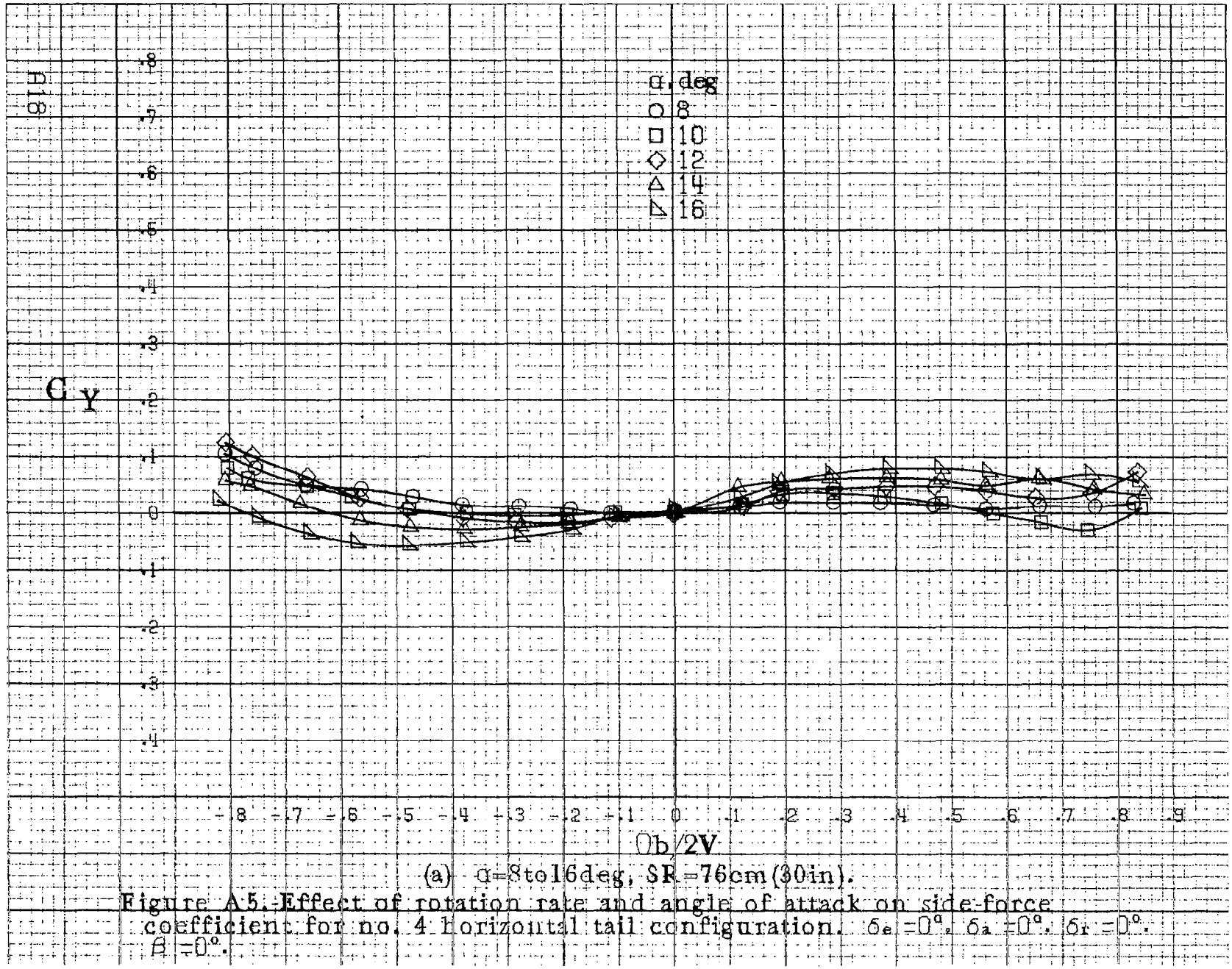

(a) α=8to16deg, S_R=76cm(30in).

Figure A5.-Effect of rotation rate and angle of attack on side-force coefficient for no. 4 horizontal tail configuration. $\delta_e = 0°$, $\delta_a = 0°$, $\delta_r = 0°$, $\beta = 0°$.

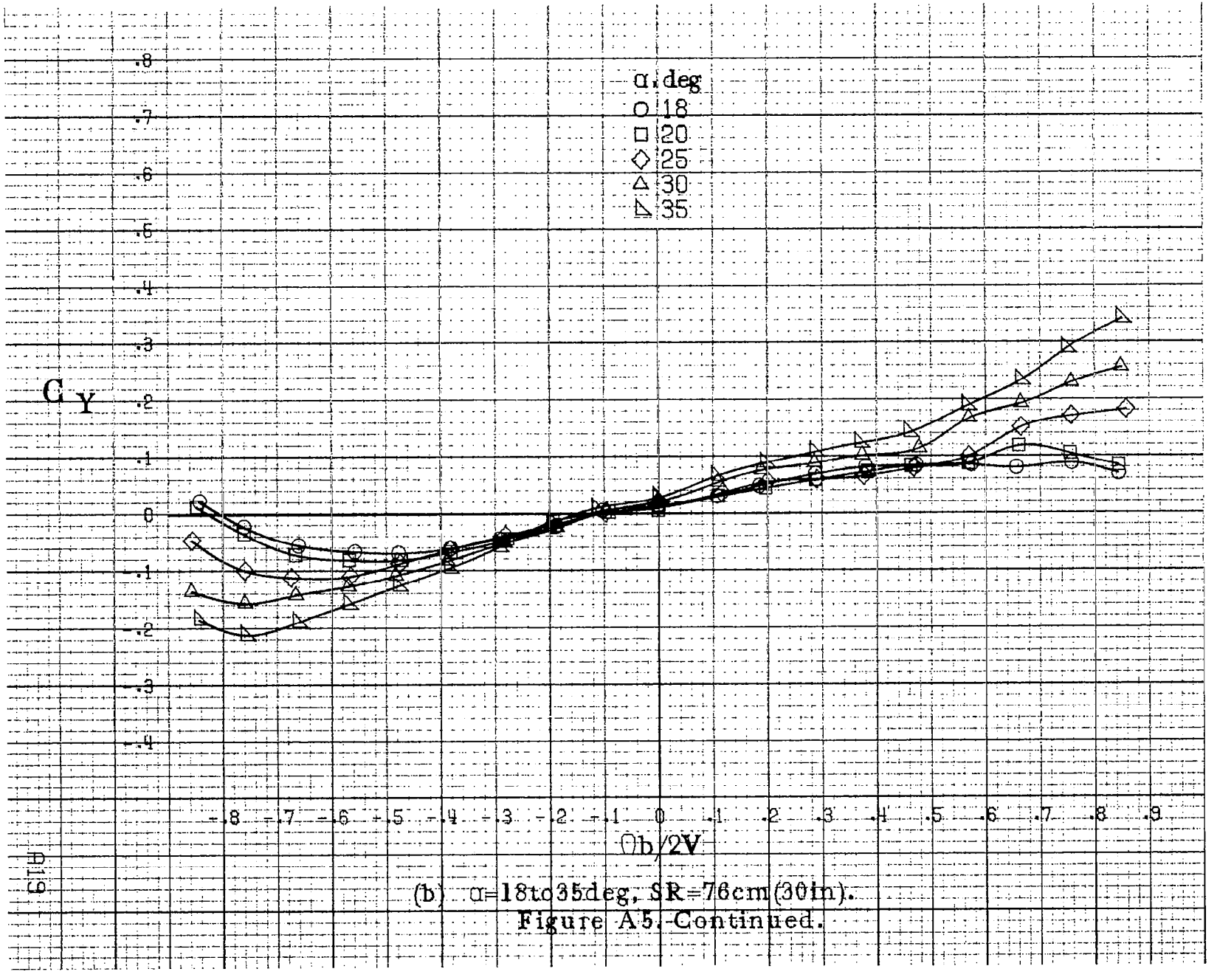

(b) α=18to35deg, SR=76cm(30in).

Figure A5.-Continued.

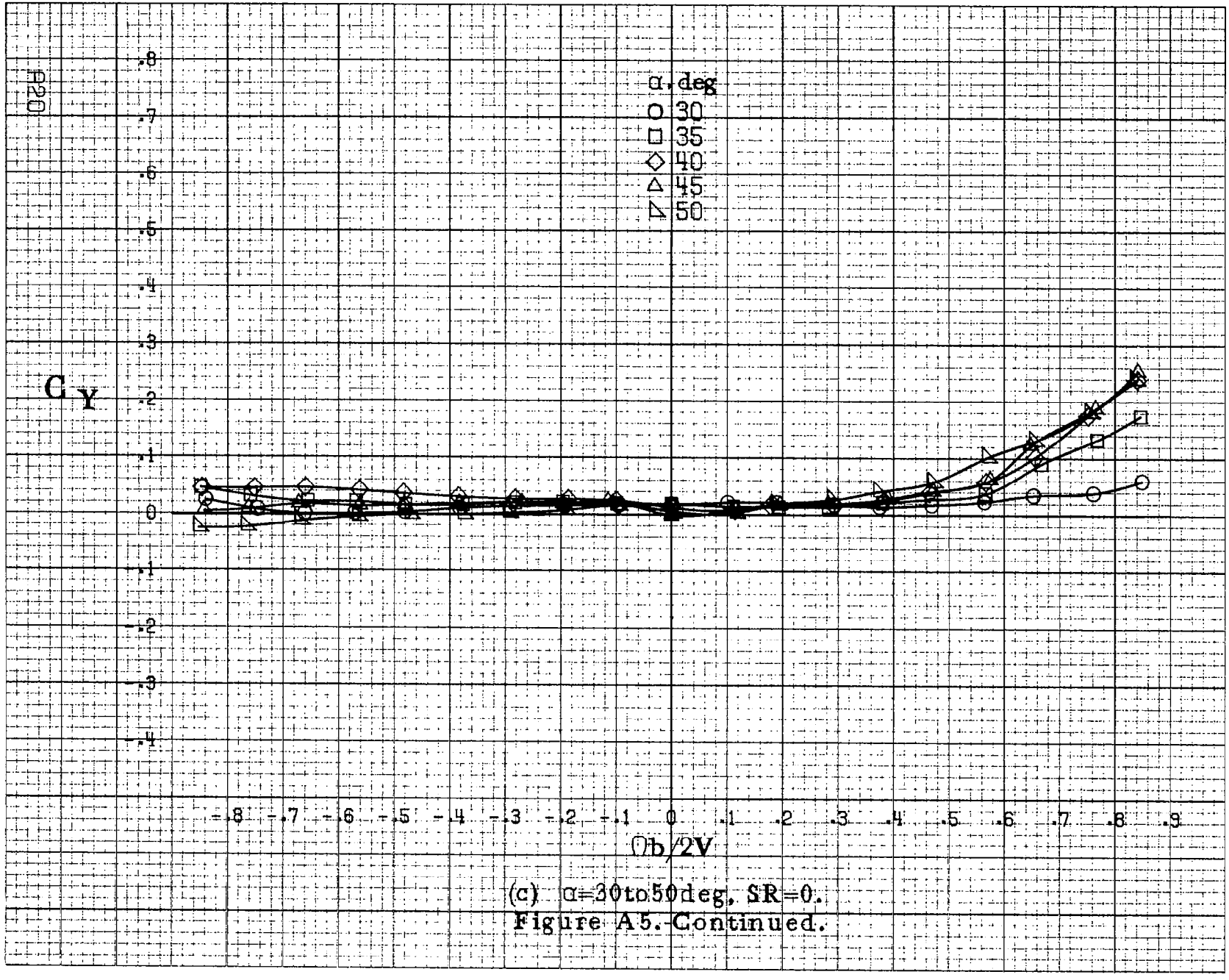

(c) α=30to50deg, SR=0.

Figure A5.-Continued.

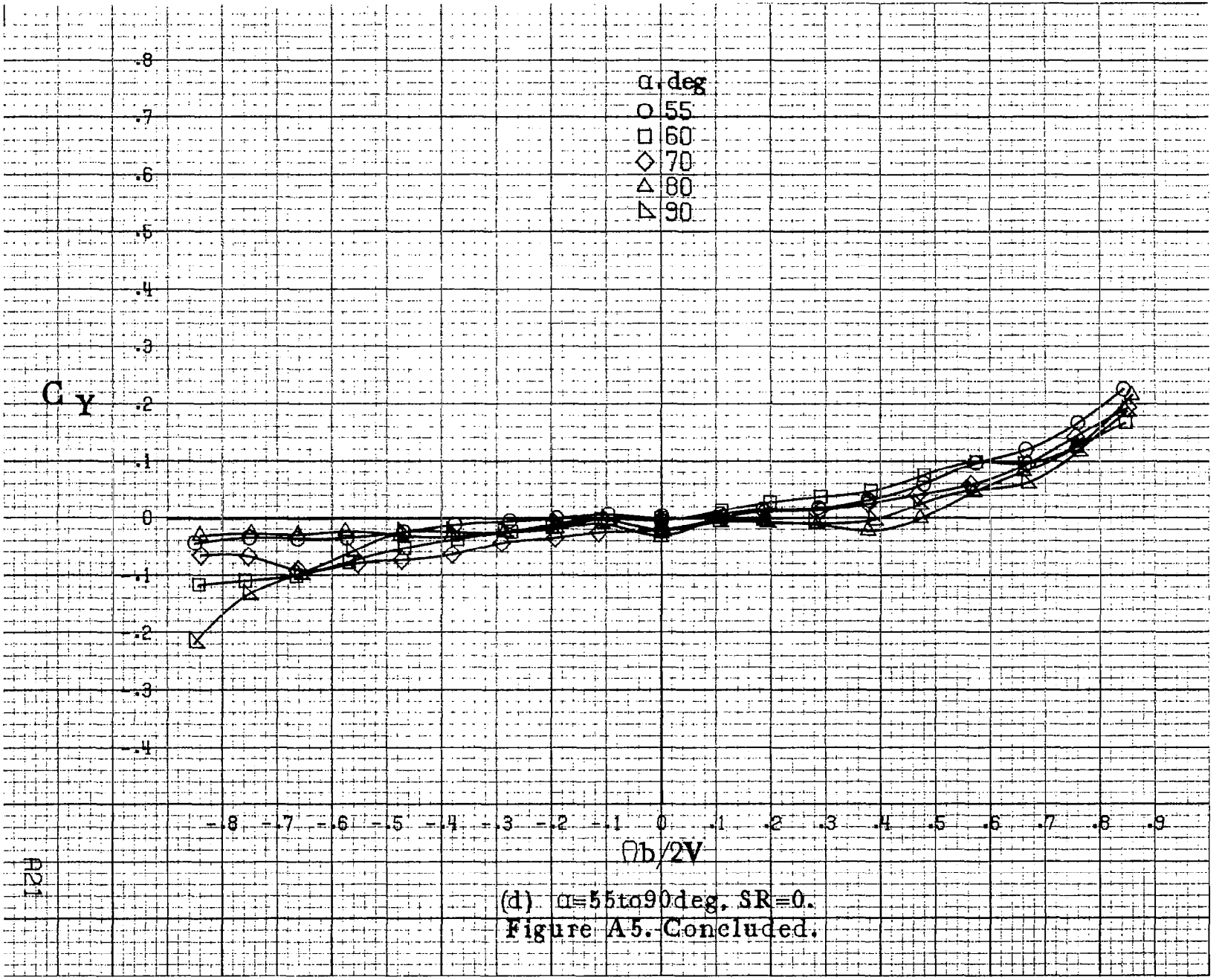

(d) α=55to90deg, SR=0.

Figure A5. Concluded.

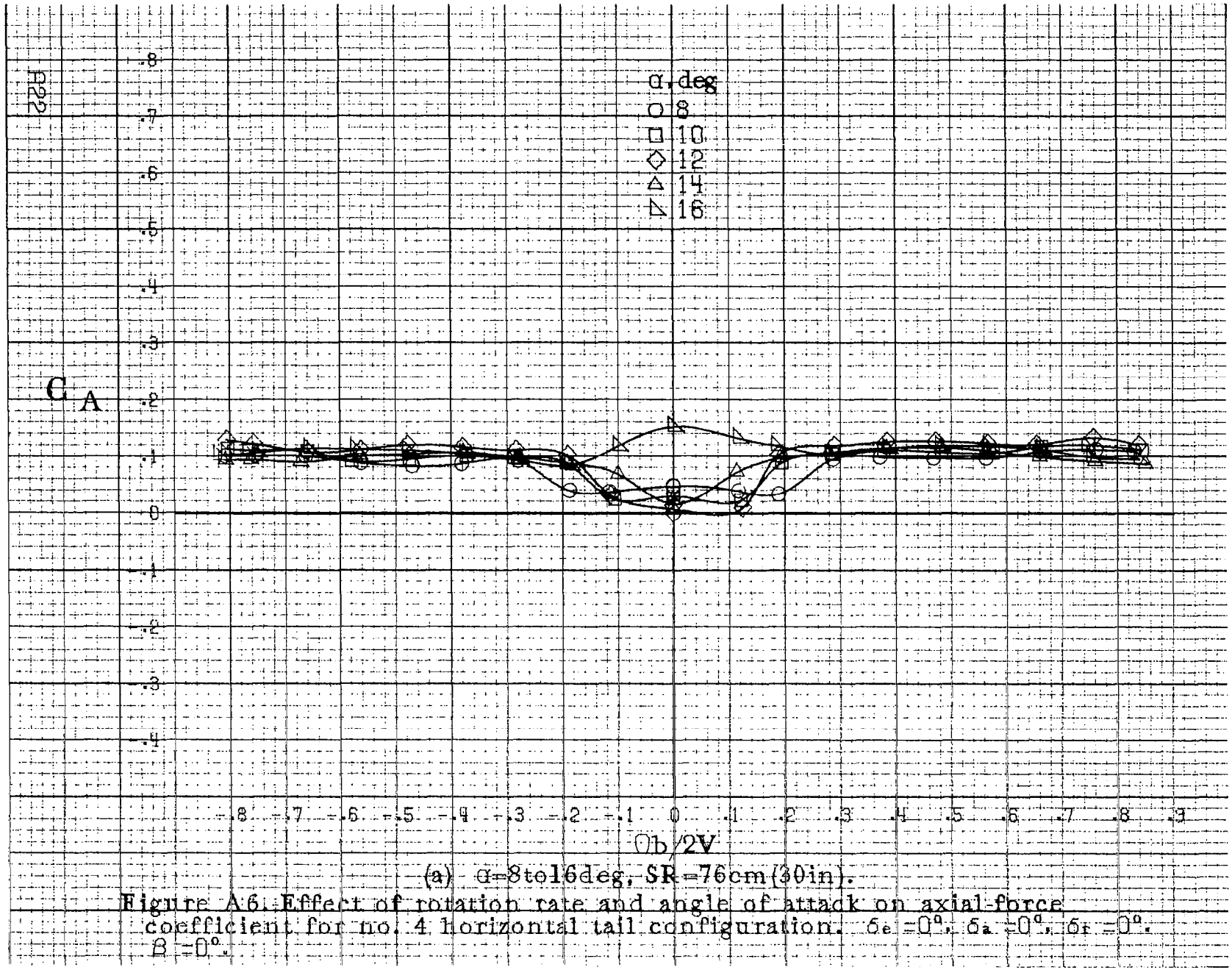

(a) α=8to16deg, SR=76cm(30in).

Figure A6. Effect of rotation rate and angle of attack on axial-force coefficient for no. 4 horizontal tail configuration. $\delta_e = 0^\circ$, $\delta_a = 0^\circ$, $\delta_r = 0^\circ$, $\beta = 0^\circ$.

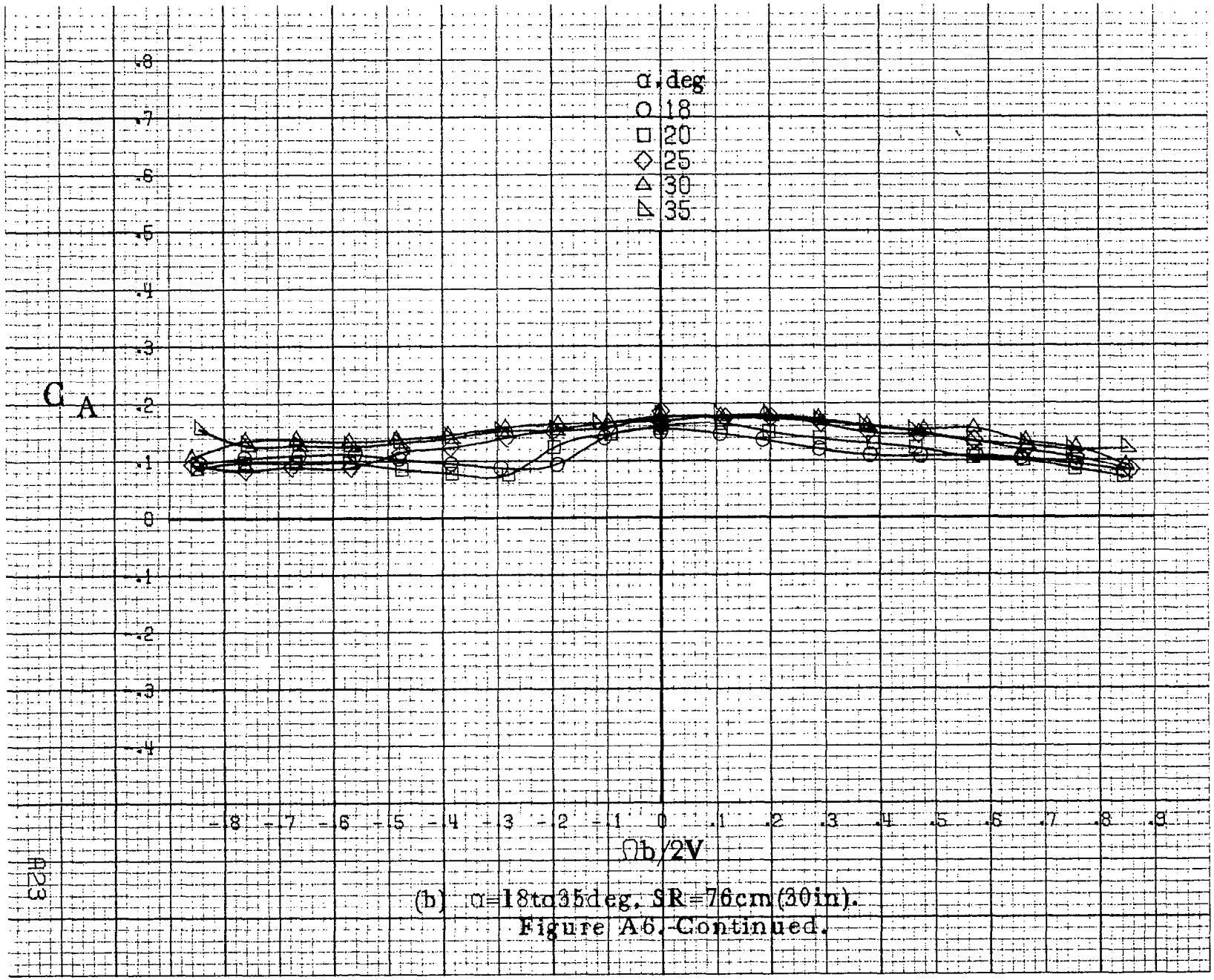

(b) α=18to35deg, SR=76cm(30in).

Figure A6.-Continued.

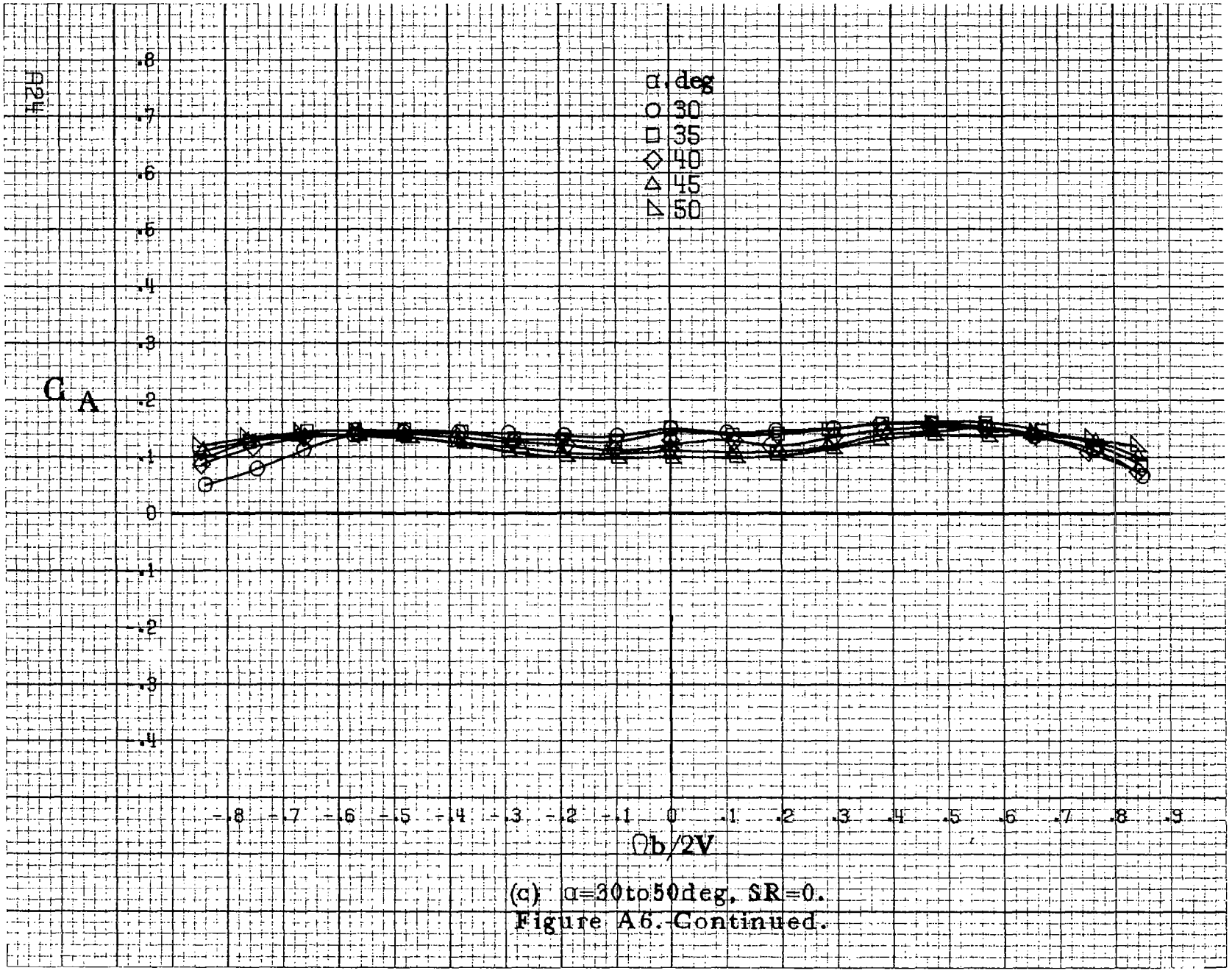

(c) α=30to50deg, SR=0.

Figure A6. Continued.

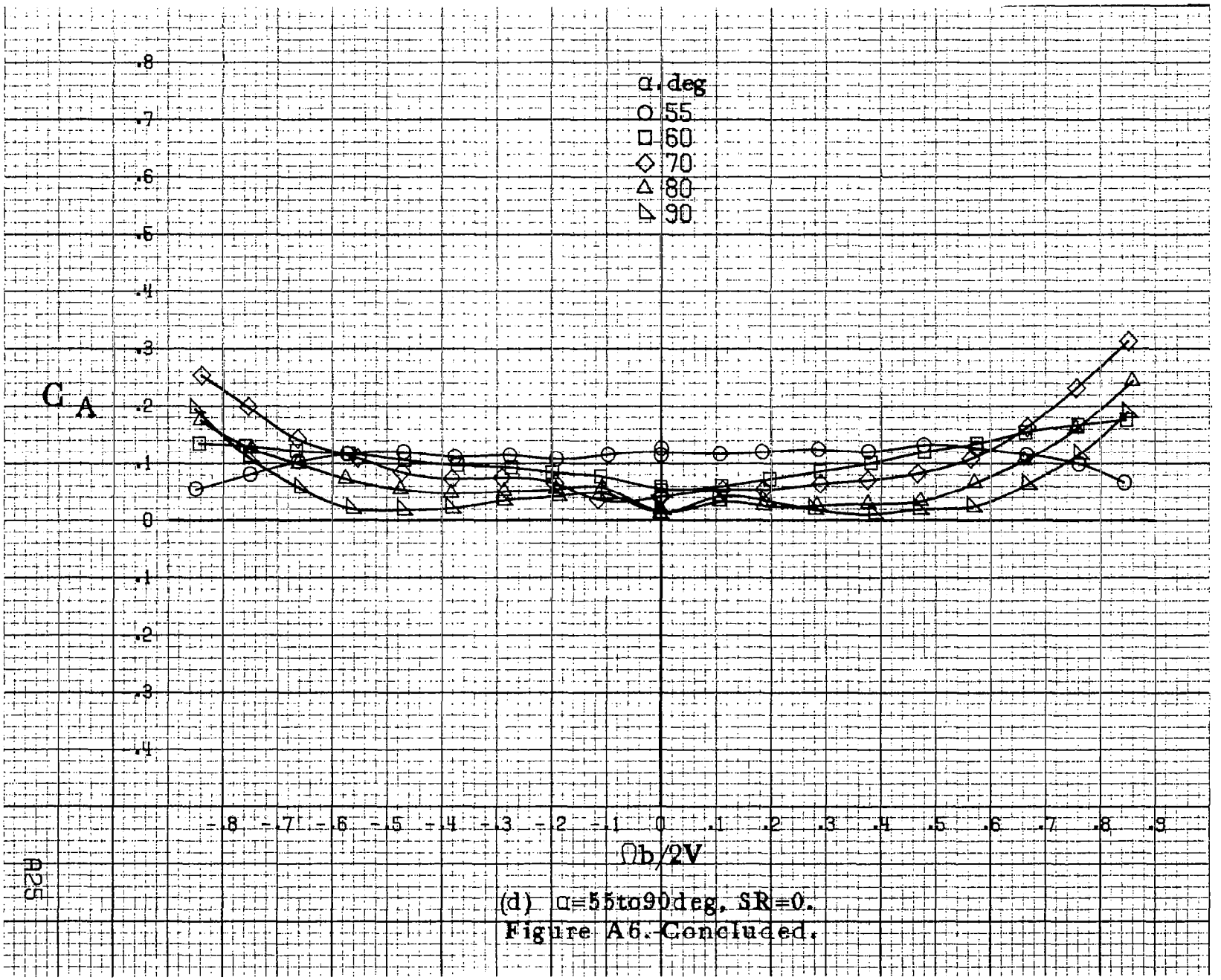

(d) α=55to90deg, SR=0.

Figure A6.-Concluded.

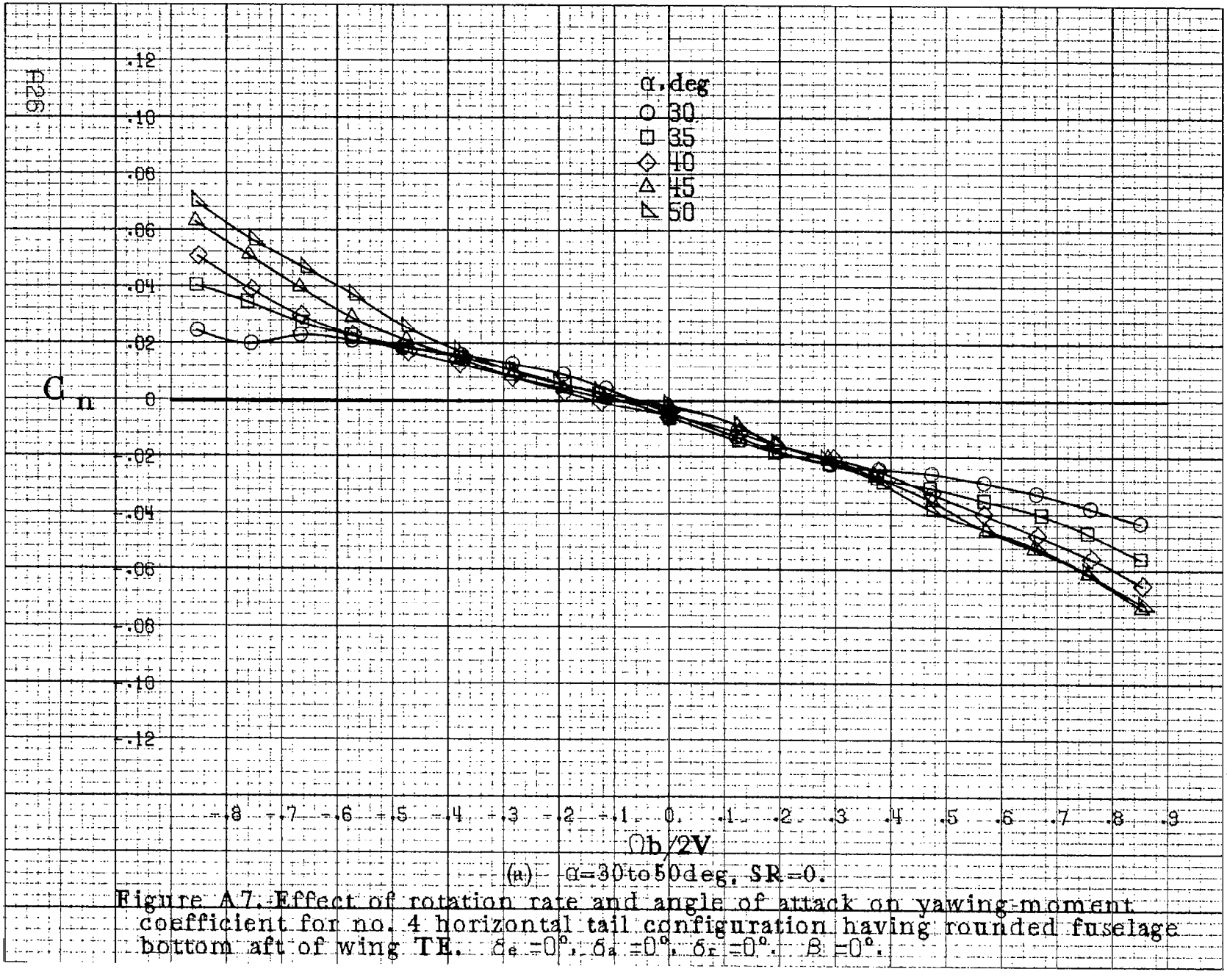

(a) α=30 to 50 deg, SR=0.

Figure A7. Effect of rotation rate and angle of attack on yawing-moment coefficient for no. 4 horizontal tail configuration having rounded fuselage bottom aft of wing TE. $\delta_e = 0°$, $\delta_a = 0°$, $\delta_r = 0°$, $\beta = 0°$.

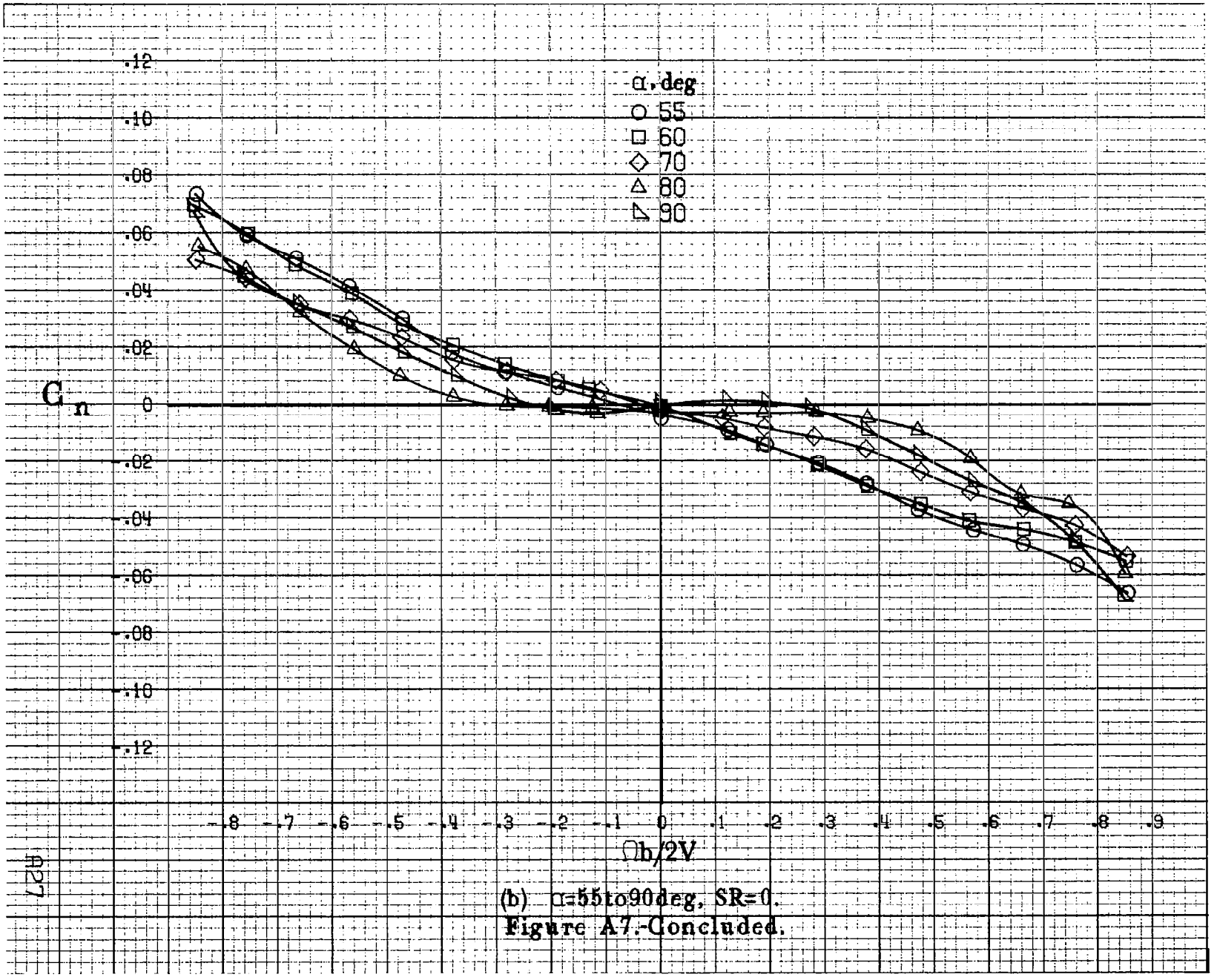

(b) α=55to90deg, SR=0.

Figure A7.-Concluded.

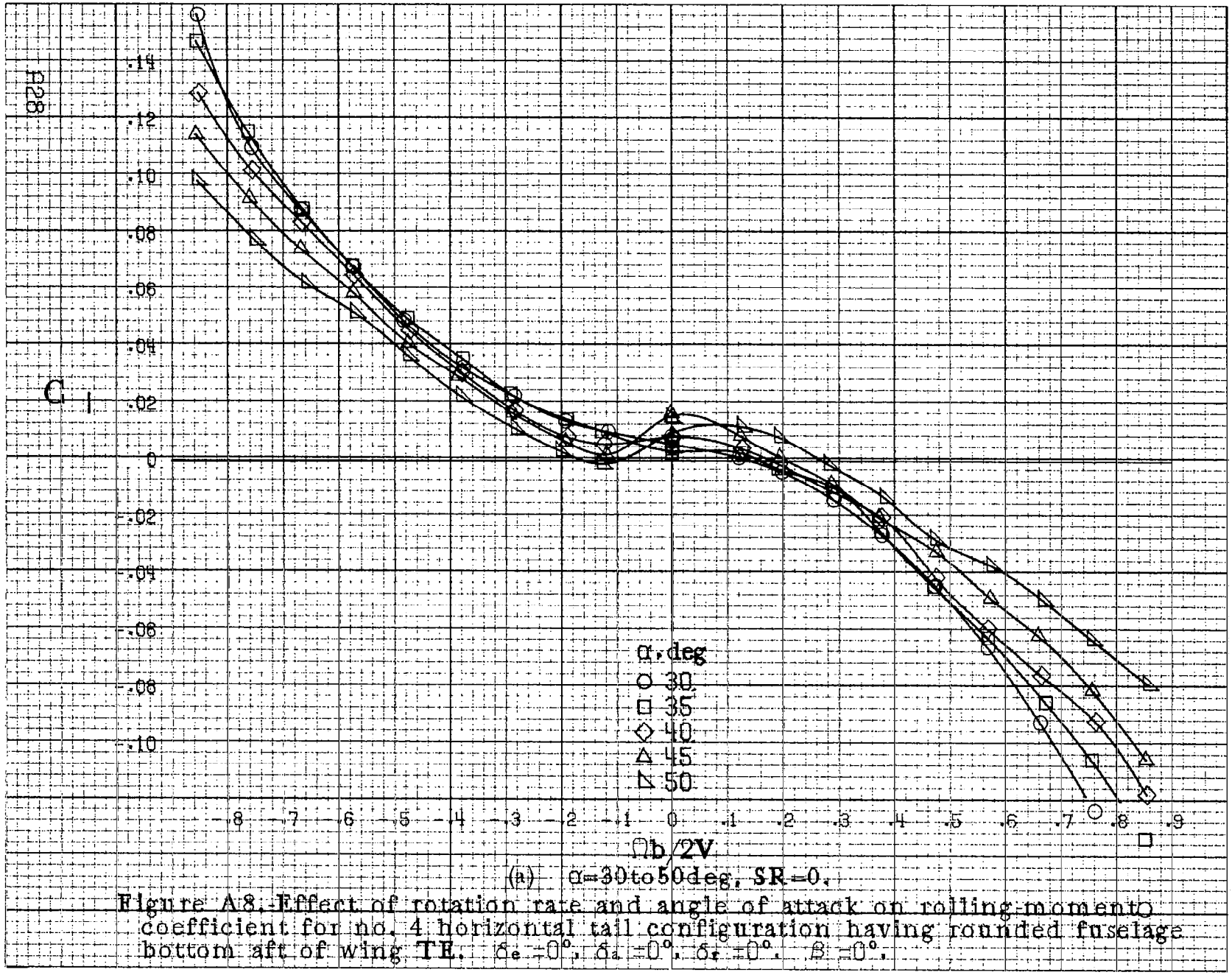

(a) α=30to50deg, SR=0.

Figure A8. Effect of rotation rate and angle of attack on rolling-moment coefficient for no. 4 horizontal tail configuration having rounded fuselage bottom aft of wing TE. δ_e=0°, δ_a=0°, δ_r=0°, β=0°.

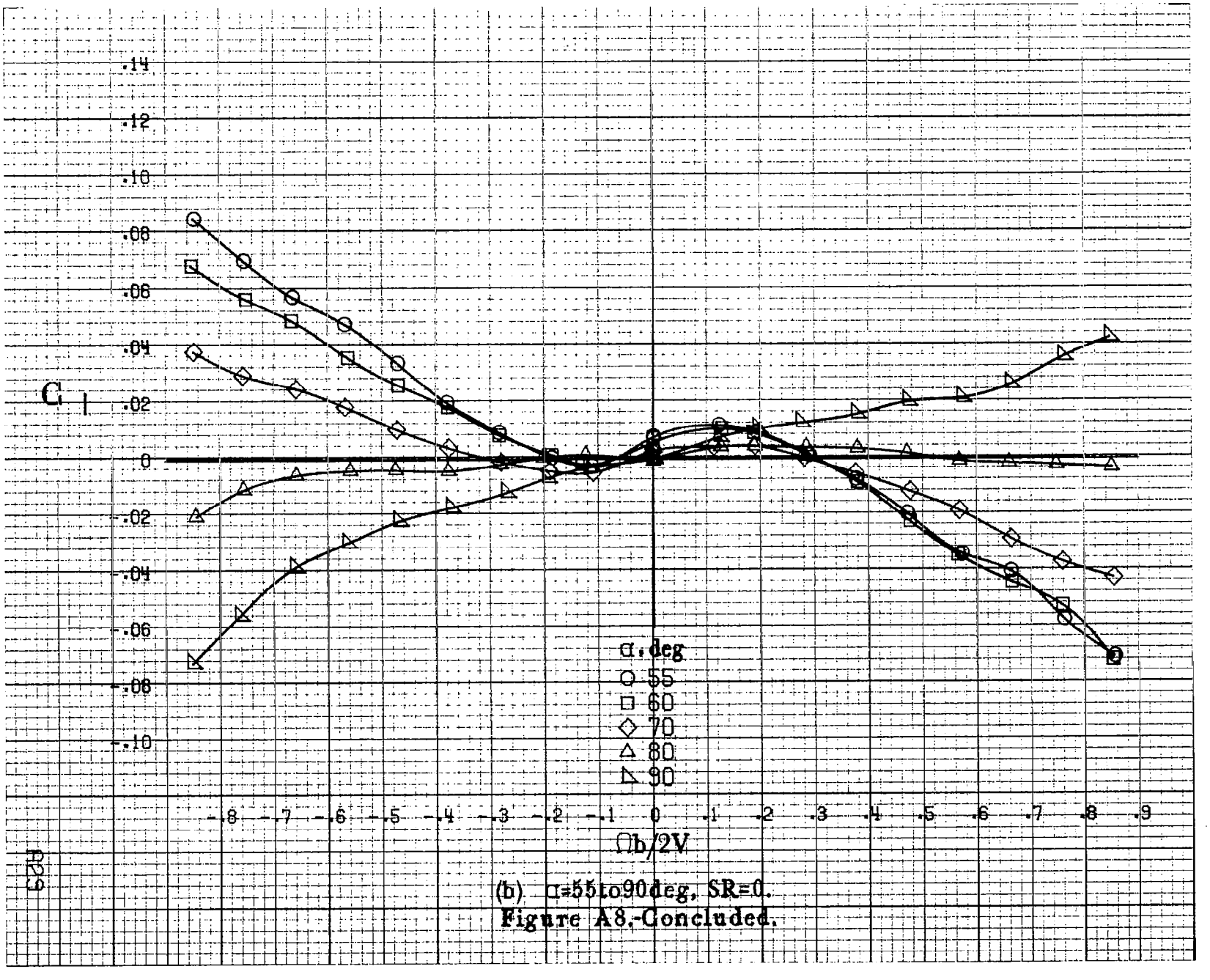

(b) α=55 to 90 deg, SR=0.

Figure A8.-Concluded.

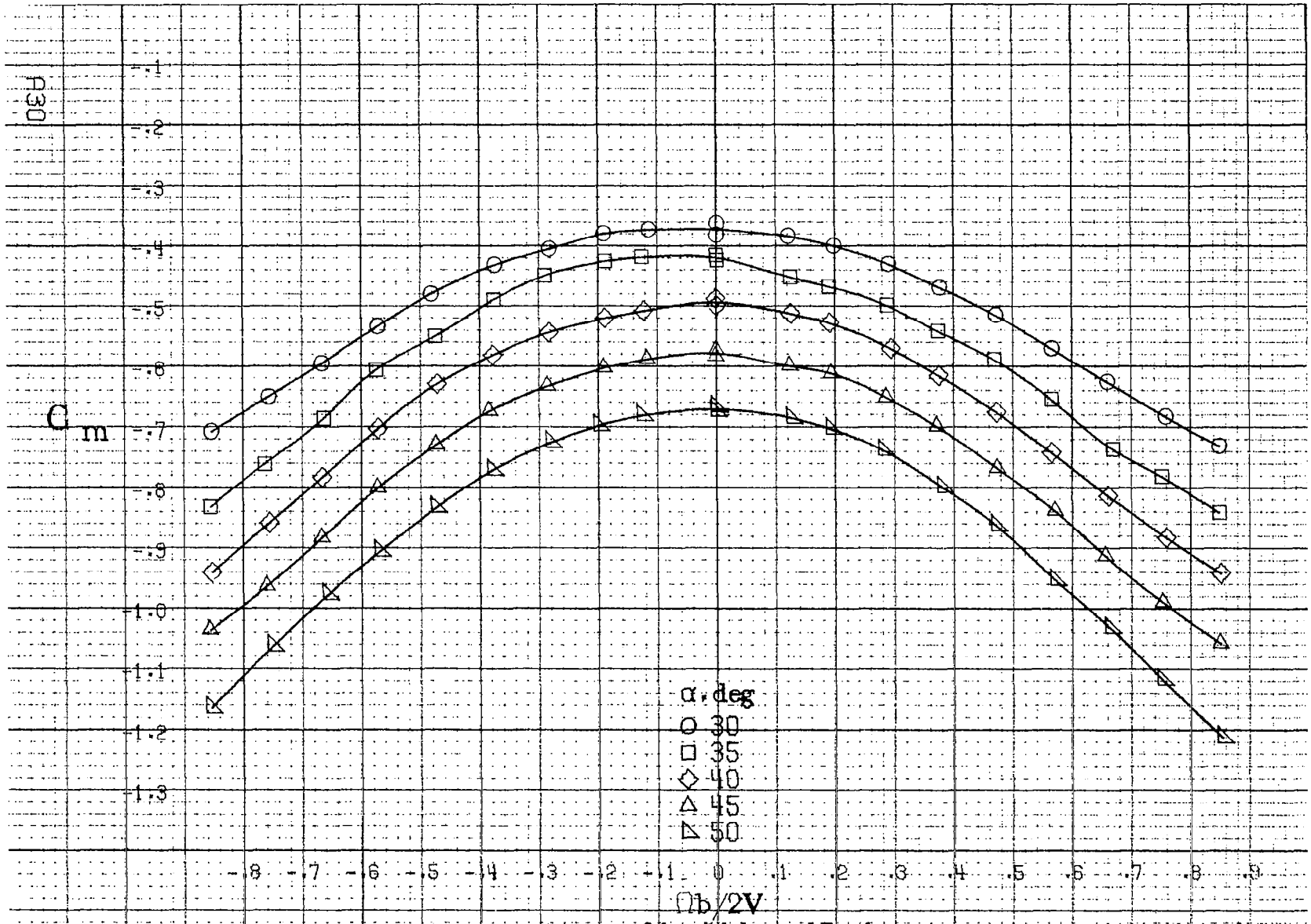

(a) α=30to50deg, SR=0.

Figure A9.-Effect of rotation rate and angle of attack on pitching-moment coefficient for no. 4 horizontal tail configuration having rounded fuselage bottom aft of wing TE. δ_e =0°, δ_a =0°, δ_r =0°, β =0°.

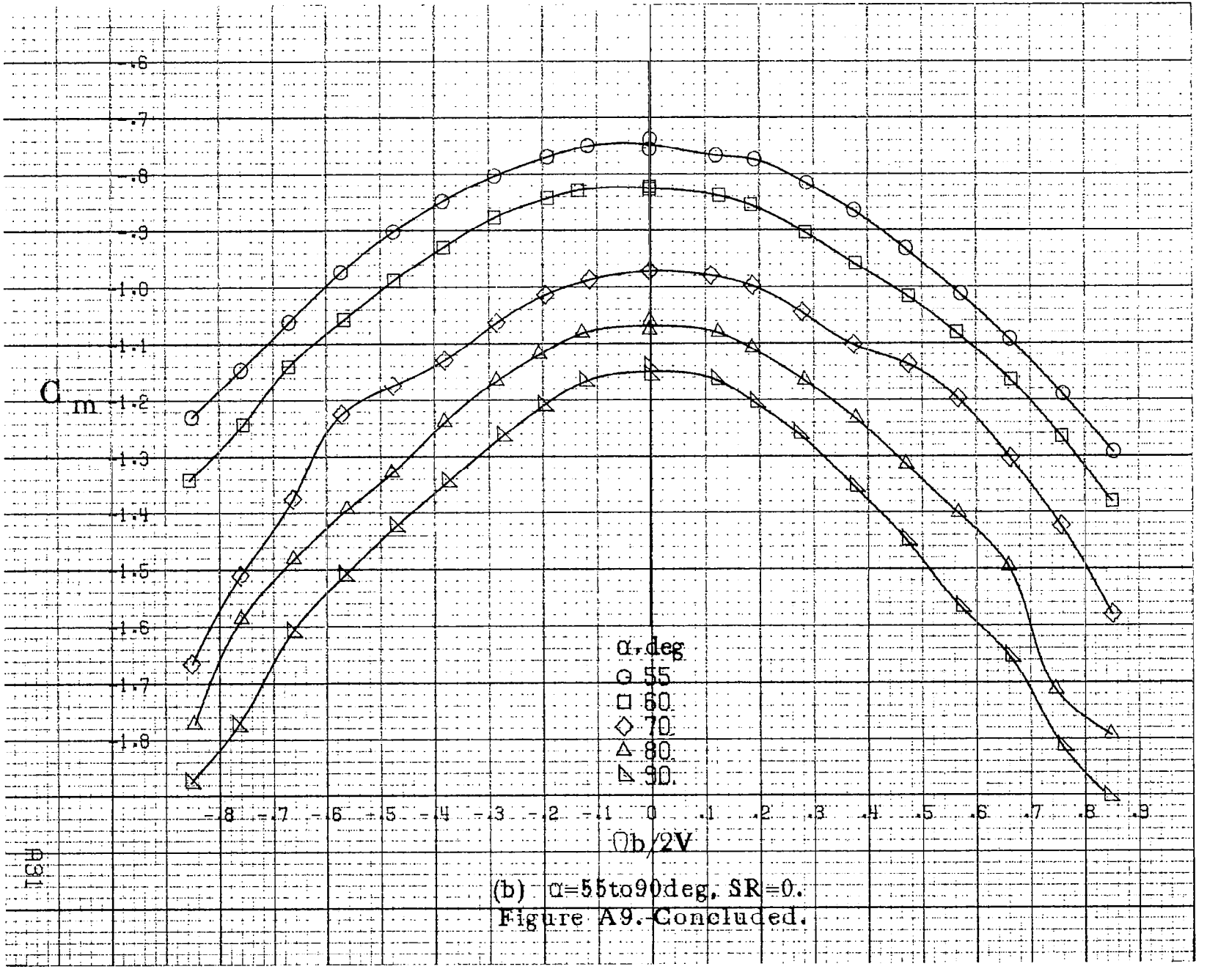

(b) α=55to90deg, SR=0.

Figure A9. Concluded.

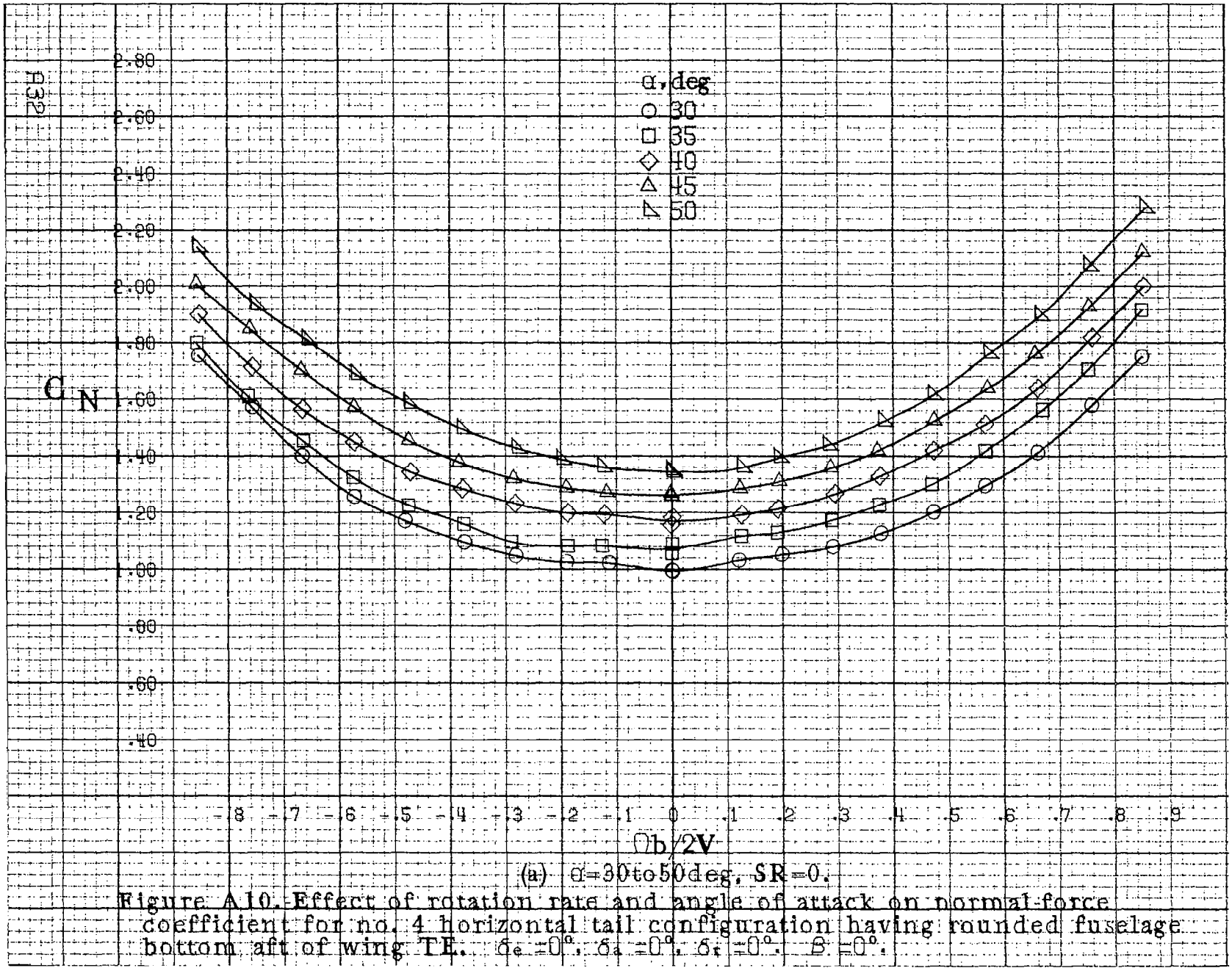

(a) α=30to50deg, SR=0.

Figure A10. Effect of rotation rate and angle of attack on normal-force coefficient for no. 4 horizontal tail configuration having rounded fuselage bottom aft of wing TE. $\delta_e = 0°$, $\delta_a = 0°$, $\delta_r = 0°$, $\beta = 0°$.

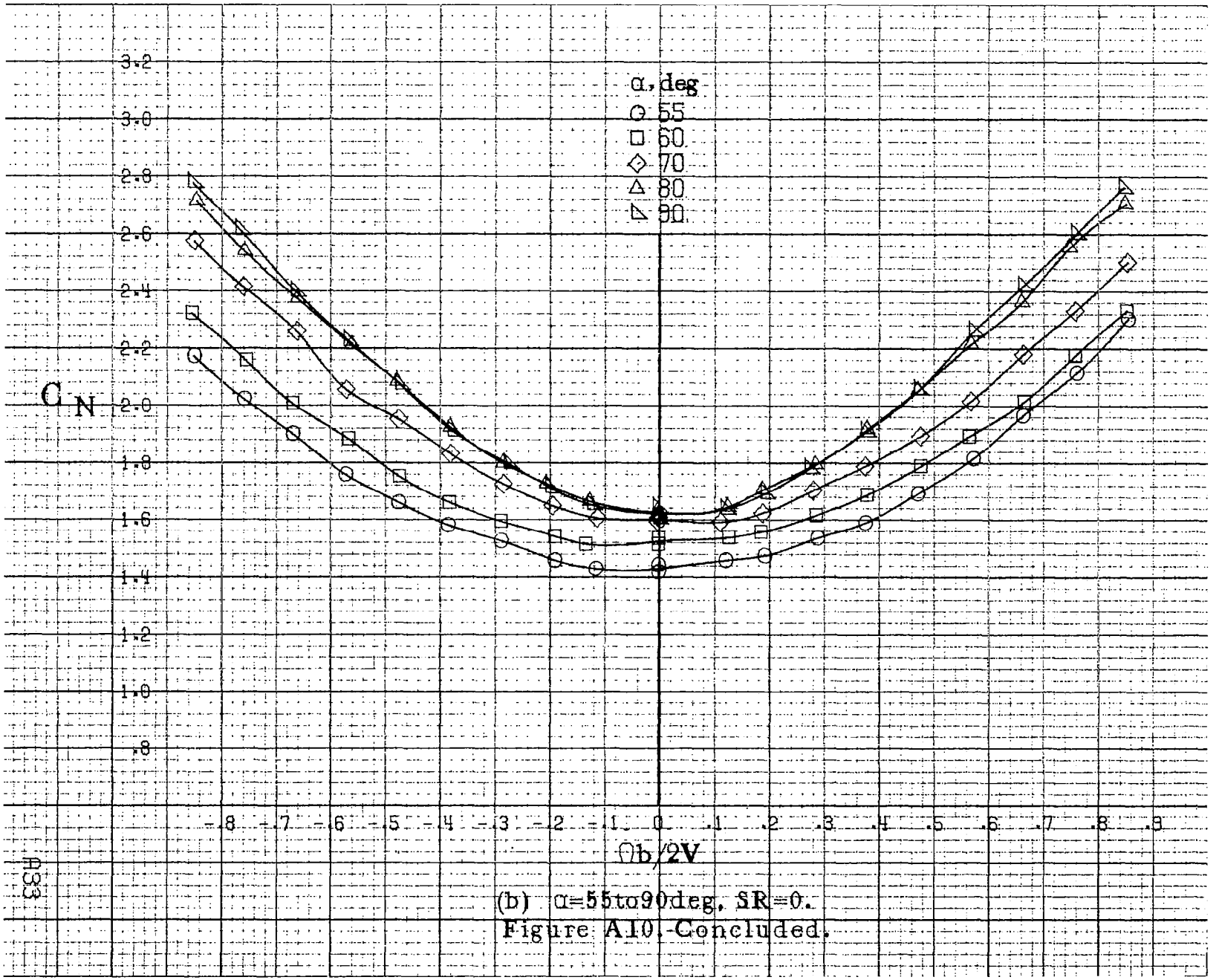

(b) α=55 to 90 deg, SR=0.

Figure A10. Concluded.

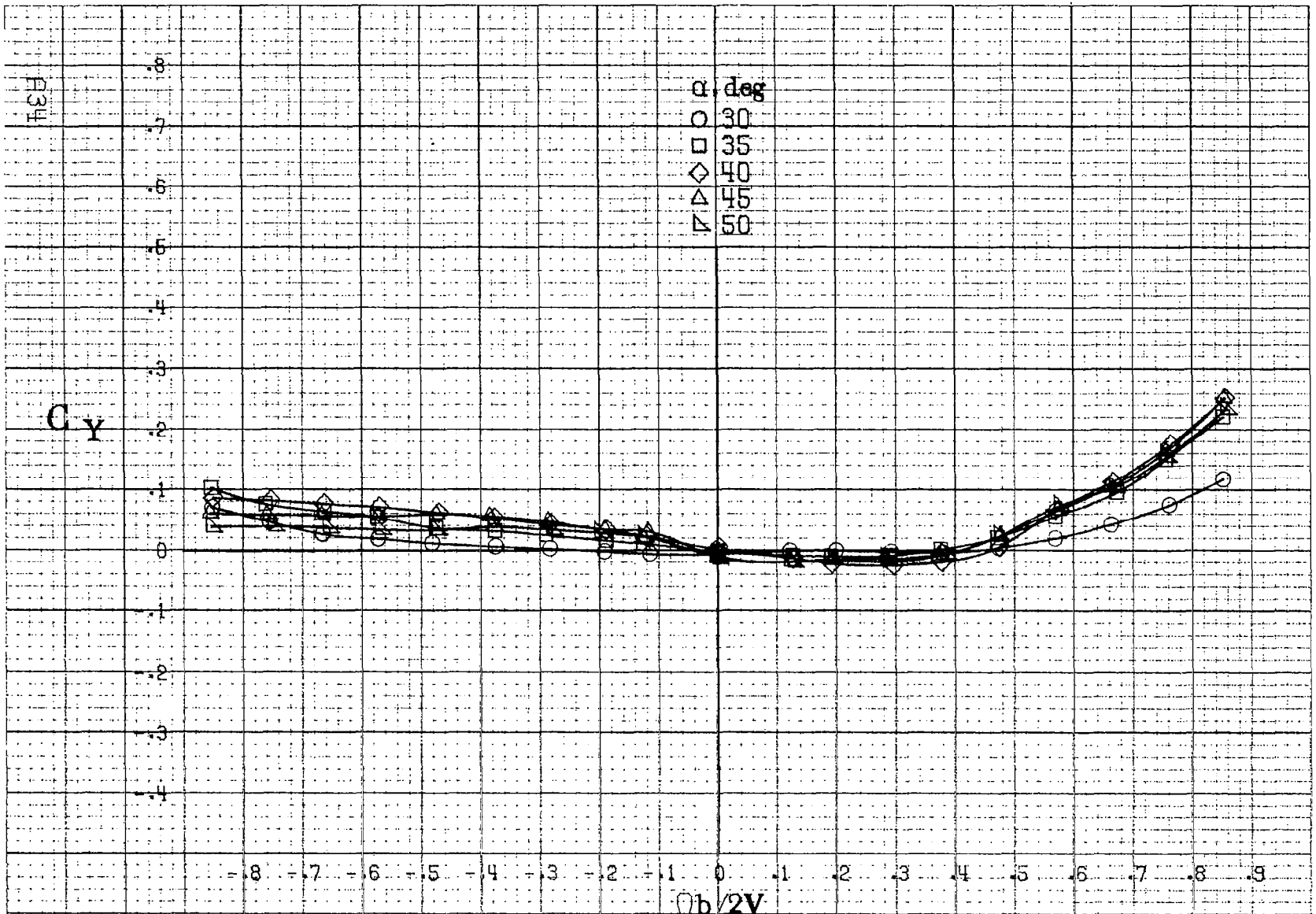

(a) α=30 to 50 deg, SR=0.

Figure A11. Effect of rotation rate and angle of attack on side-force coefficient for no. 4 horizontal tail configuration having rounded fuselage bottom aft of wing TE. $\delta_e = 0°$, $\delta_a = 0°$, $\delta_r = 0°$, $\beta = 0°$.

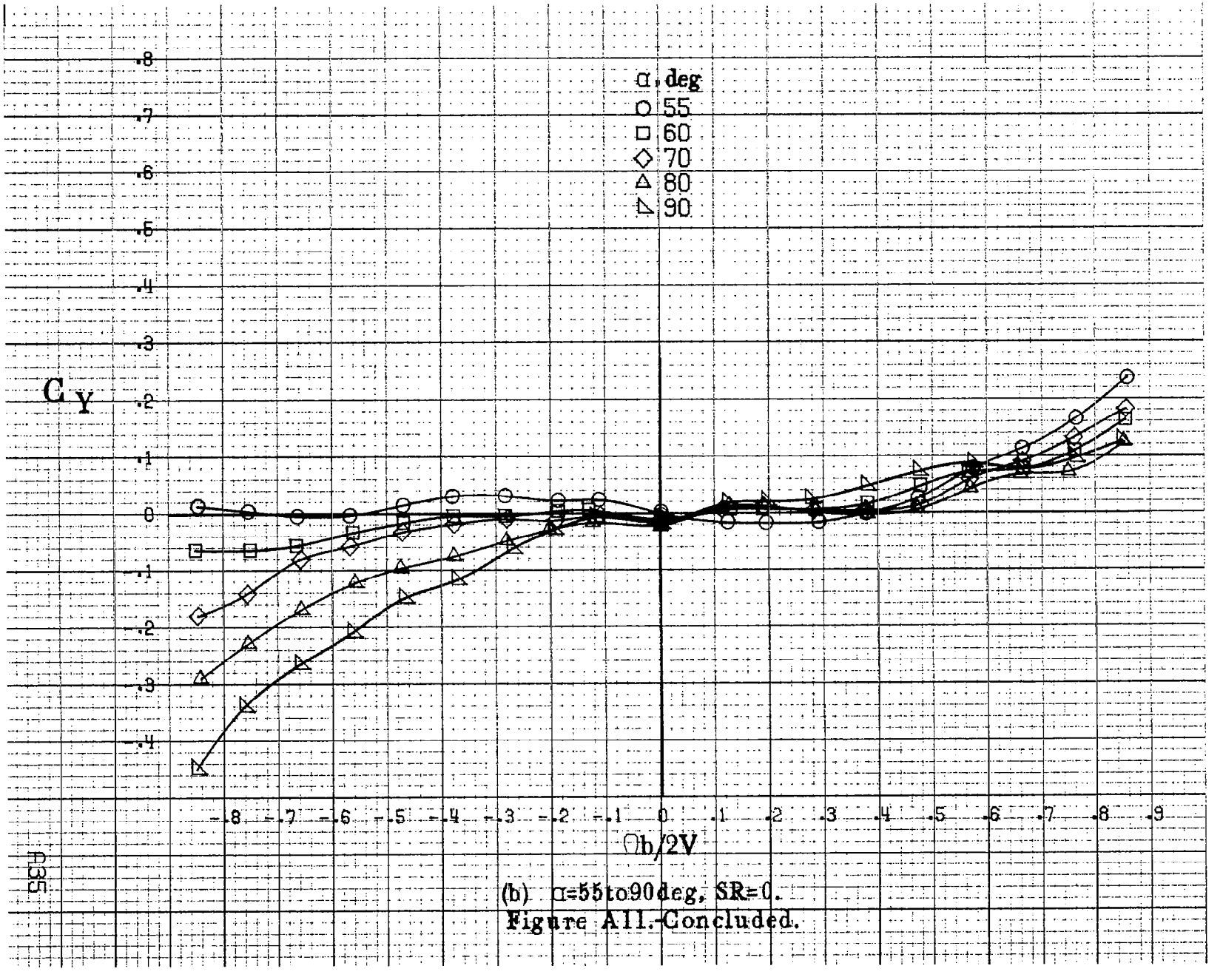

(b) α=55 to 90 deg, SR=0.

Figure A11.-Concluded.

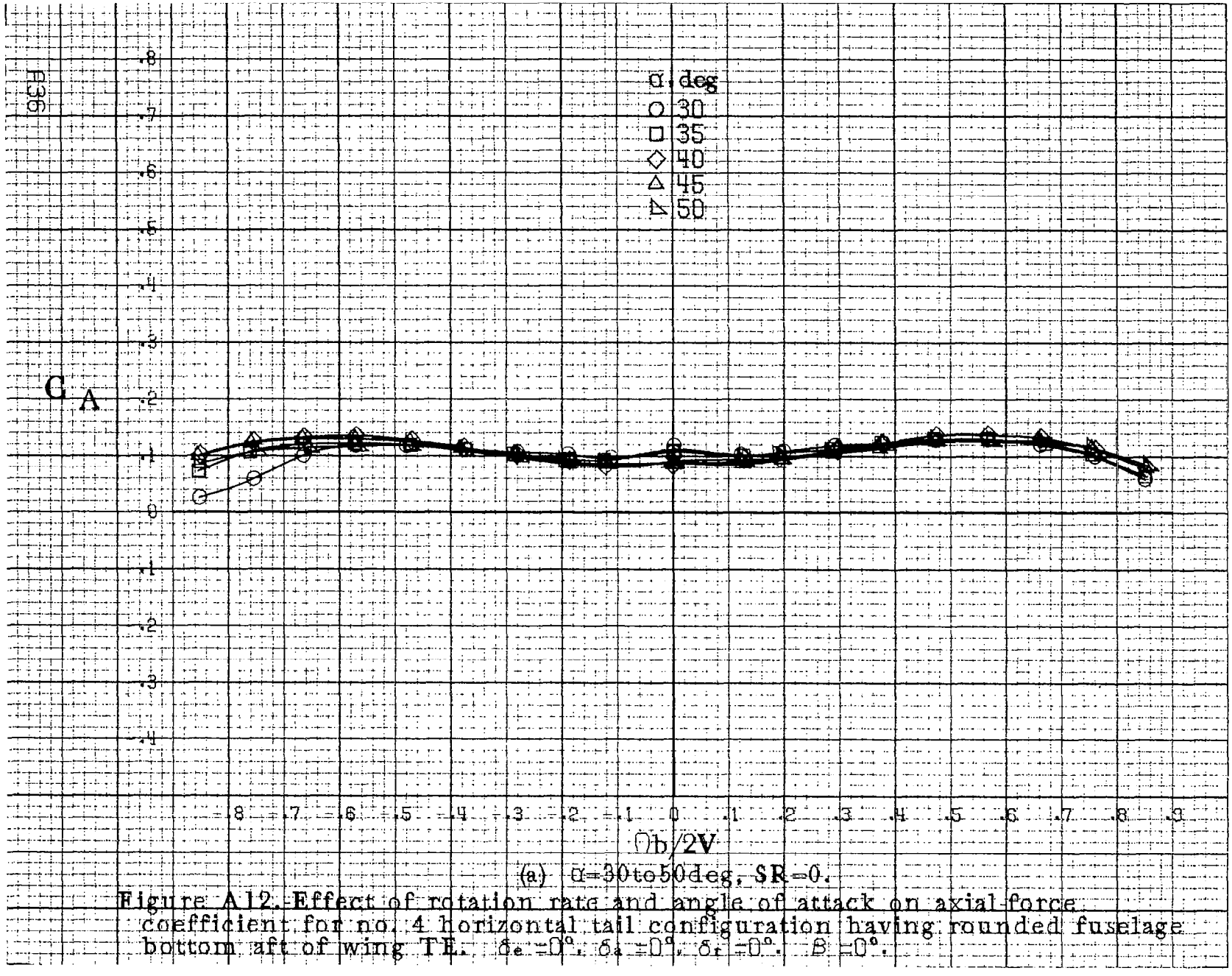

(a) α=30to50deg, SR=0.

Figure A12. Effect of rotation rate and angle of attack on axial force coefficient for no. 4 horizontal tail configuration having rounded fuselage bottom aft of wing TE. $\delta_e = 0°$, $\delta_a = 0°$, $\delta_r = 0°$, $\beta = 0°$.

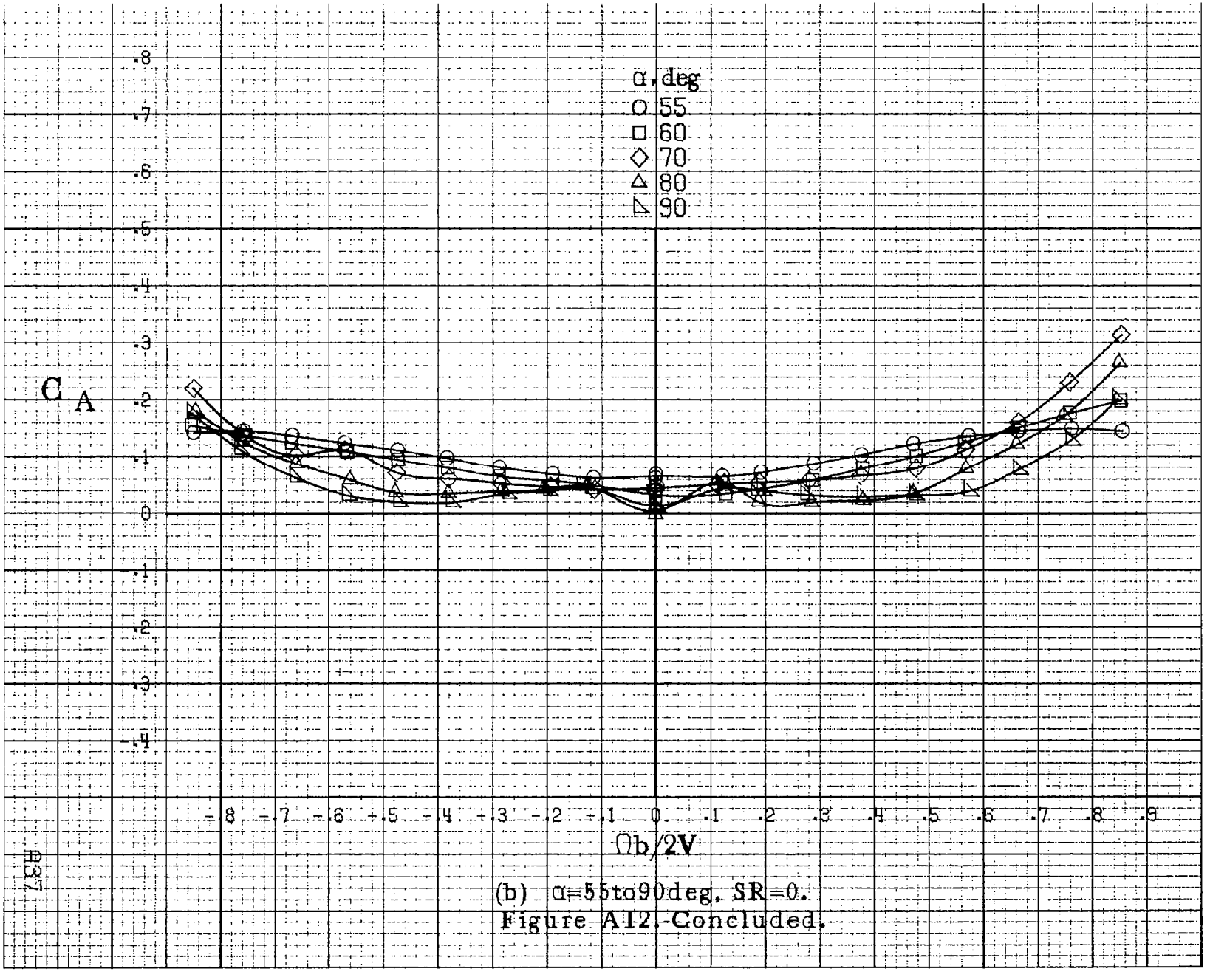

(b) α=55to90deg, SR=0.

Figure A12. Concluded.

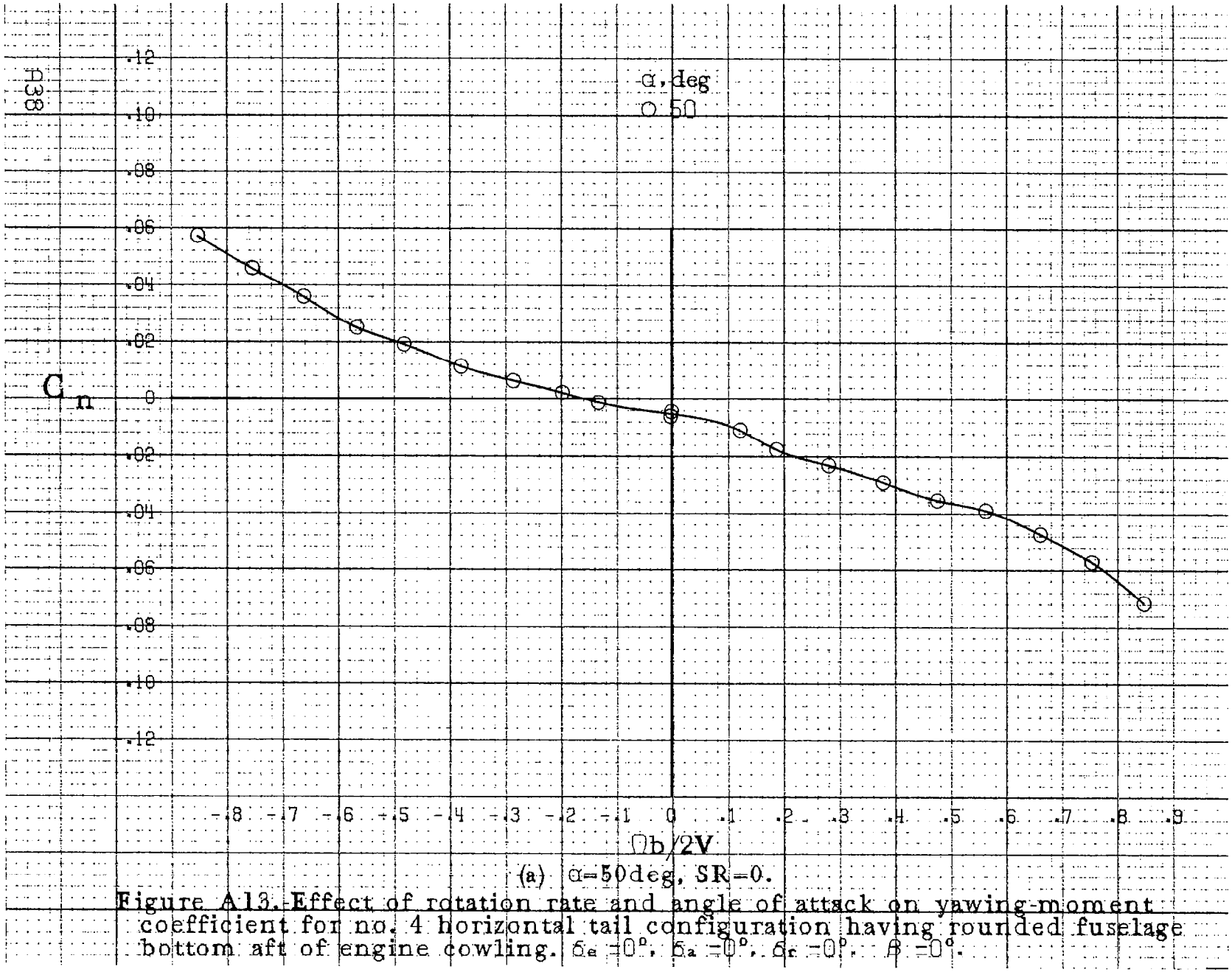

(a) α=50deg, SR=0.

Figure A13.-Effect of rotation rate and angle of attack on yawing-moment coefficient for no. 4 horizontal tail configuration having rounded fuselage bottom aft of engine cowling. $\delta_e = 0°$, $\delta_a = 0°$, $\delta_r = 0°$, $\beta = 0°$.

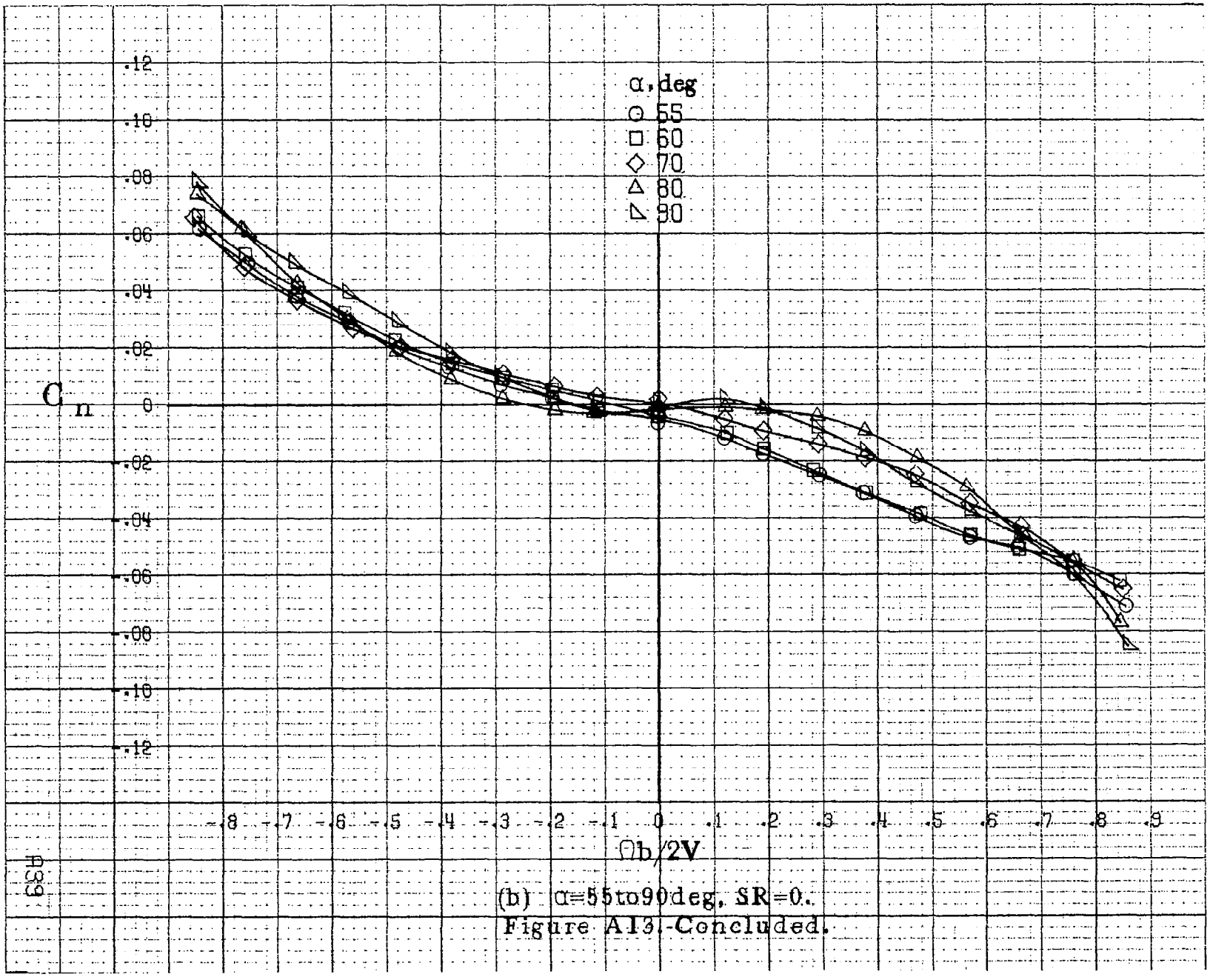

(b) α=55to90deg, SR=0.

Figure A13.-Concluded.

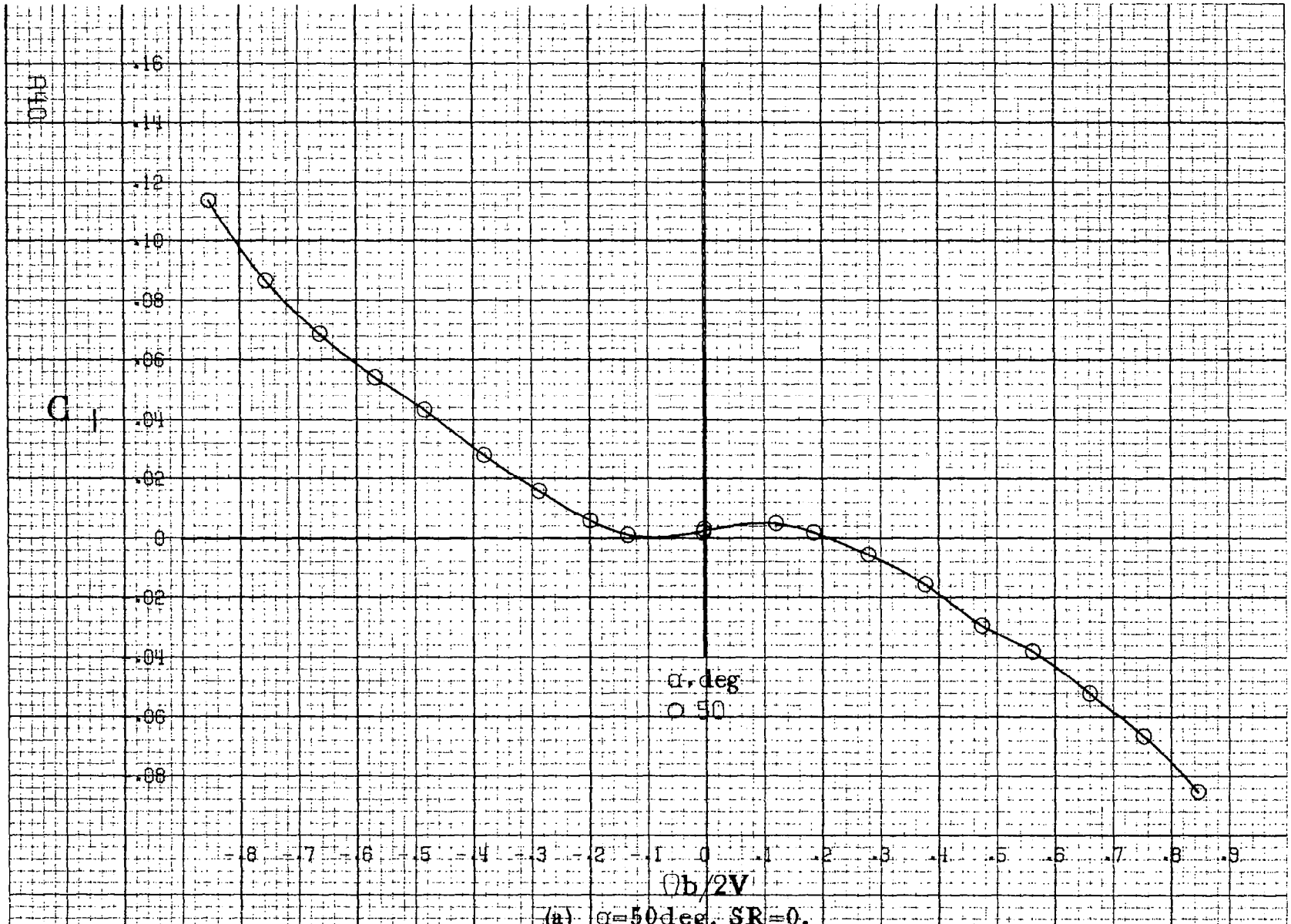

(a) α=50deg, SR=0.

Figure A14. Effect of rotation rate and angle of attack on rolling-moment coefficient for no. 4 horizontal tail configuration having rounded fuselage bottom aft of engine cowling. $\delta_e = 0°$, $\delta_a = 0°$, $\delta_r = 0°$, $\beta = 0°$.

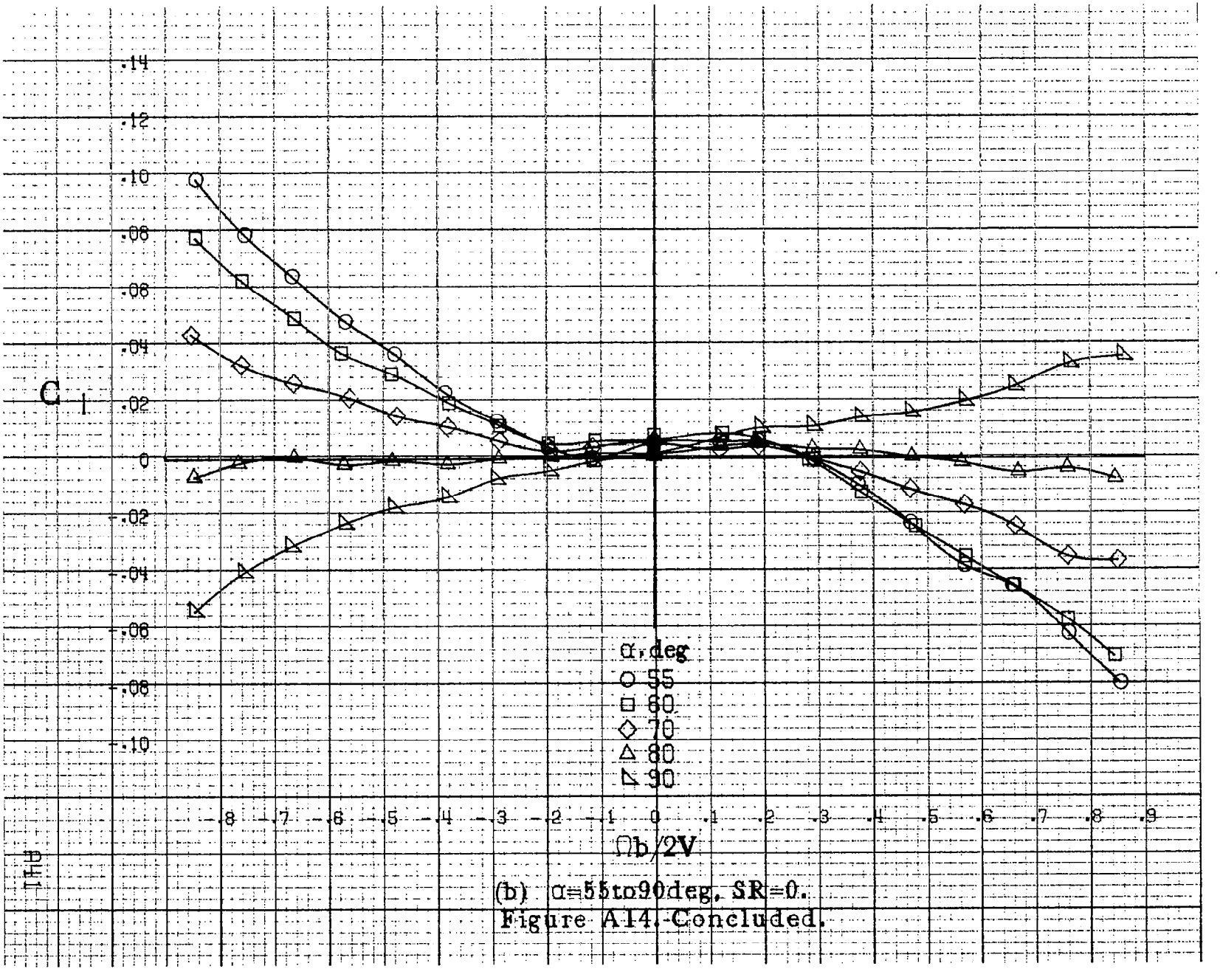

(b) α=55to90deg, SR=0.

Figure A14.-Concluded.

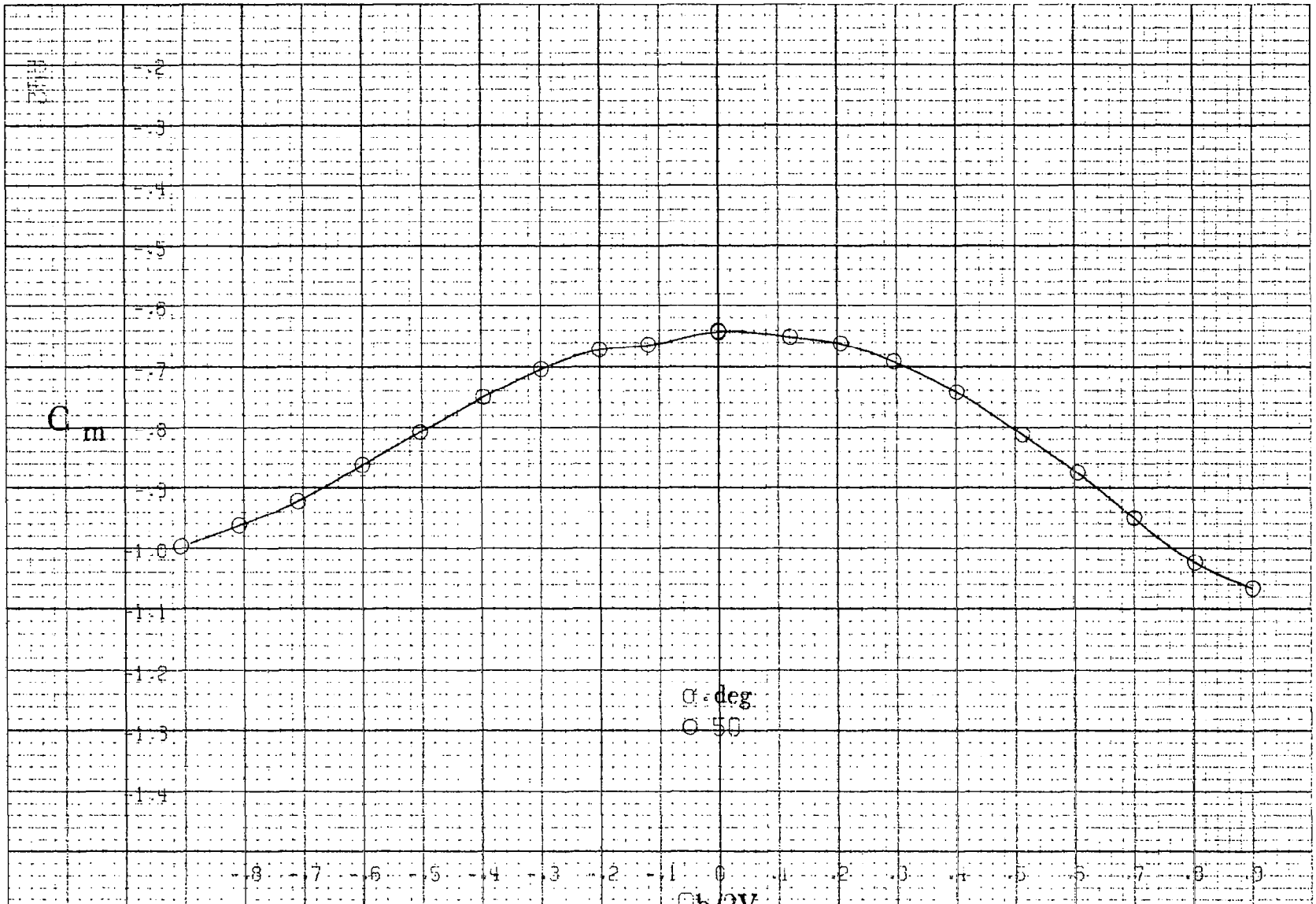

(a) i_t=50deg SR=0.

Figure A15.-Effect of rotation rate and angle of attack on pitching-moment coefficient for no. 4 horizontal tail configuration having rounded fuselage bottom aft of engine cowling. δ_e=0°, δ_a=0°, δ_r=0°, β=0°.

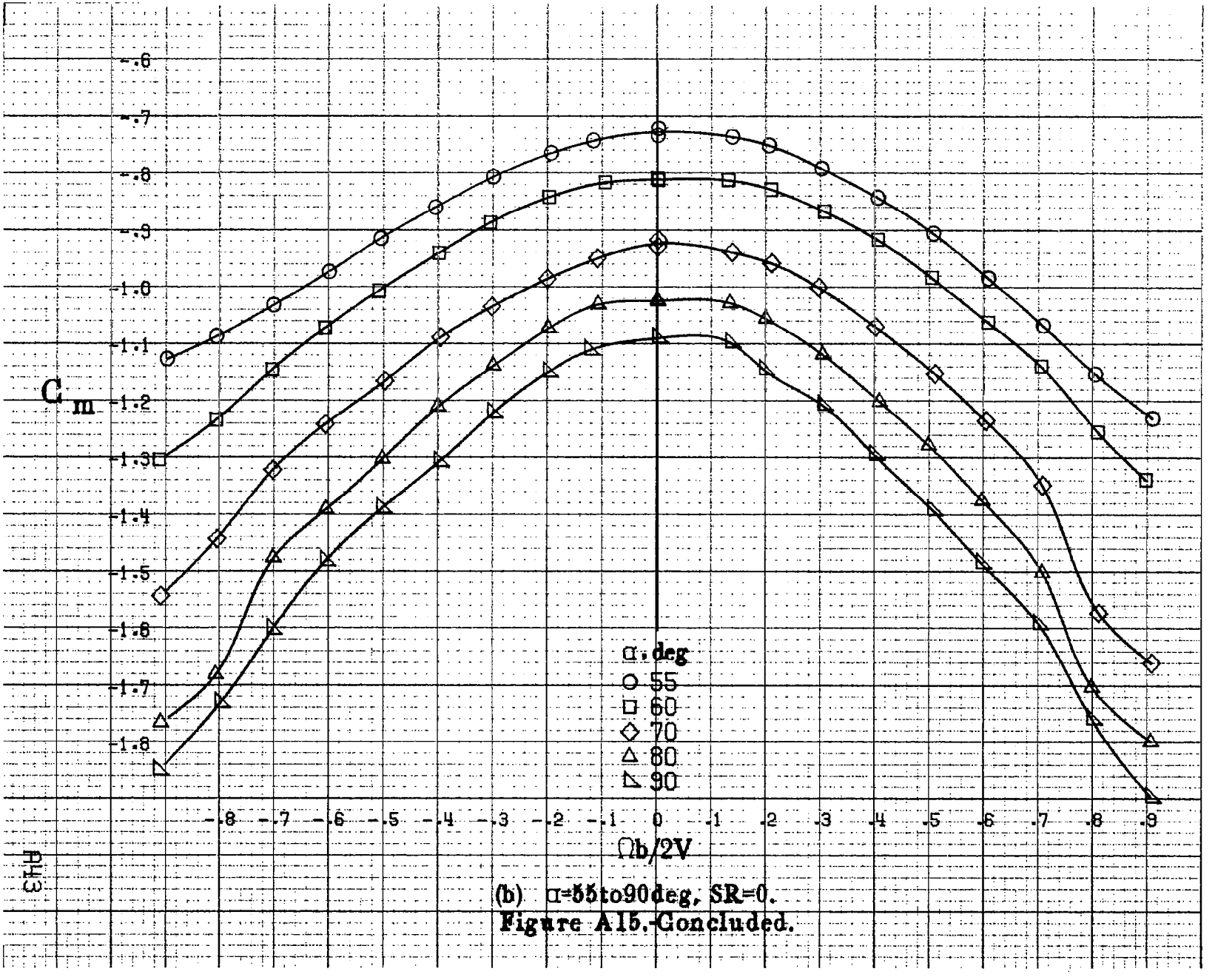

(b) α=55to90deg, SR=0.

Figure A15.-Concluded.

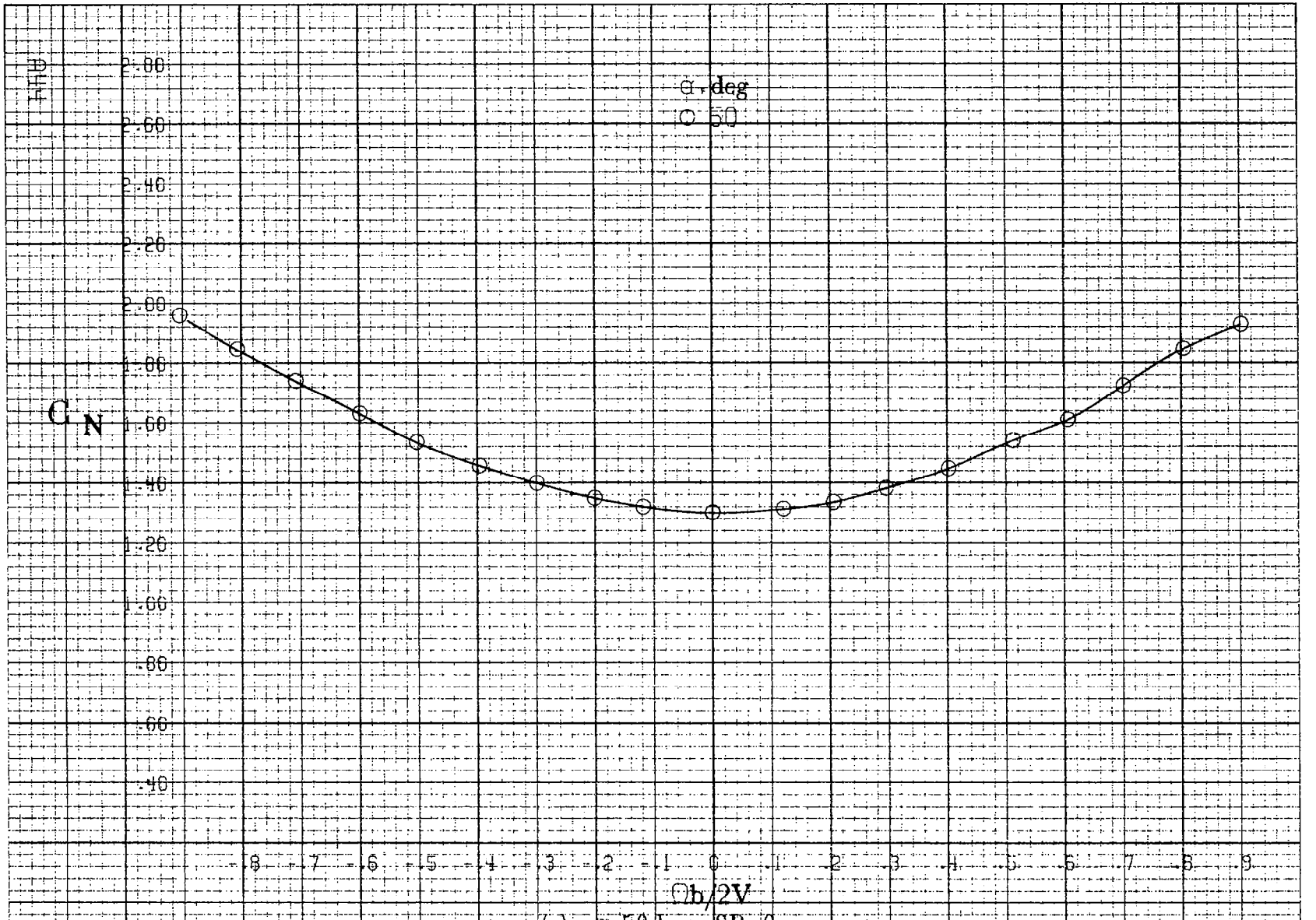

(a) α=50deg, SR=0.

Figure A16. Effect of rotation rate and angle of attack on normal-force coefficient for no. 4 horizontal tail configuration having rounded fuselage bottom aft of engine cowling. $\delta_e = 0°$, $\delta_a = 0°$, $\delta_r = 0°$, $\beta = 0°$.

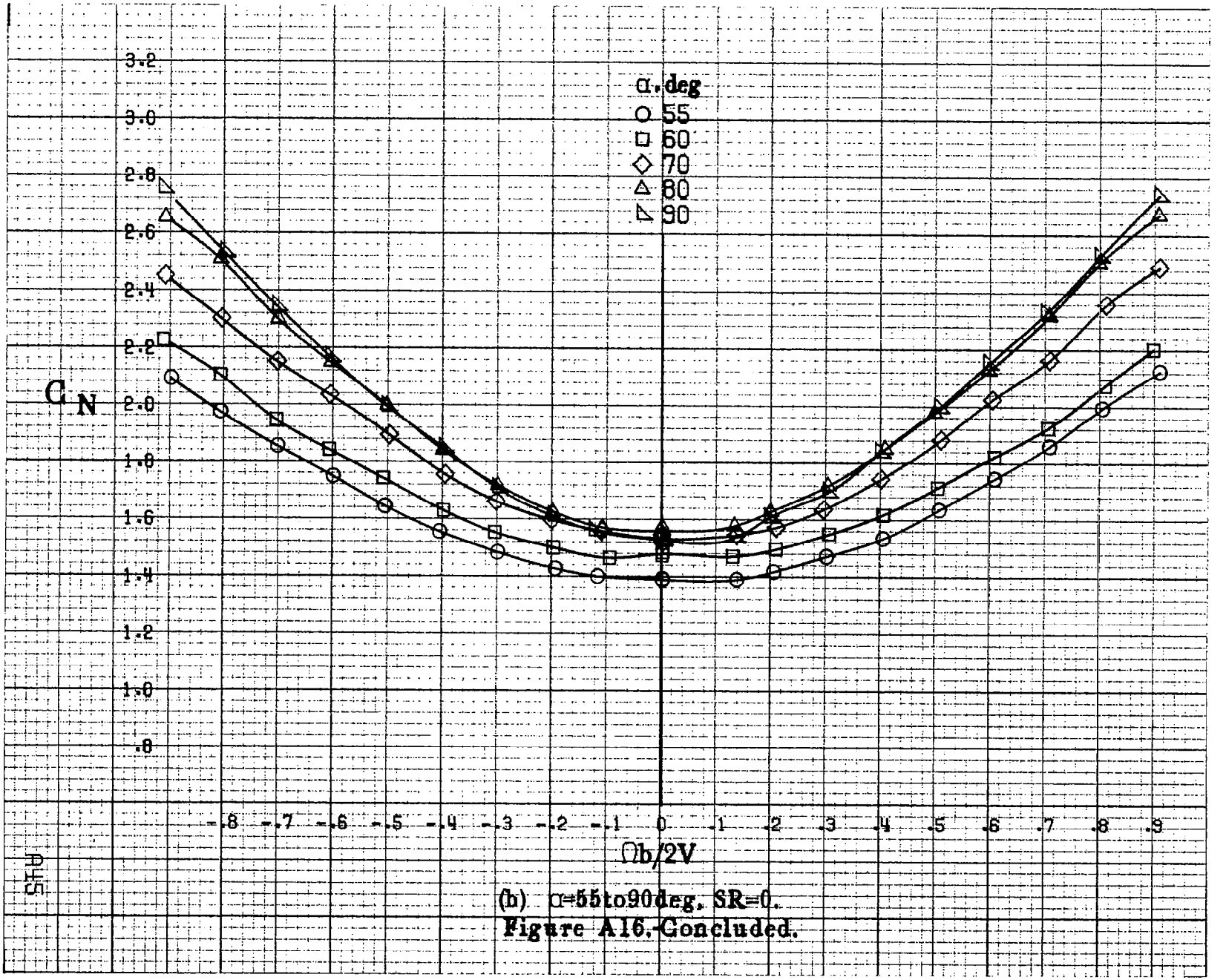

(b) α=55to90deg, SR=0.

Figure A16.-Concluded.

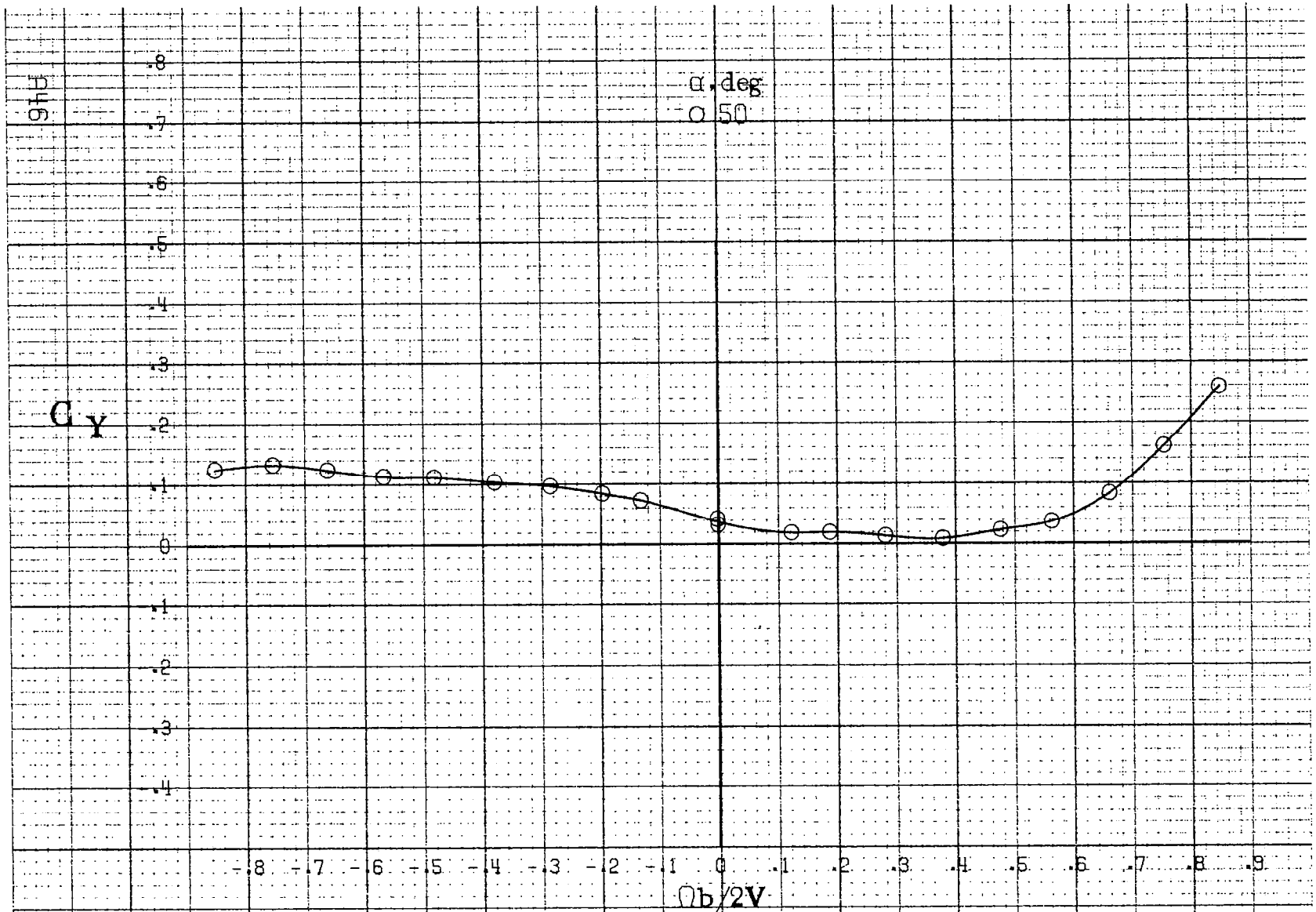

(a) α=50deg, SR=0.

Figure A17. Effect of rotation rate and angle of attack on side-force coefficient for no. 4 horizontal tail configuration having rounded fuselage bottom aft of engine cowling. $\delta_e = 0°$, $\delta_a = 0°$, $\delta_r = 0°$, $\beta = 0°$.

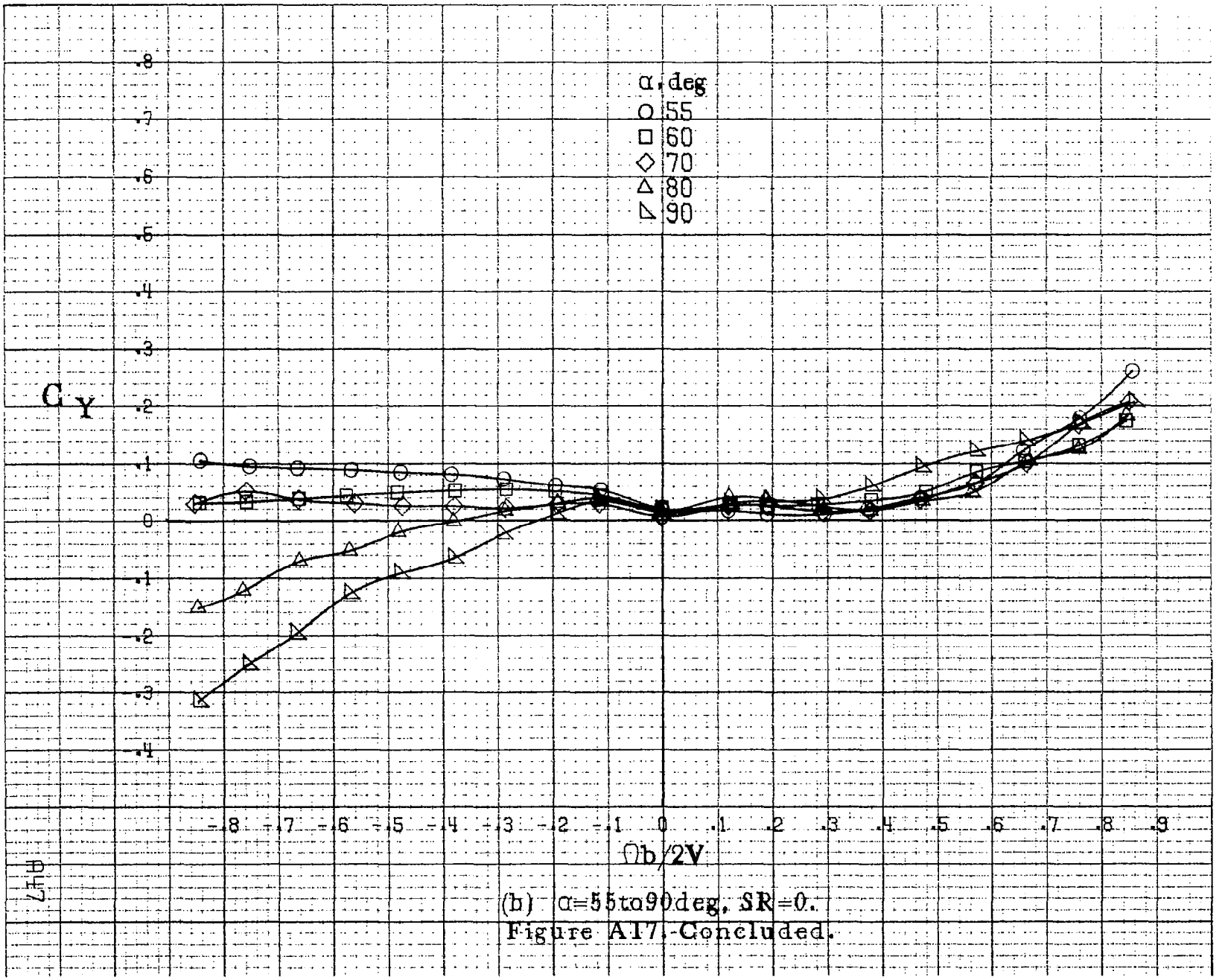

(b) α=55to90deg, SR=0.

Figure A17.-Concluded.

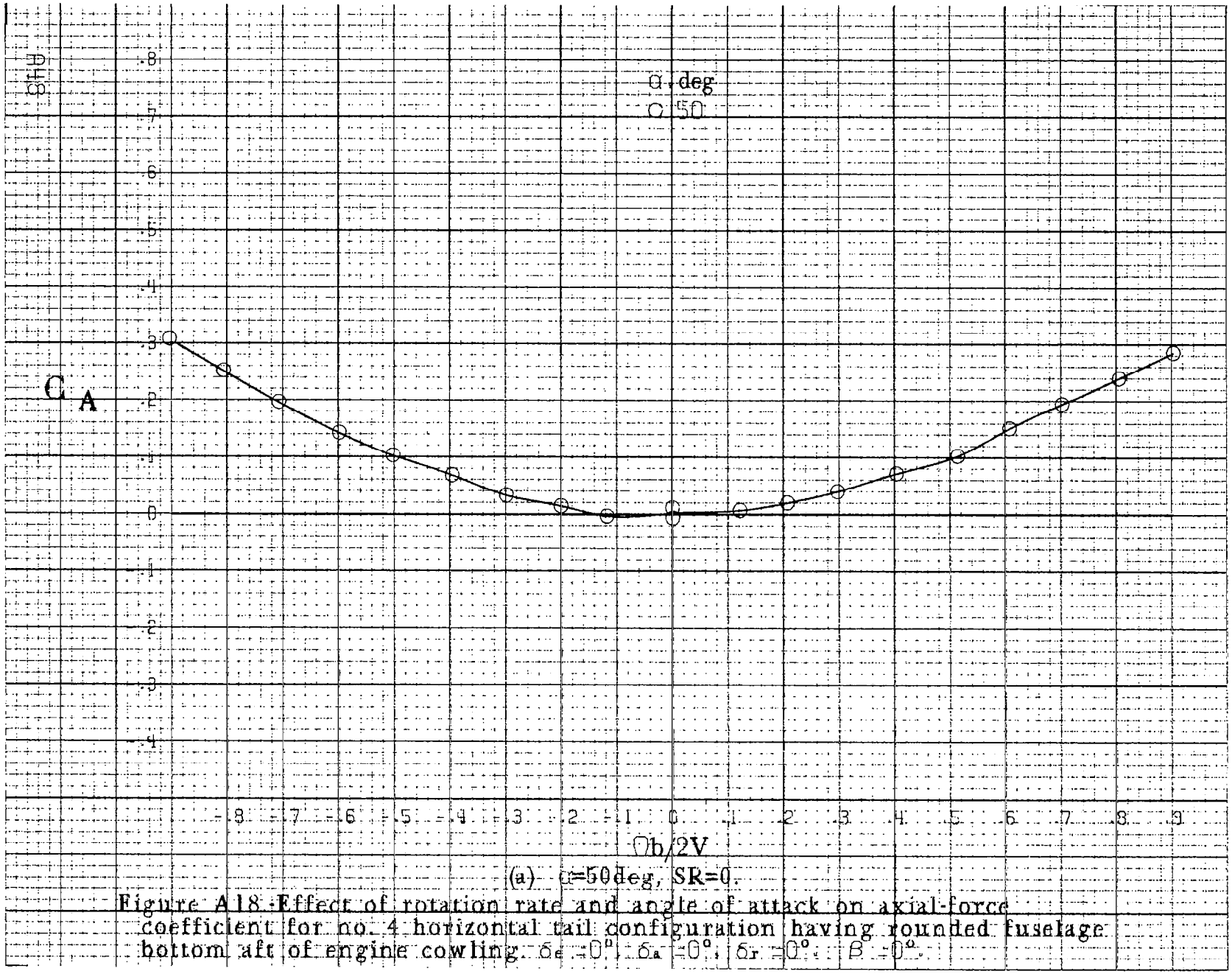

(a) α=50deg, SR=0.

Figure A18.-Effect of rotation rate and angle of attack on axial-force coefficient for no. 4 horizontal tail configuration having rounded fuselage bottom aft of engine cowling. δ_e =0°, δ_a =0°, δ_r =0°, β =0°.

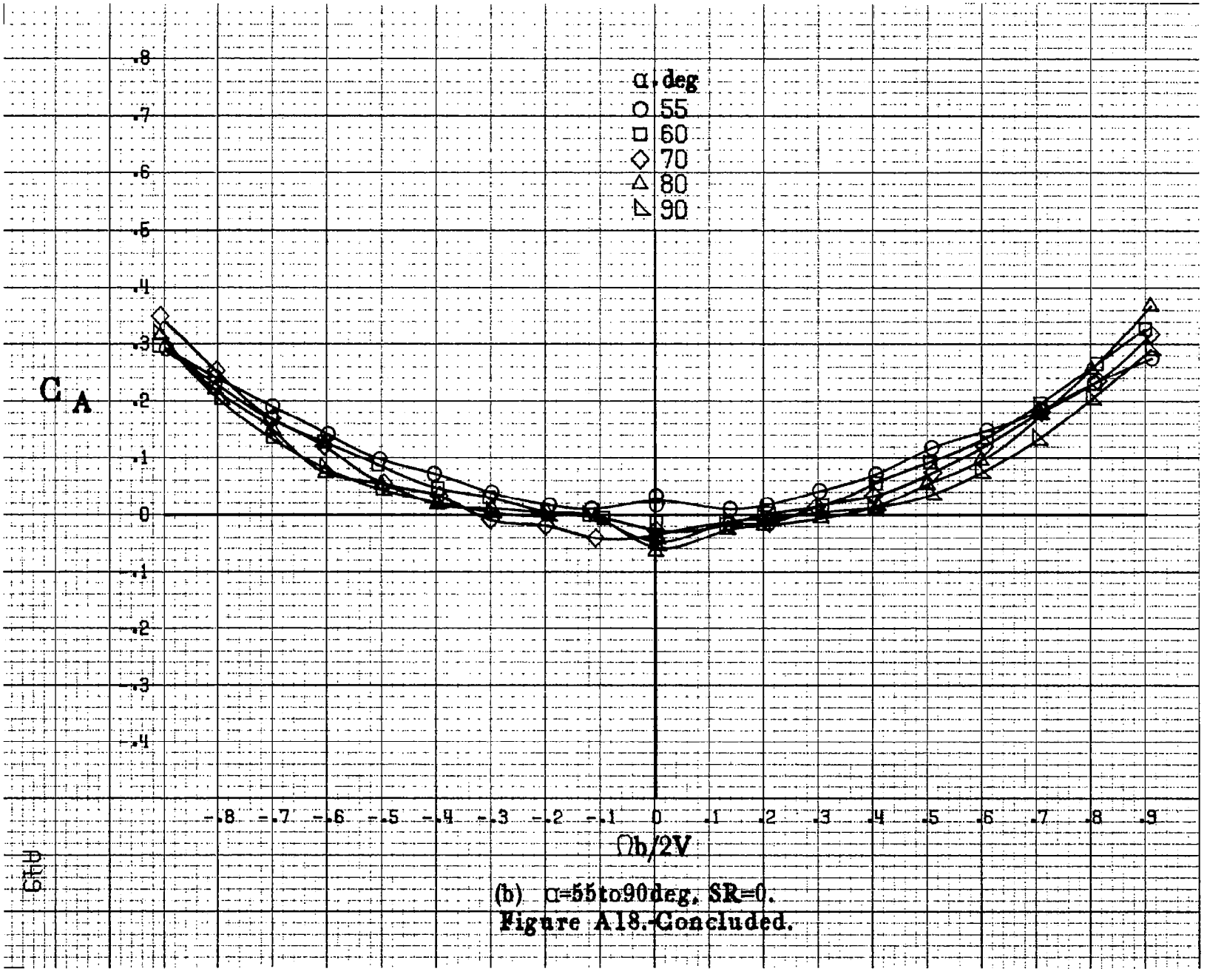

(b) α=55 to 90 deg, SR=0.

Figure A18.-Concluded.

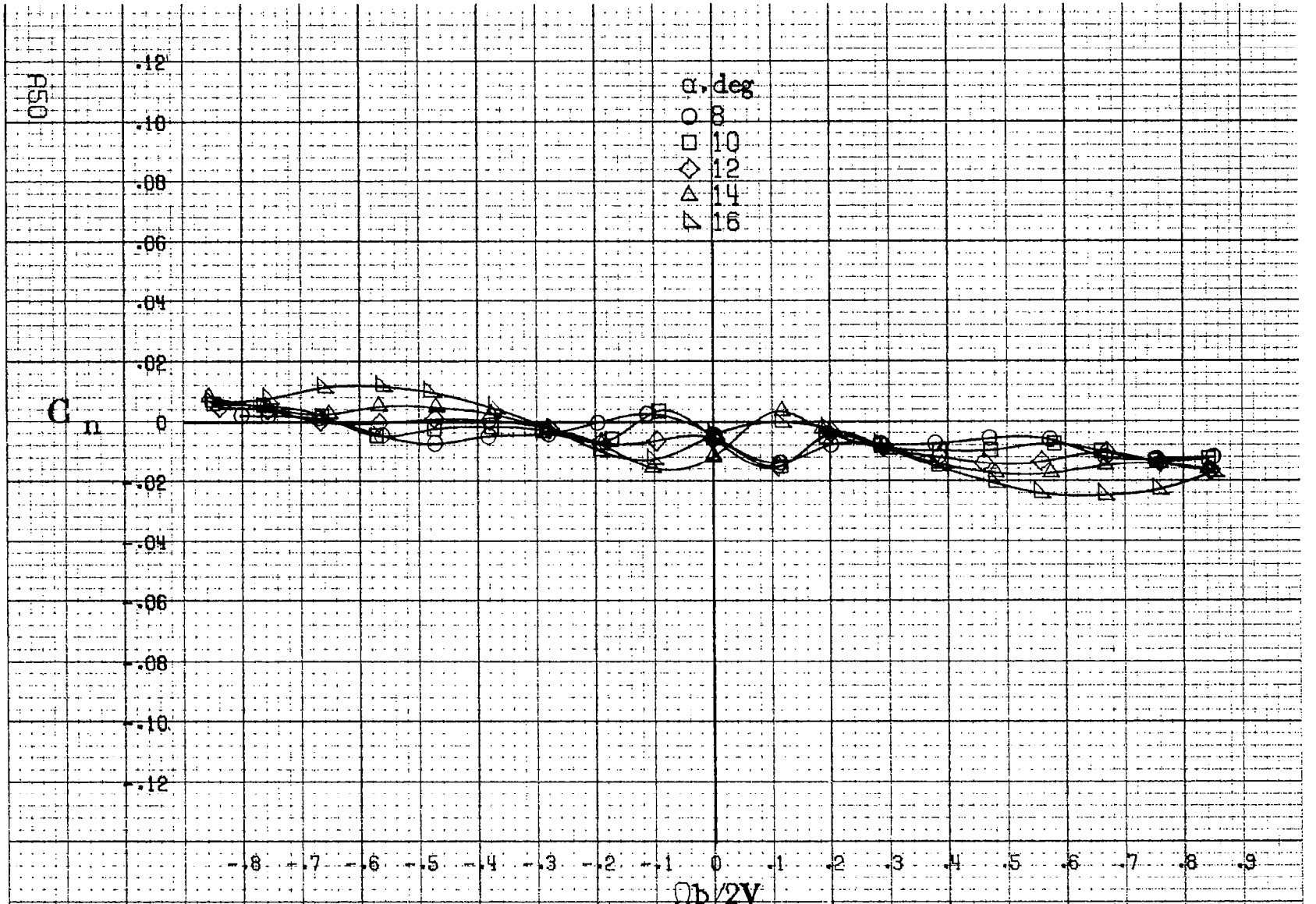

(a) α=8to16deg, SR=76cm(30in).

Figure A19.-Effect of rotation rate and angle of attack on yawing-moment coefficient for no. 3 horizontal tail configuration. δ_e =0°, δ_a =0°, δ_r =0°, β =0°.

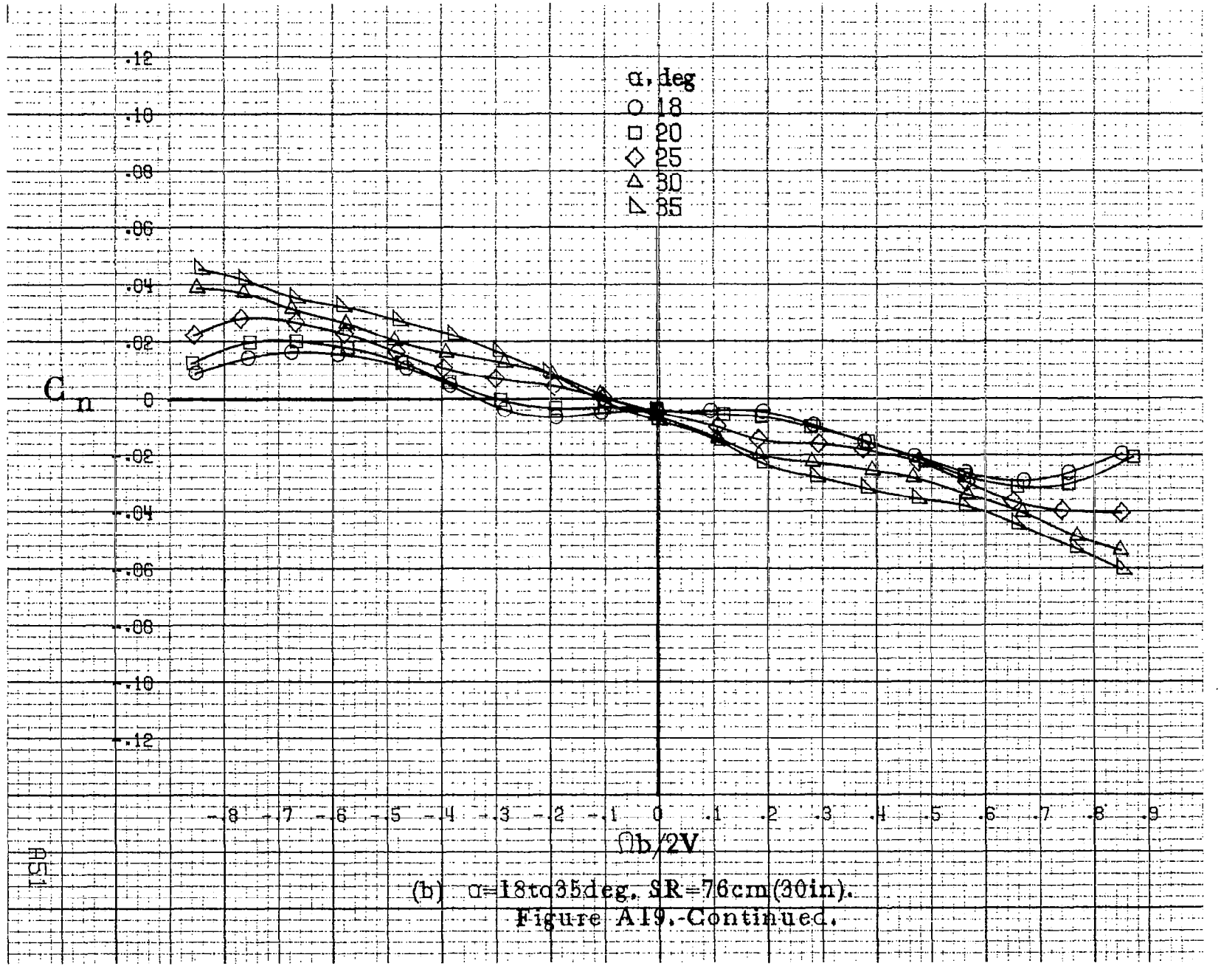

(b) α=18to35deg, SR=76cm(30in).

Figure A19.-Continued.

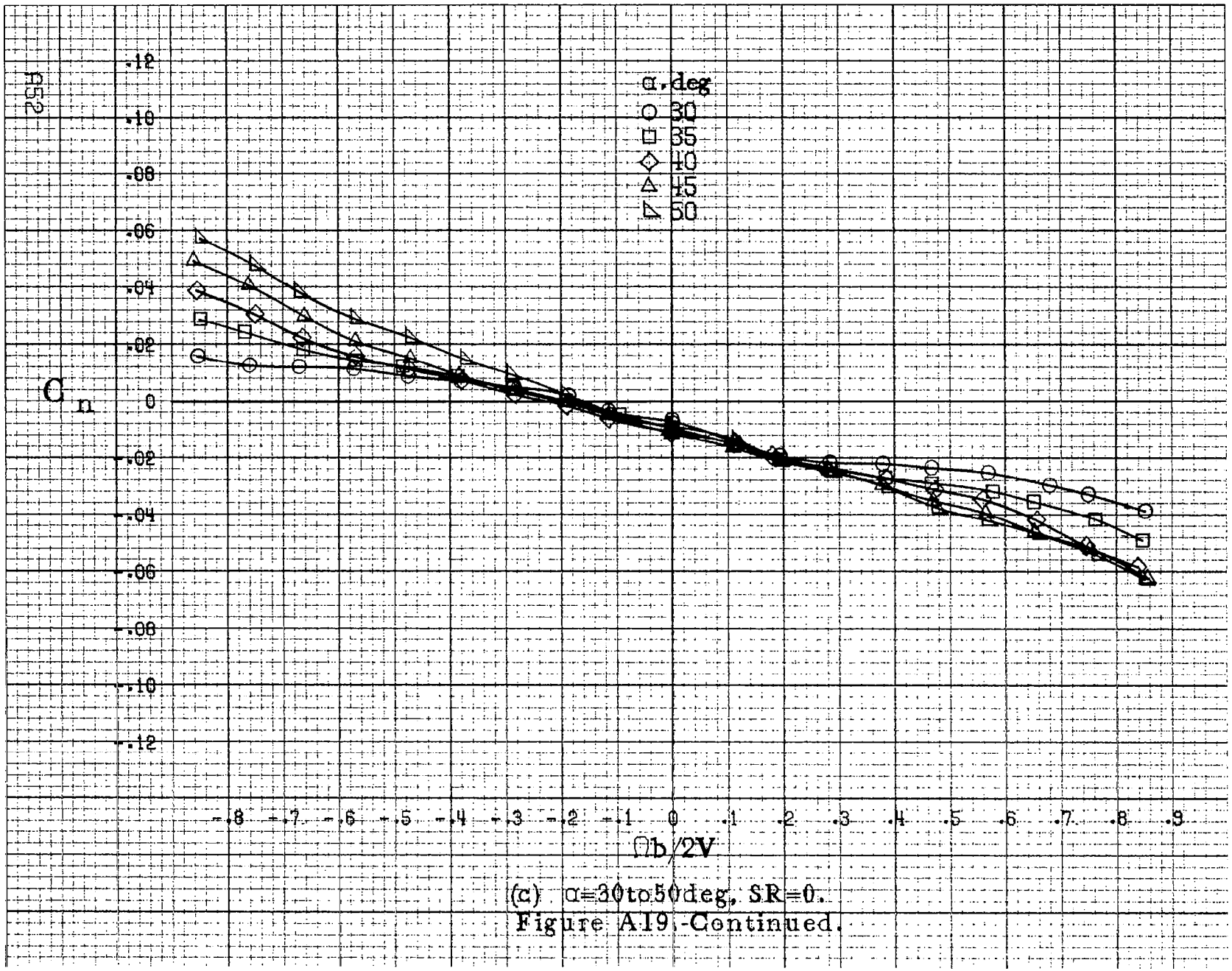

(c) α=30to50deg, SR=0.

Figure A19.-Continued.

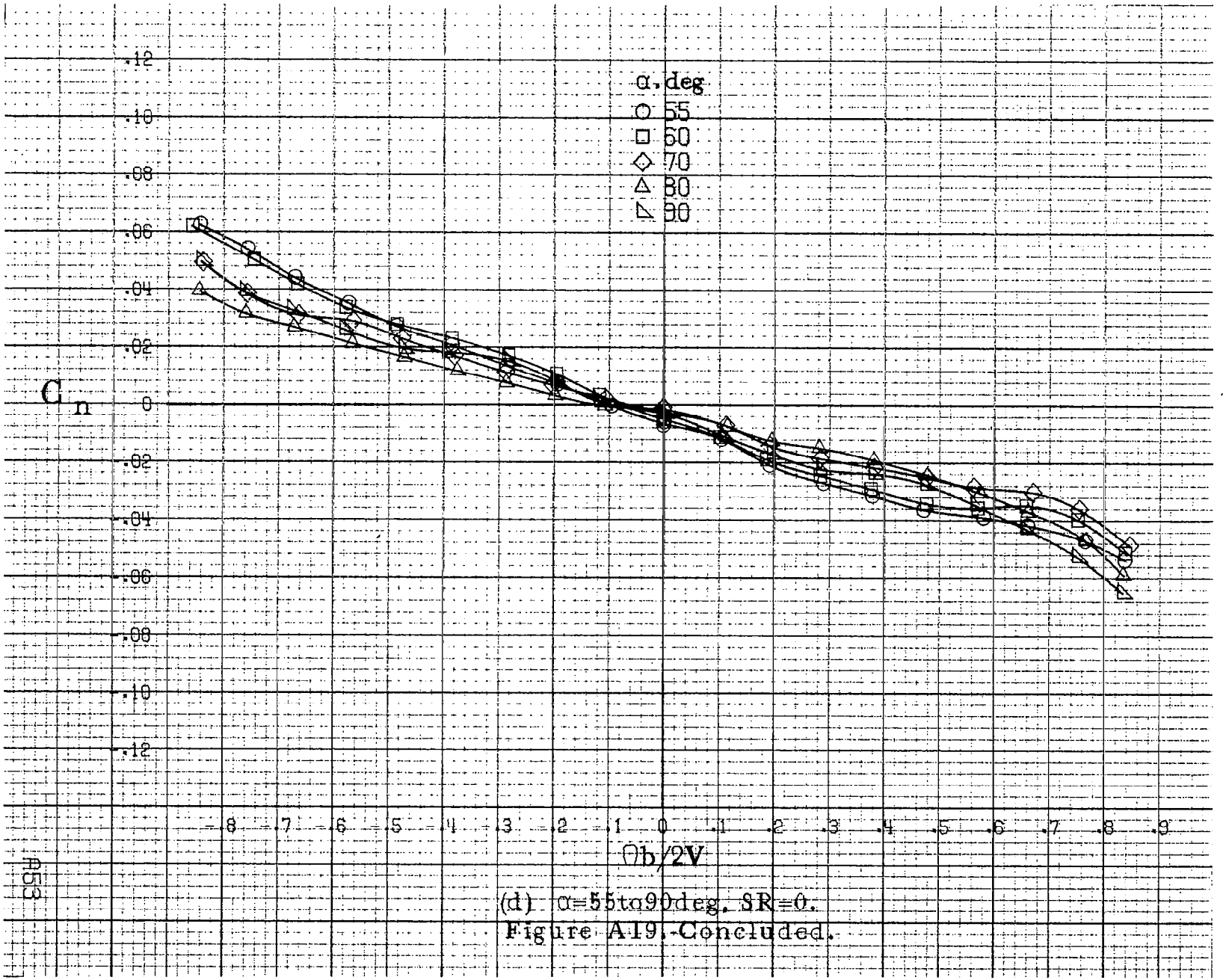

(d) α=55 to 90 deg. SR=0.

Figure A19.-Concluded.

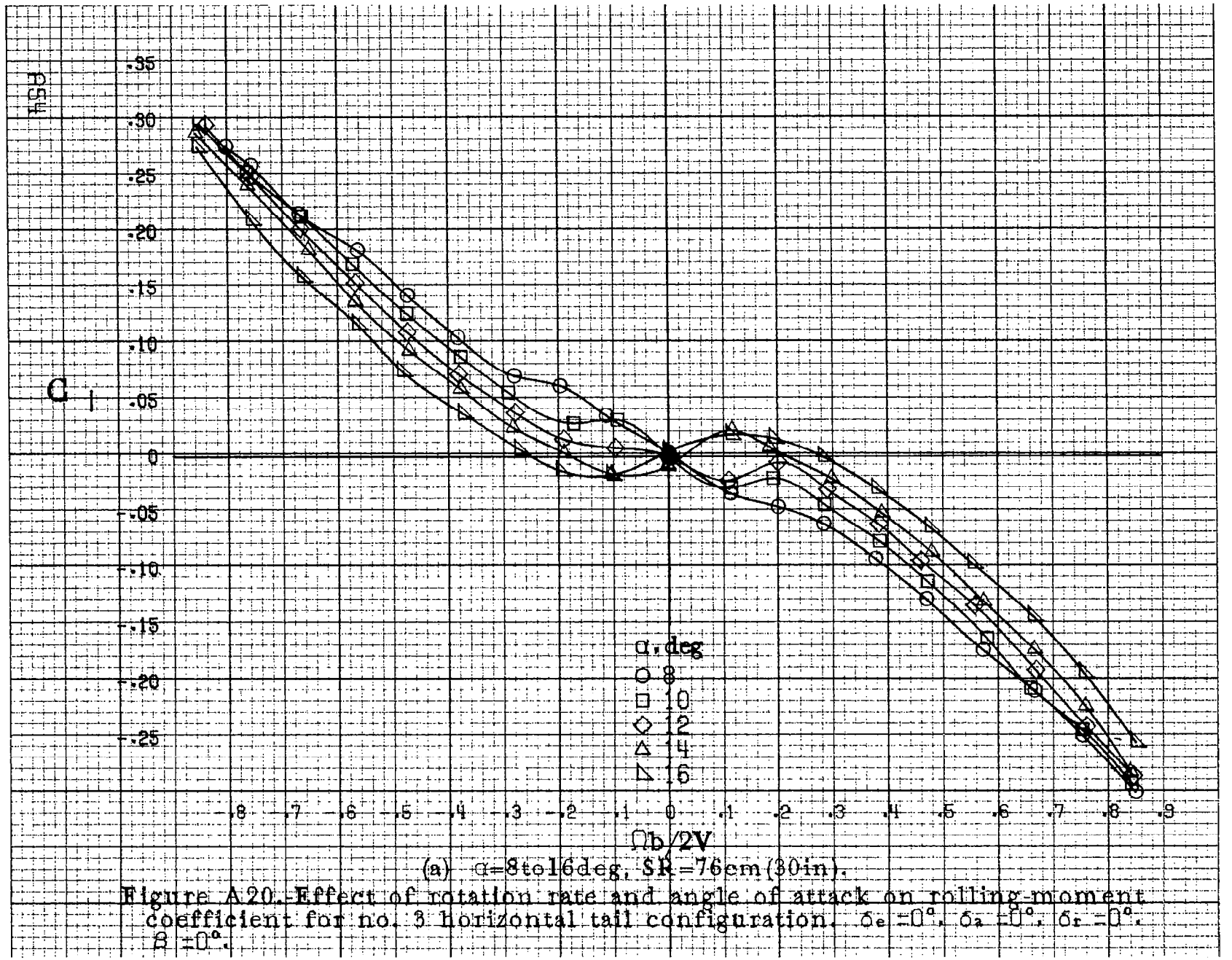

(a) α=8to16deg, S_R=76cm(30in).

Figure A20.-Effect of rotation rate and angle of attack on rolling-moment coefficient for no. 3 horizontal tail configuration. δ_e =0°, δ_a =0°, δ_r =0°, β =0°.

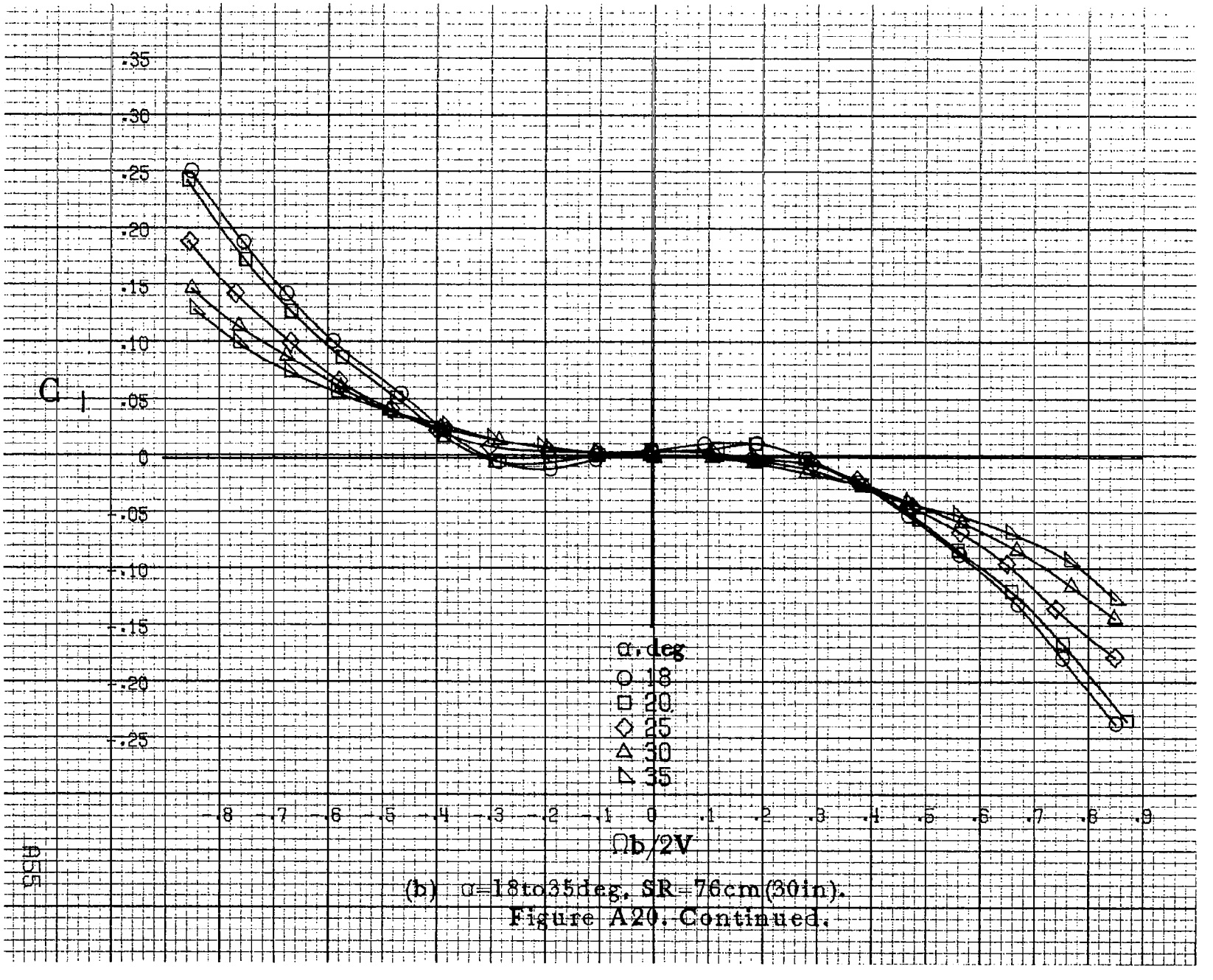

(b) α=18to35deg, SR=76cm(30in).

Figure A20. Continued.

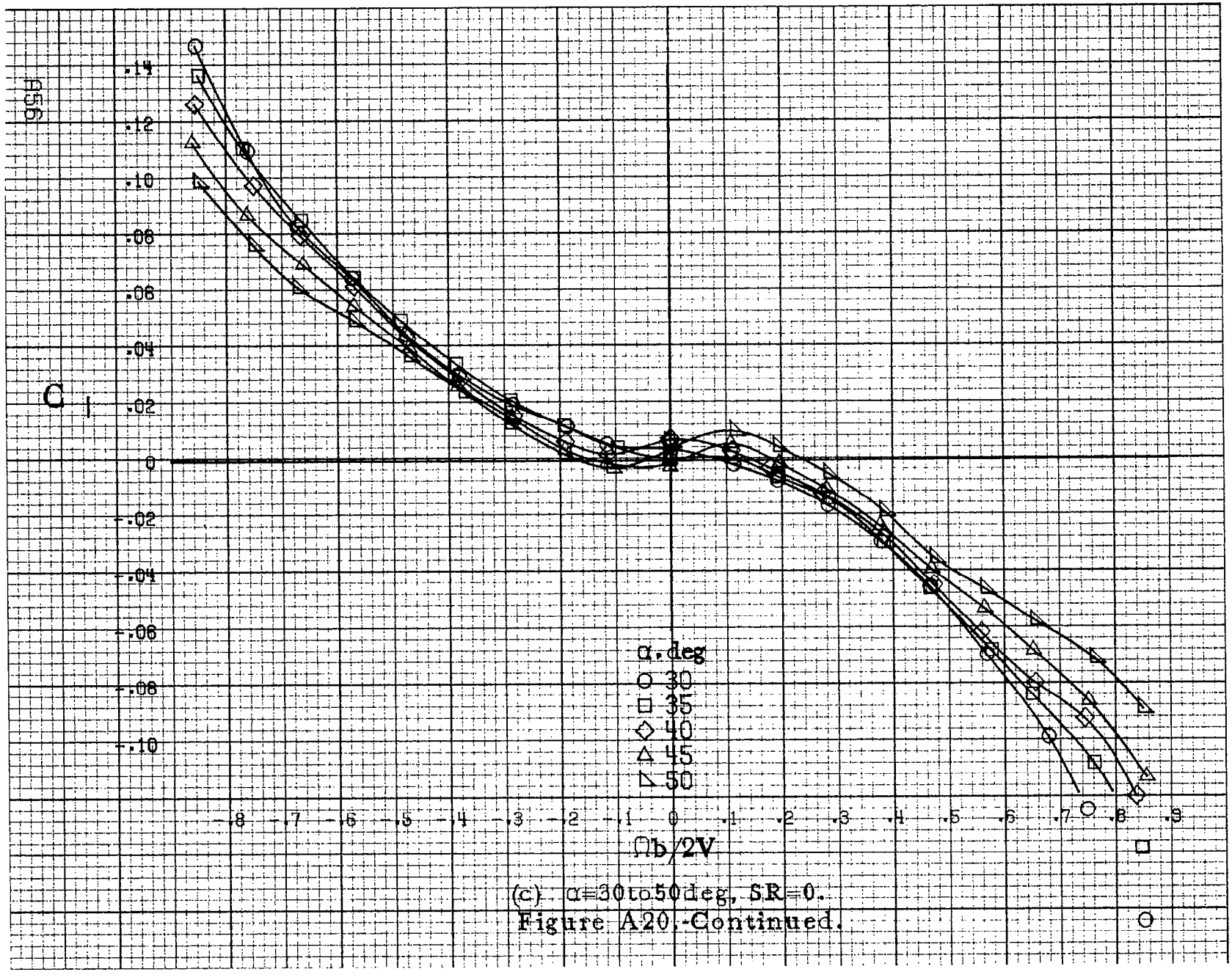

(c) α=30 to 50 deg, SR=0.

Figure A20.-Continued.

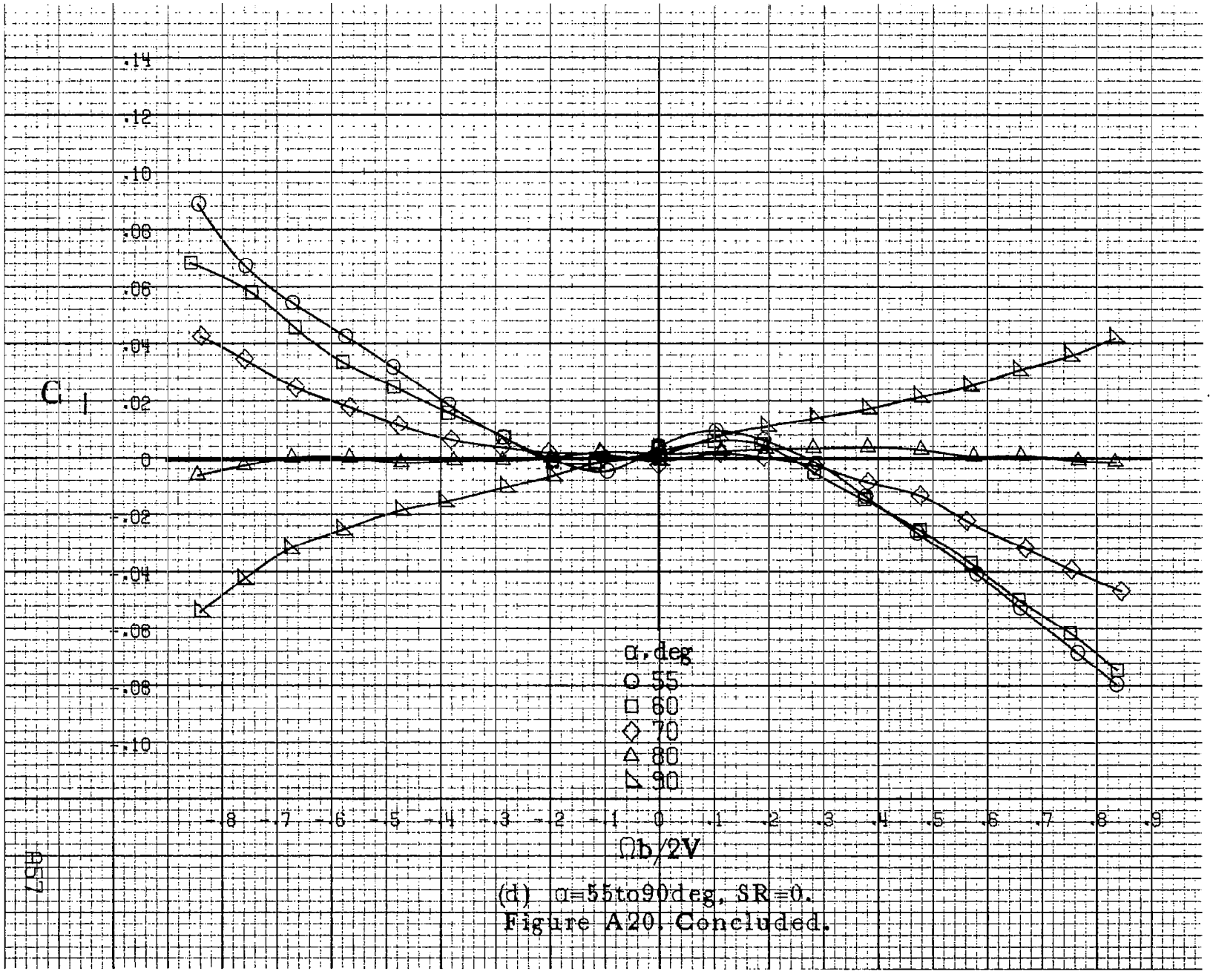

(d) α=55to90deg, SR=0.

Figure A20. Concluded.

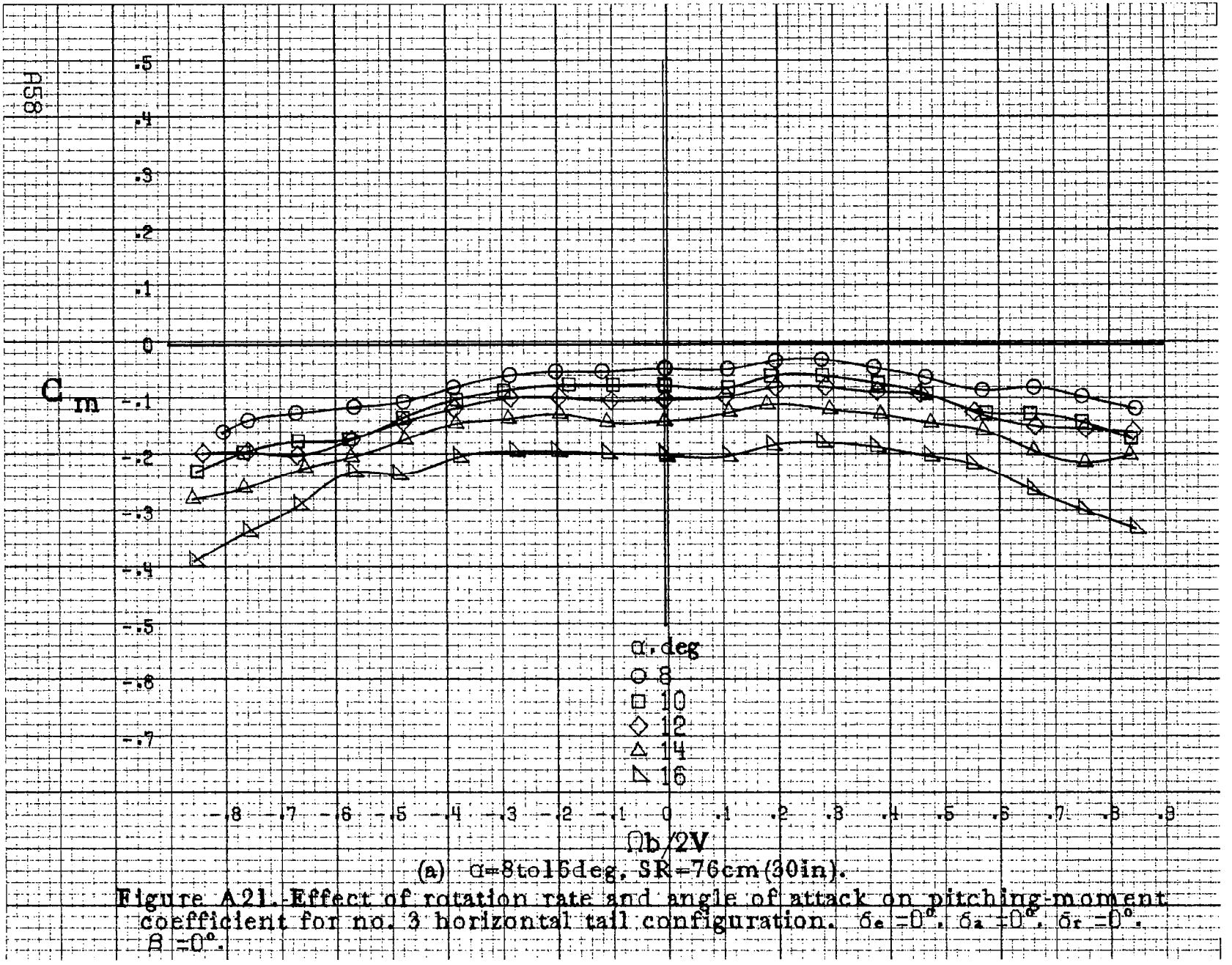

(a) α=8to16deg, SR=76cm(30in).

Figure A21.-Effect of rotation rate and angle of attack on pitching-moment coefficient for no. 3 horizontal tail configuration. $\delta_e = 0°$, $\delta_a = 0°$, $\delta_r = 0°$, $\beta = 0°$.

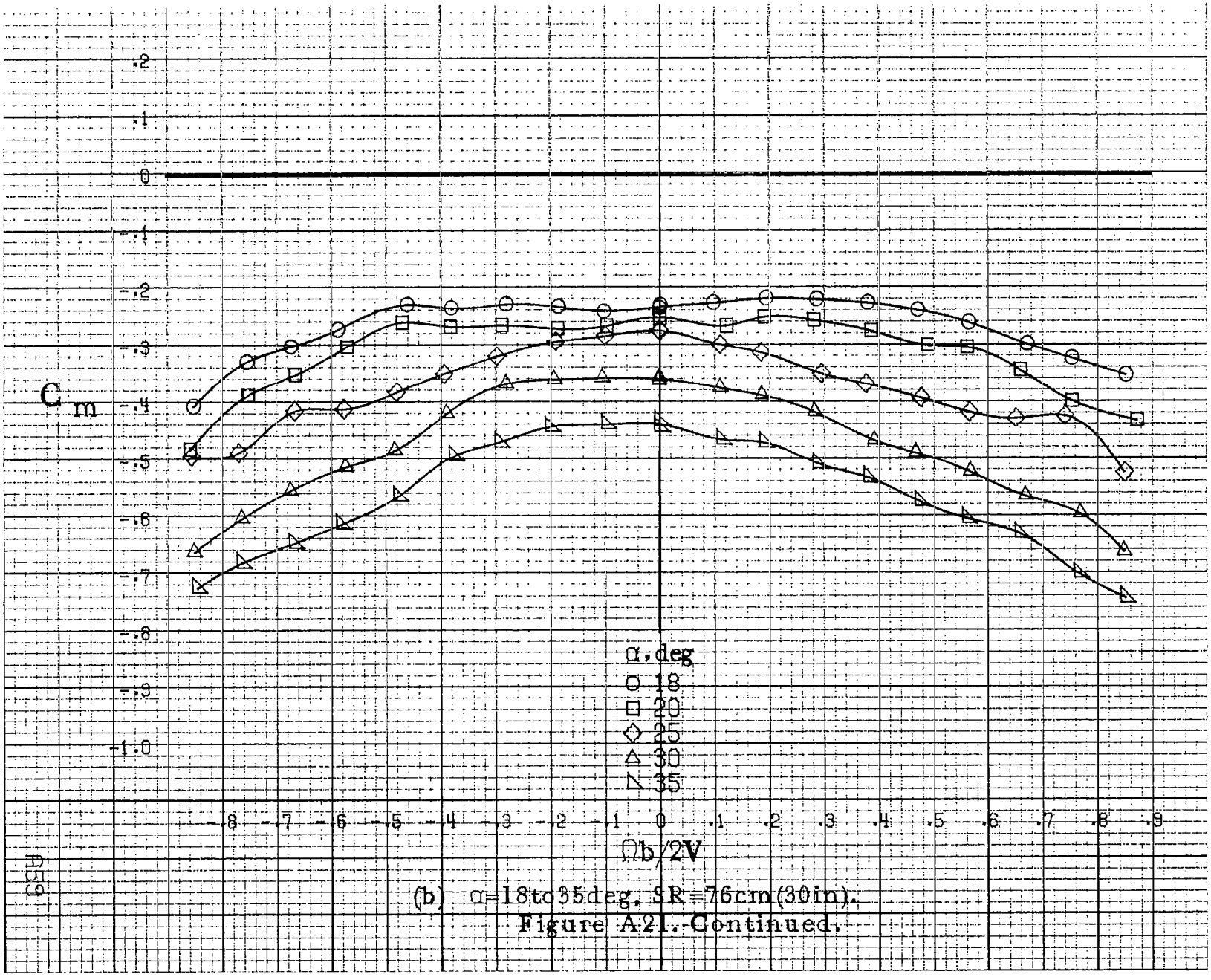

(b) α=18to35deg, SR=76cm(30in).

Figure A21.-Continued.

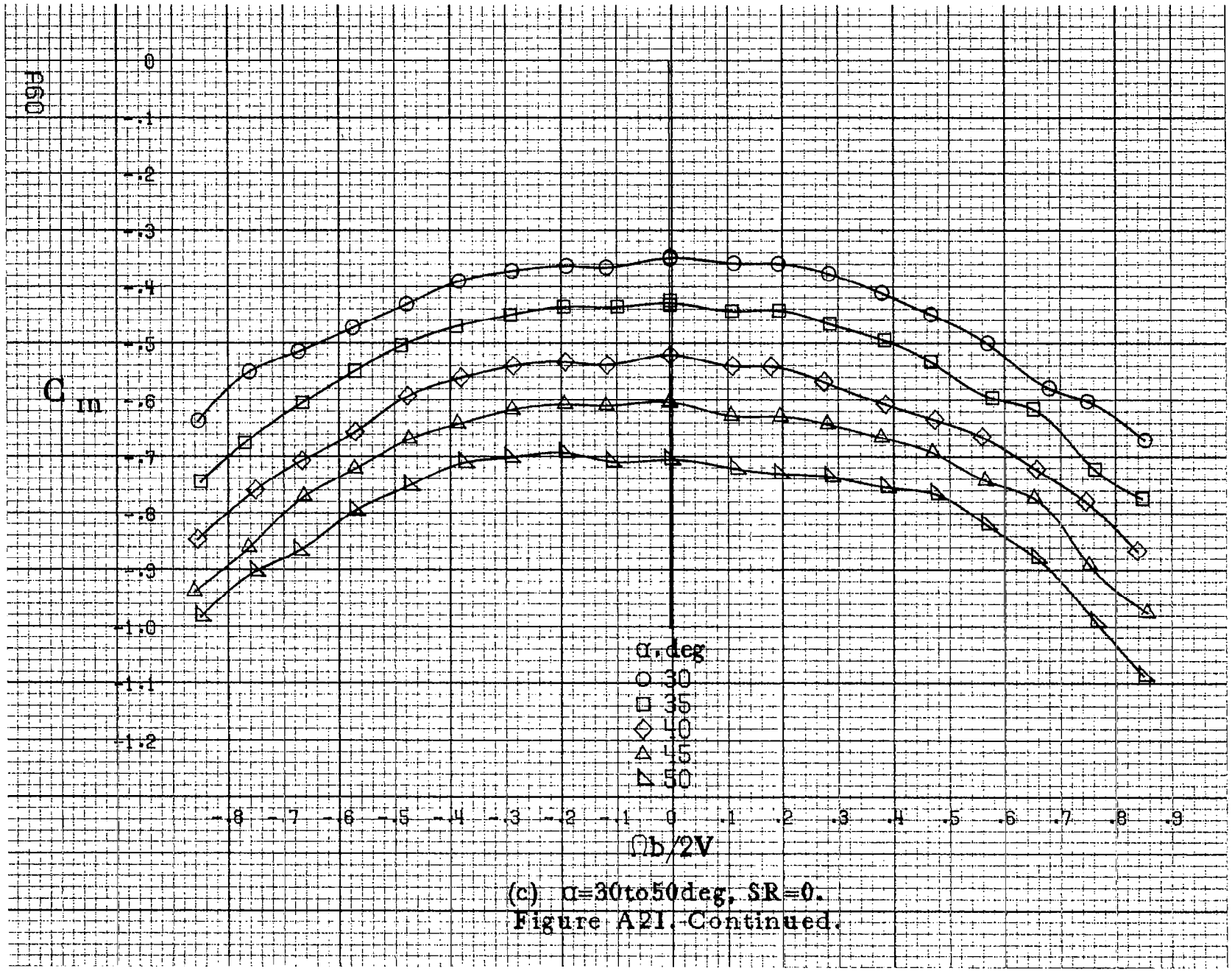

(c) α=30to50deg, SR=0.

Figure A21.-Continued.

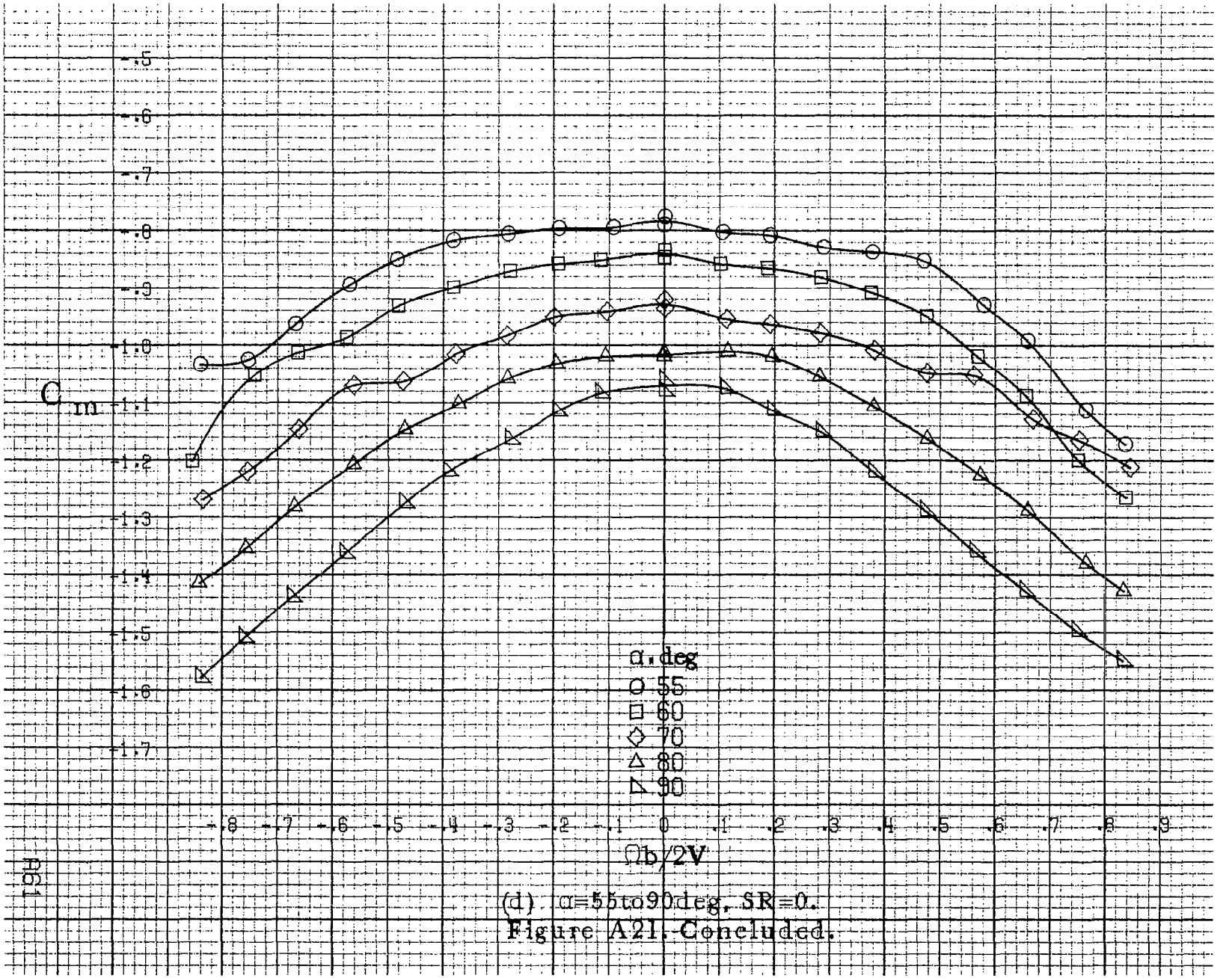

(d) α=55to90deg, SR=0.

Figure A21. Concluded.

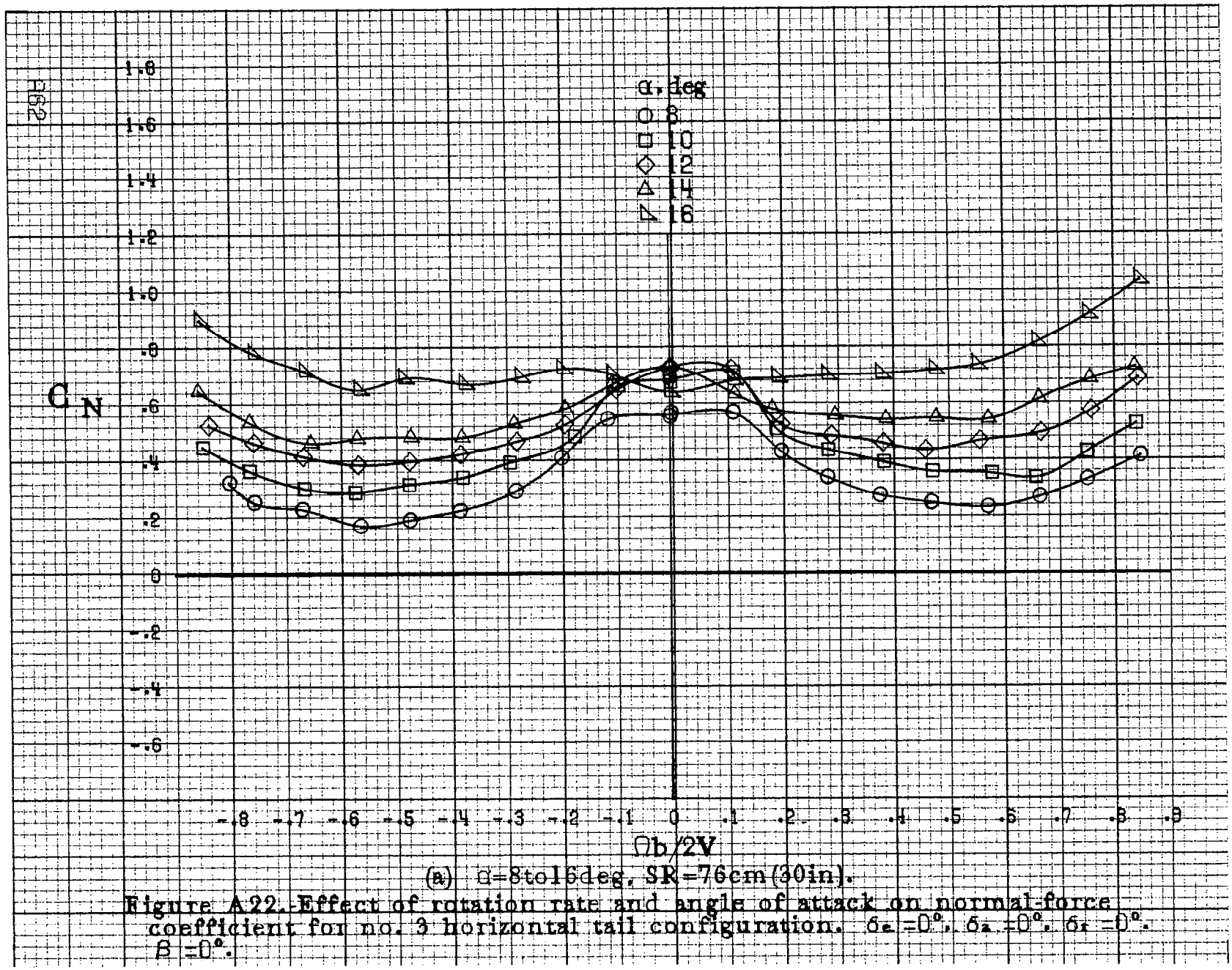

(a) α=8to16deg, SR=76cm(30in).

Figure A22.-Effect of rotation rate and angle of attack on normal-force coefficient for no. 3 horizontal tail configuration. $\delta_e = 0°$, $\delta_a = 0°$, $\delta_r = 0°$, $\beta = 0°$.

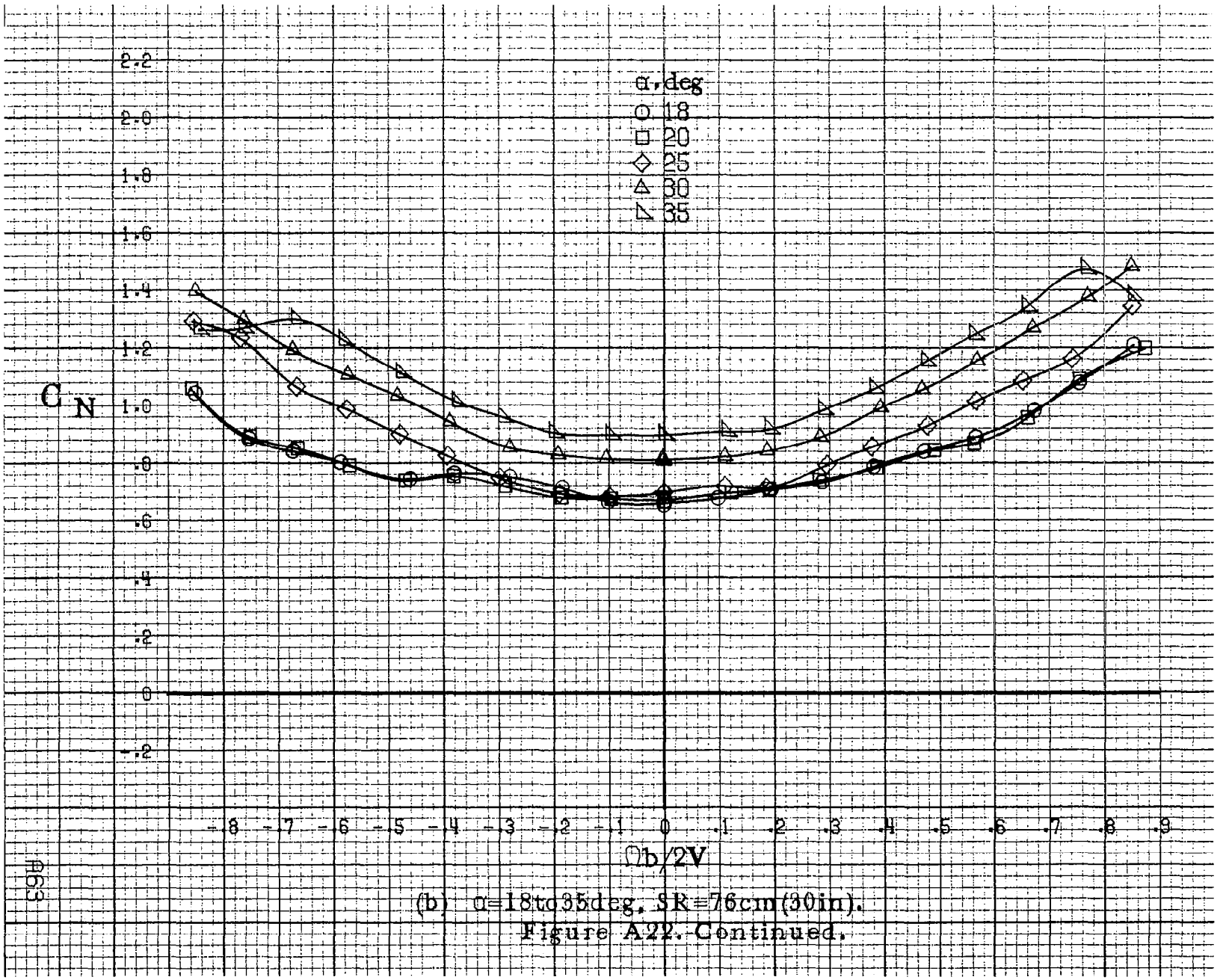

(b) α=18to35deg, SR=76cm(30in).

Figure A22. Continued.

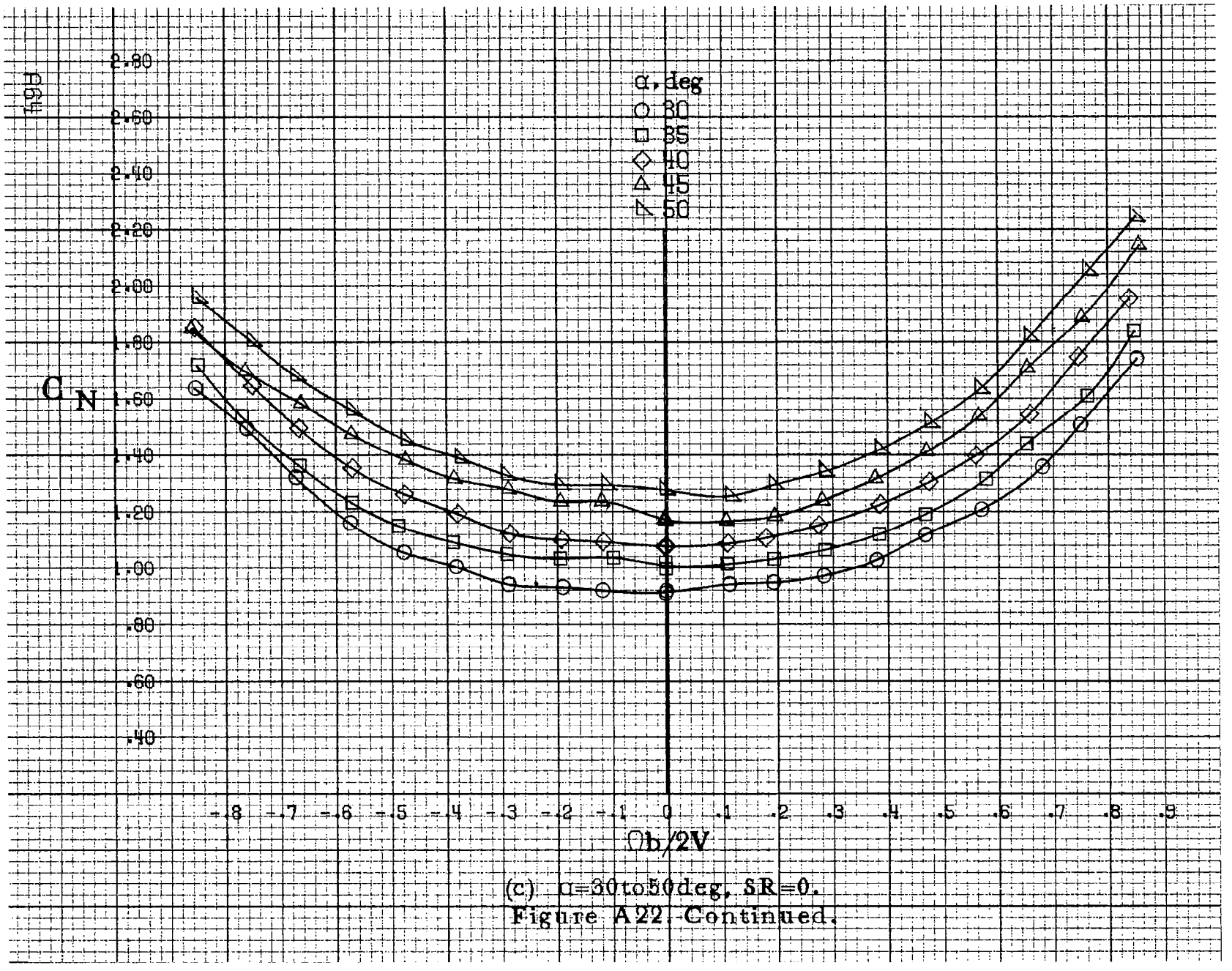

(c) α=30 to 50 deg, δR=0.

Figure A22.-Continued.

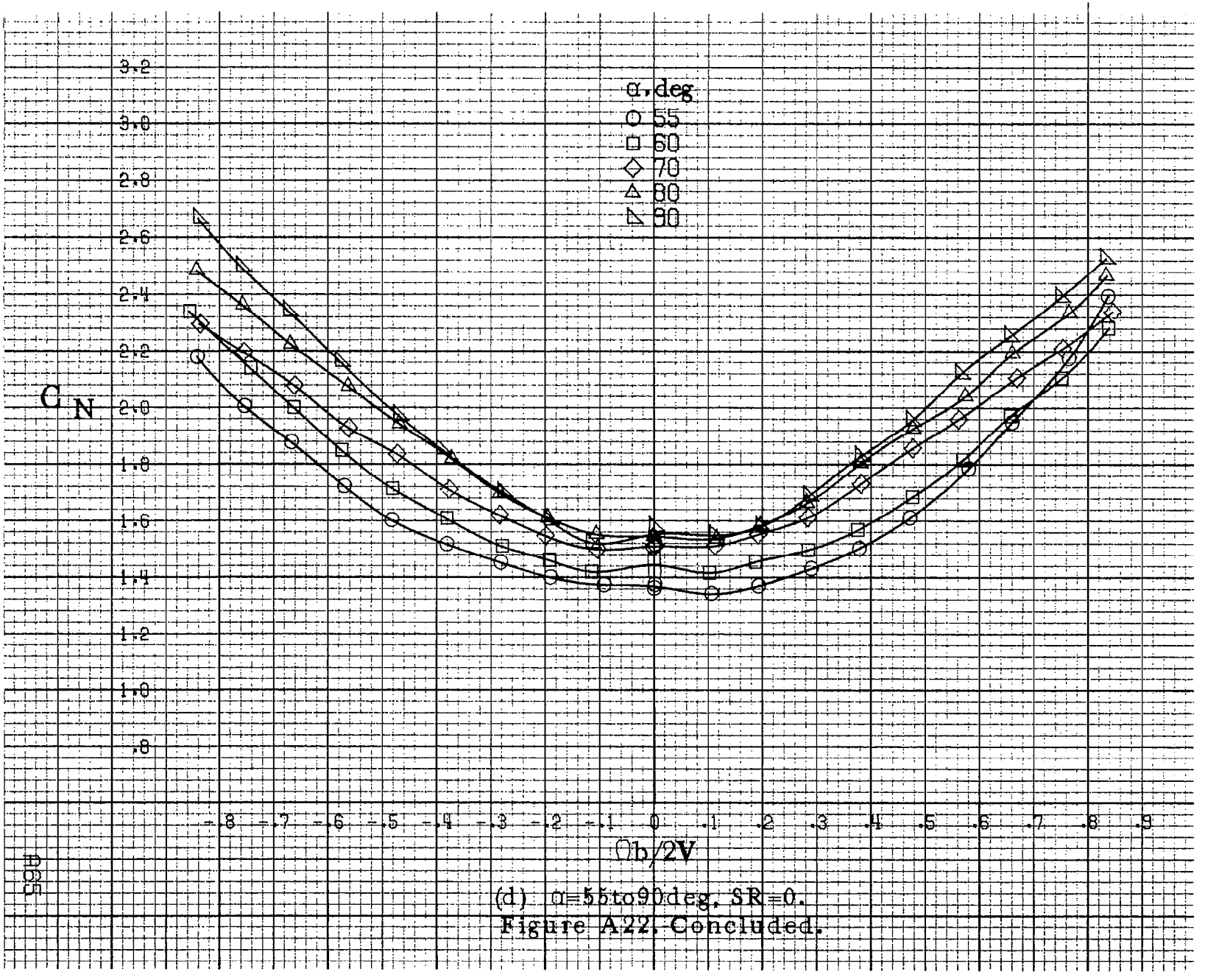

(d) α=55 to 90 deg, SR=0.

Figure A22. Concluded.

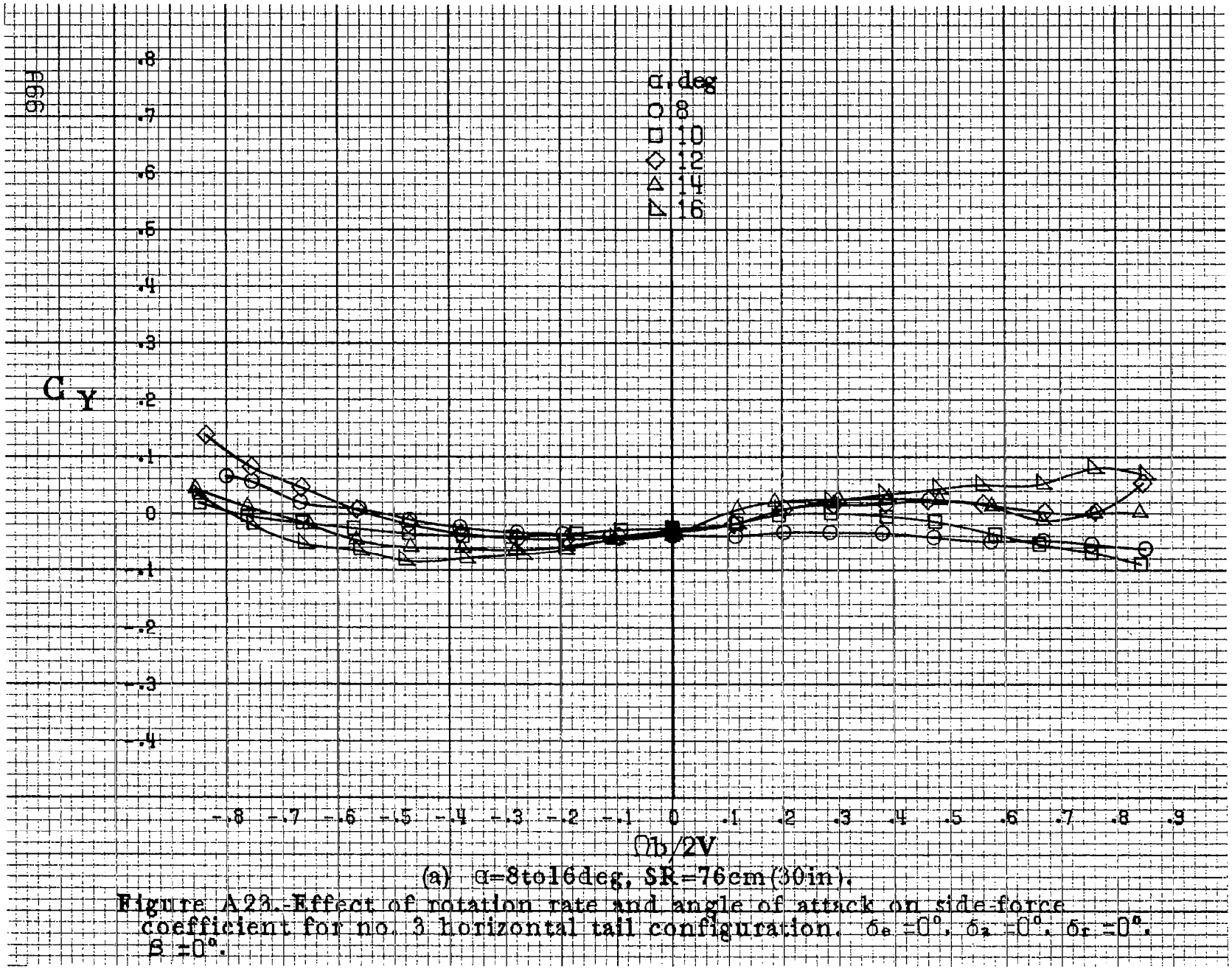

(a) α=8to16deg, SR=76cm(30in).

Figure A23.-Effect of rotation rate and angle of attack on side-force coefficient for no. 3 horizontal tail configuration. $\delta_e = 0°$, $\delta_a = 0°$, $\delta_r = 0°$, $\beta = 0°$.

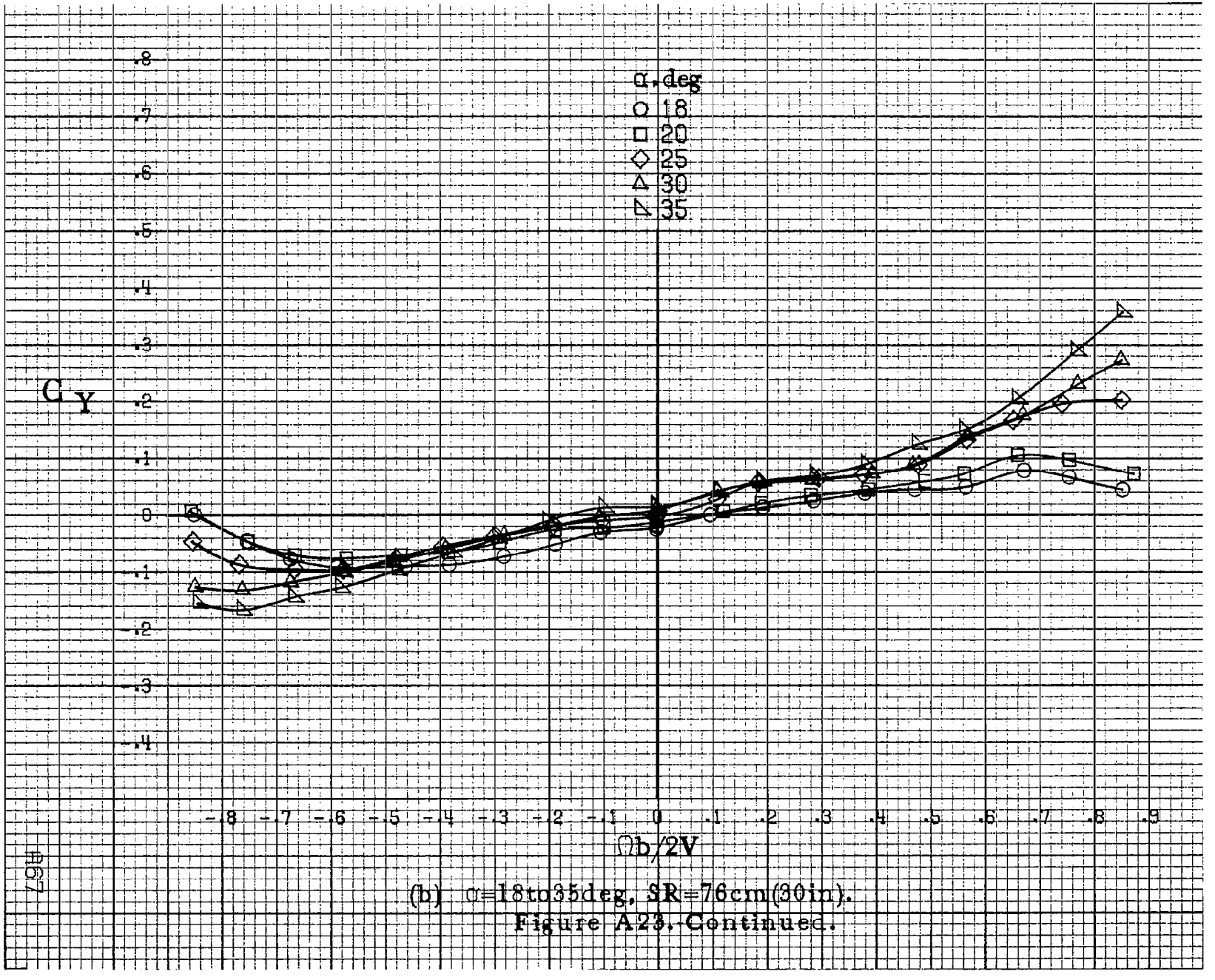

(b) α=18to35deg, SR=76cm(30in).

Figure A23.-Continued.

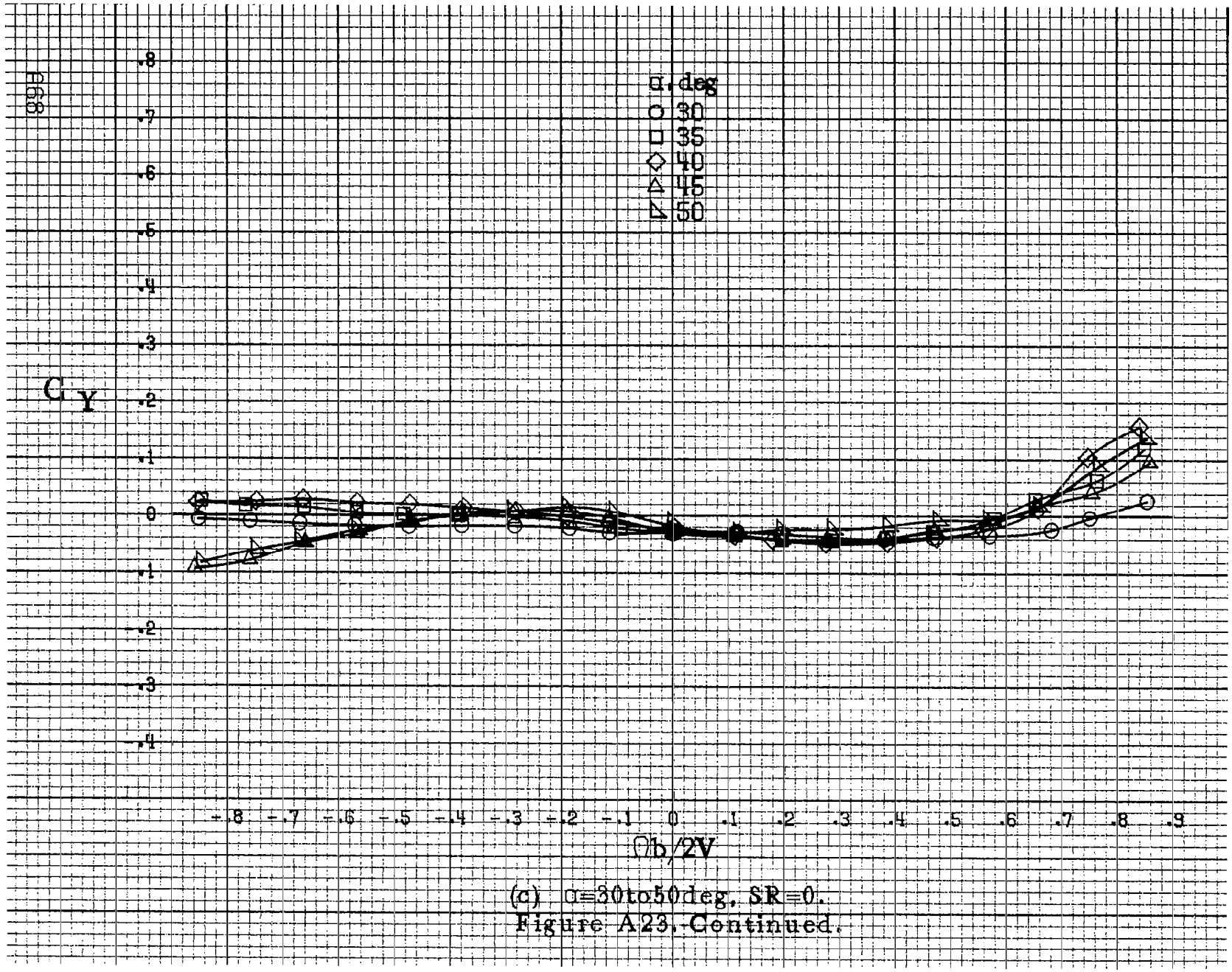

(c) $\alpha = 30$ to 50 deg, $SR = 0$.

Figure A23.-Continued.

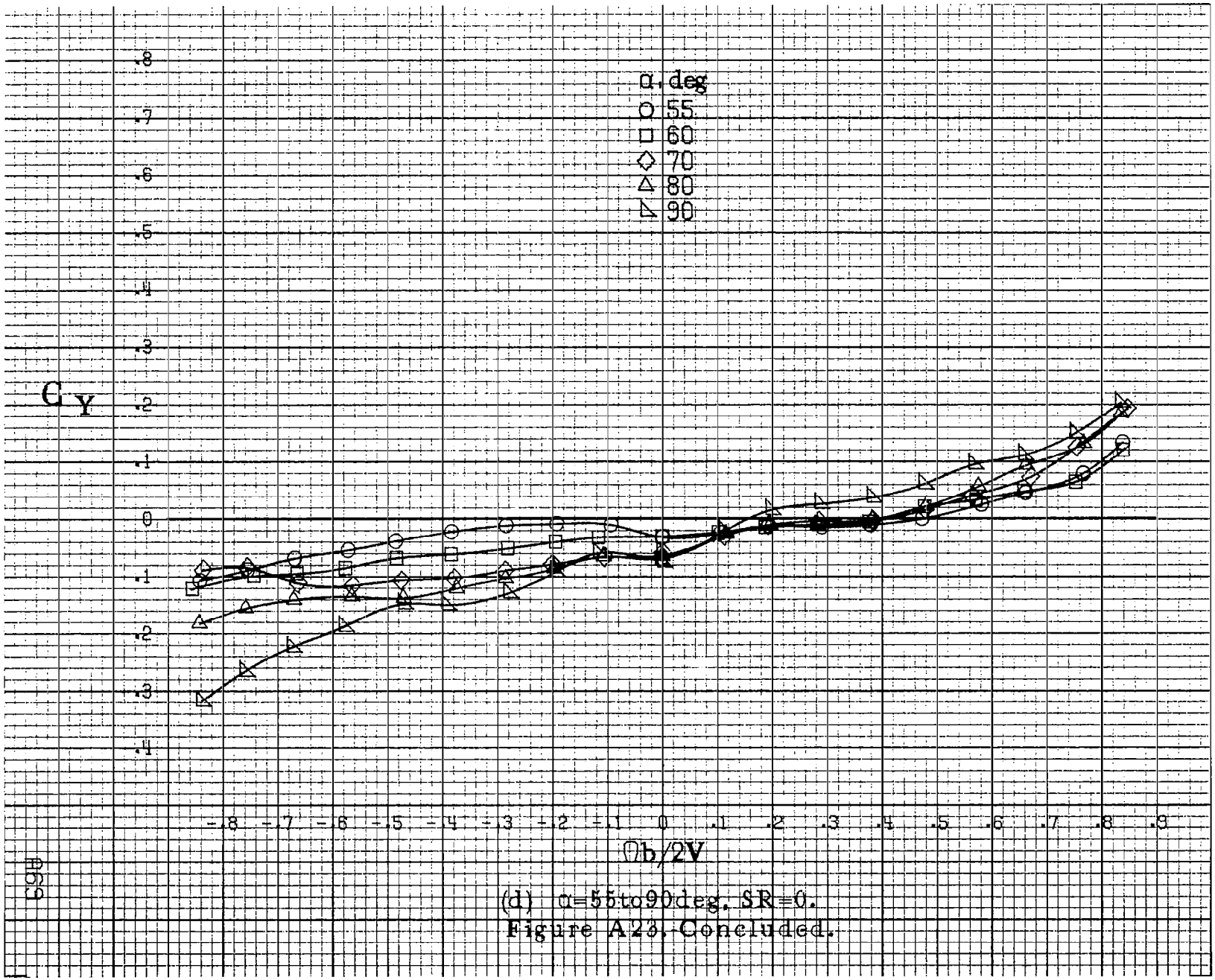

(d) α=55 to 90 deg. SR=0.

Figure A23. Concluded.

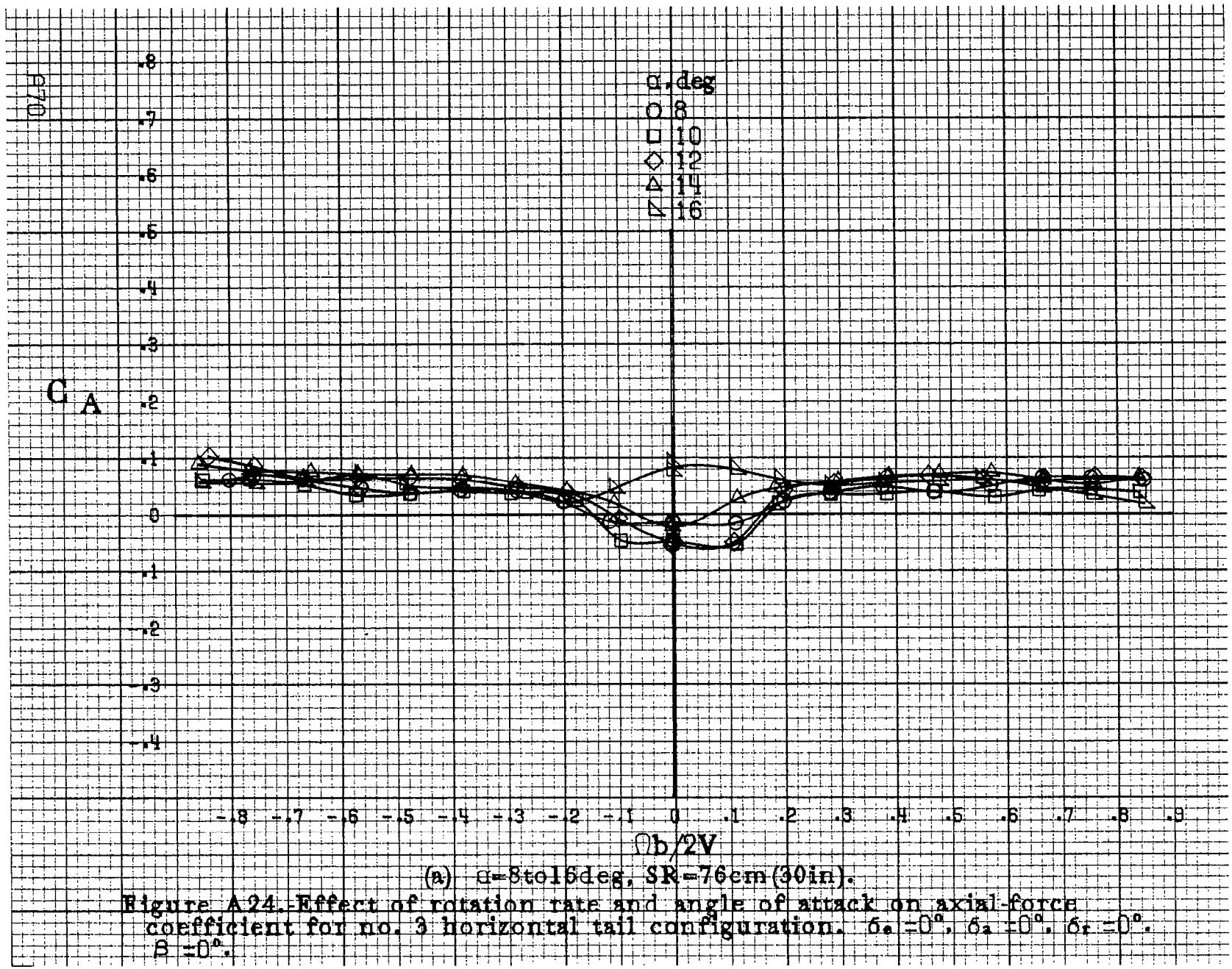

(a) α=8to16deg, SR=76cm(30in).

Figure A24.-Effect of rotation rate and angle of attack on axial-force coefficient for no. 3 horizontal tail configuration. $\delta_e = 0°$, $\delta_a = 0°$, $\delta_r = 0°$, $\beta = 0°$.

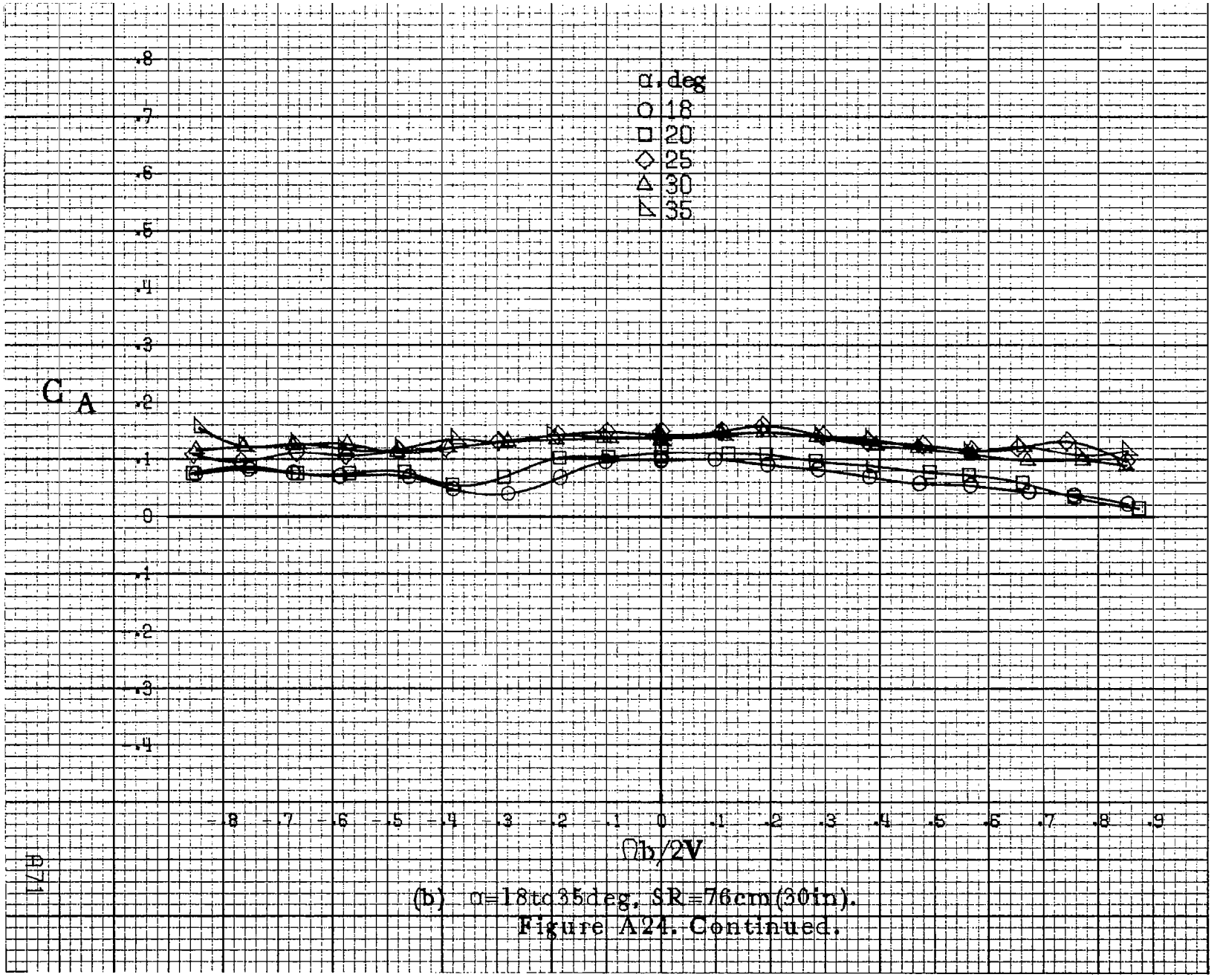

(b) α=18 to 35 deg, SR=76 cm (30 in).

Figure A24. Continued.

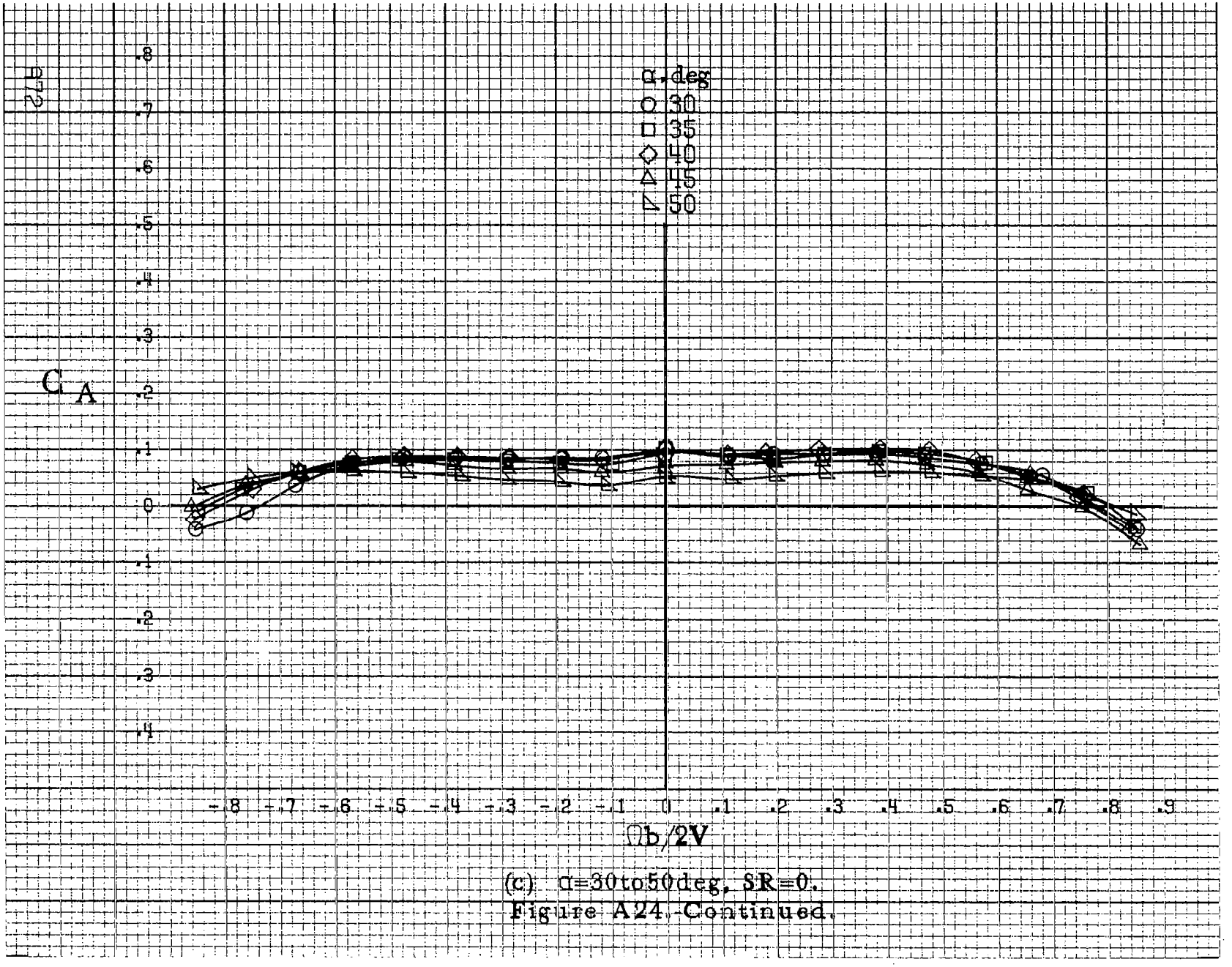

(c) α=30 to 50 deg, SR=0.

Figure A24.-Continued.

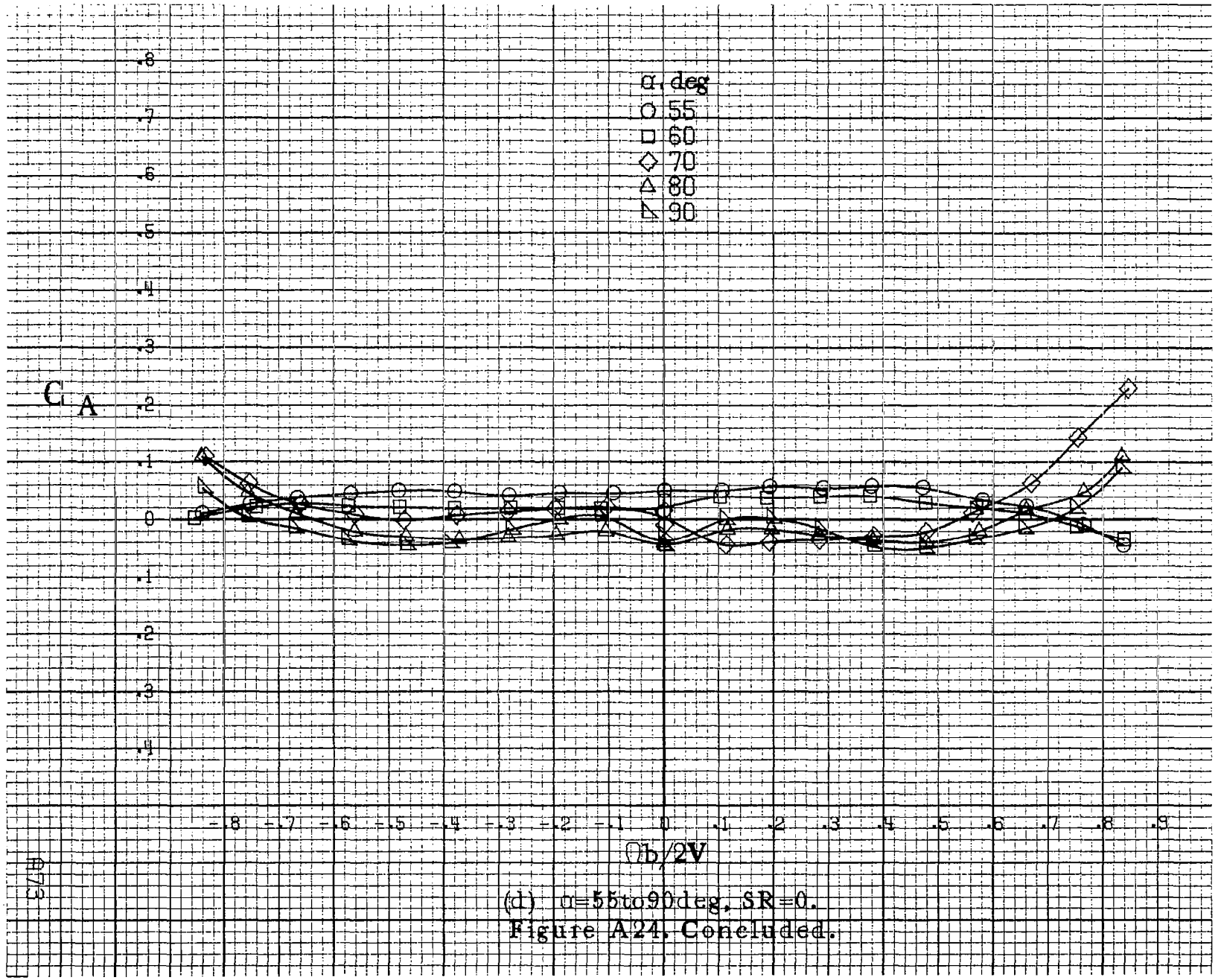

(d) α=55to90deg, SR=0.

Figure A24. Concluded.

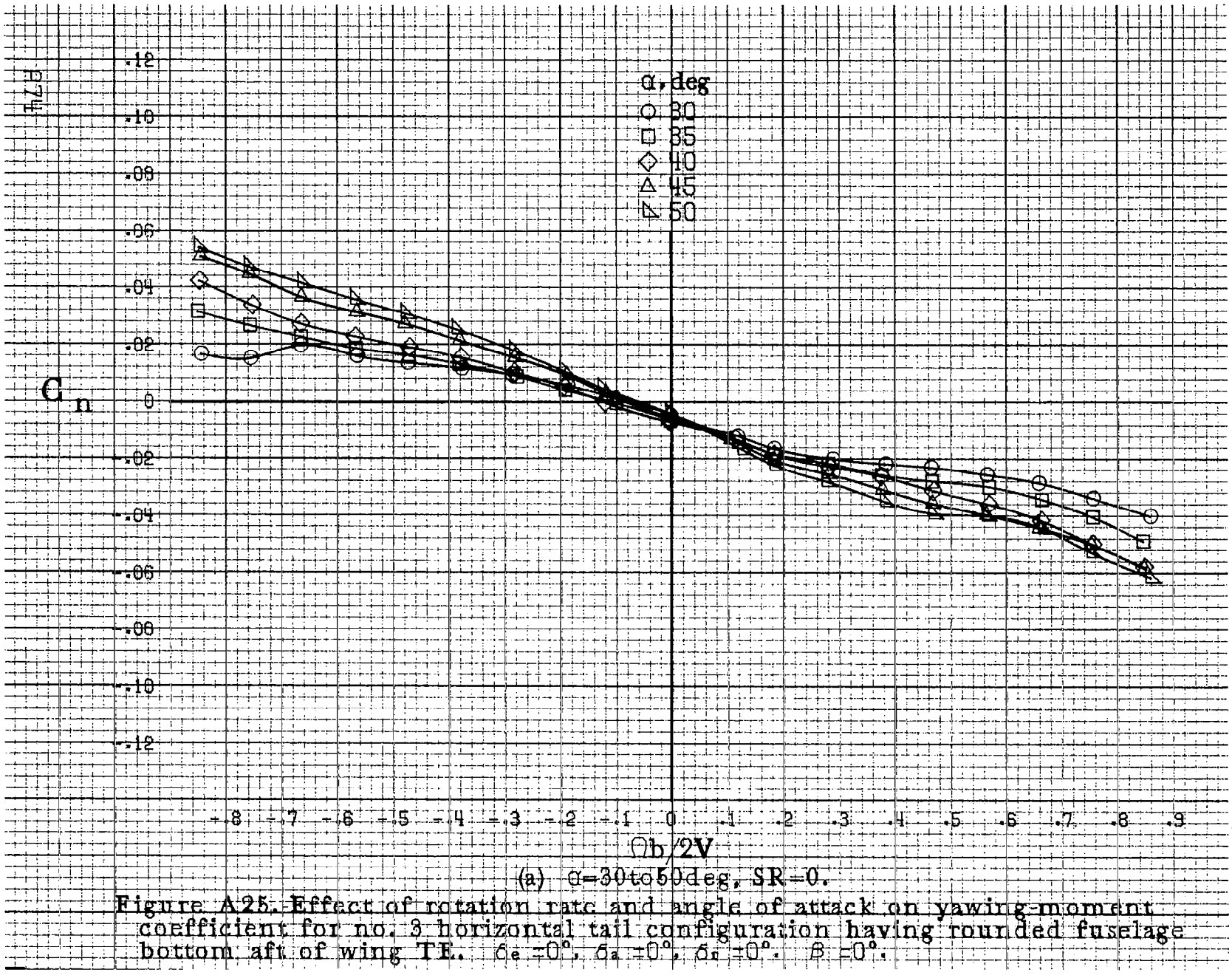

(a) α=30to50deg, SR=0.

Figure A25. Effect of rotation rate and angle of attack on yawing-moment coefficient for no. 3 horizontal tail configuration having rounded fuselage bottom aft of wing TE. δ_e =0°, δ_a =0°, δ_r =0°. β =0°.

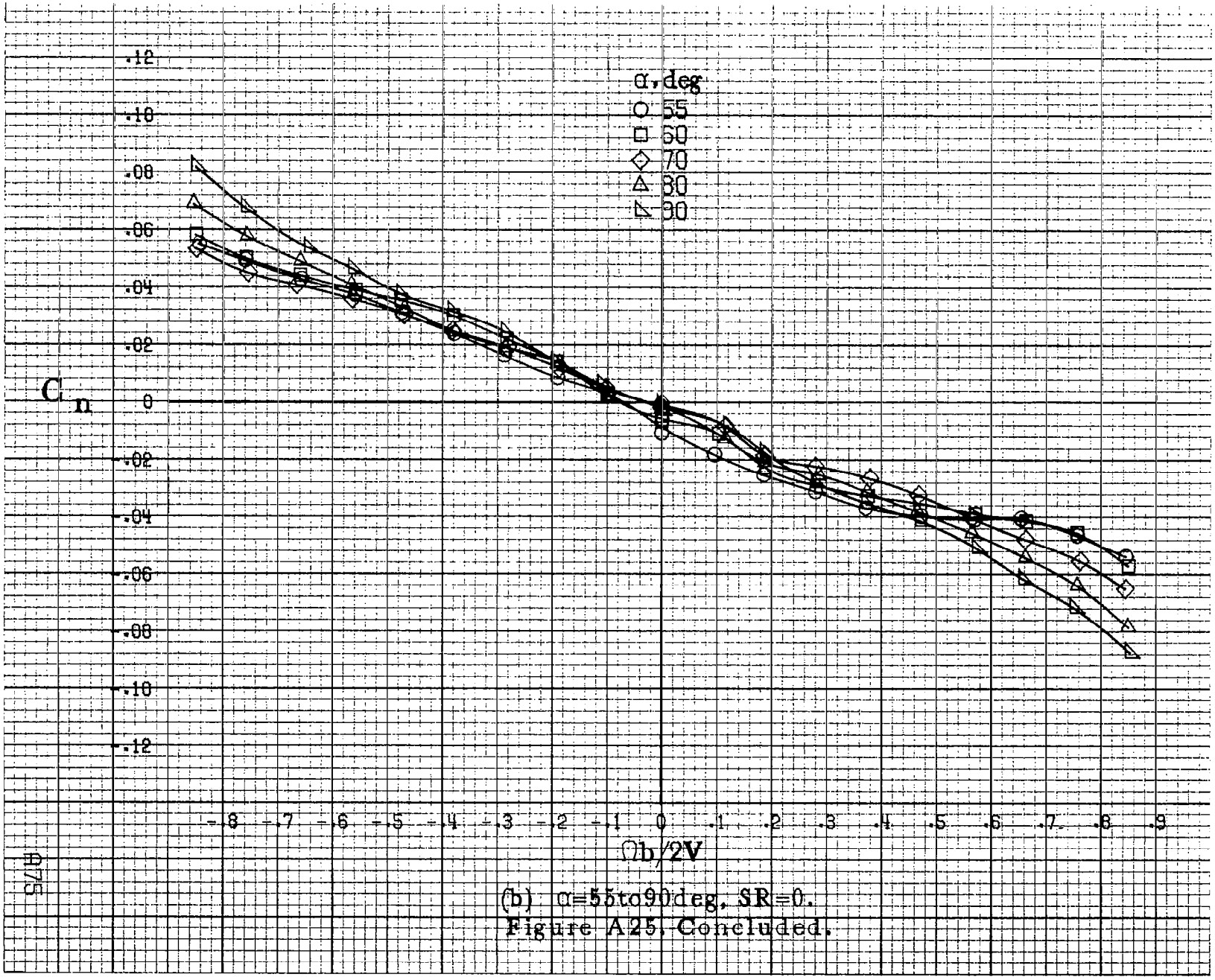

(b) α=55to90deg, SR=0.

Figure A25. Concluded.

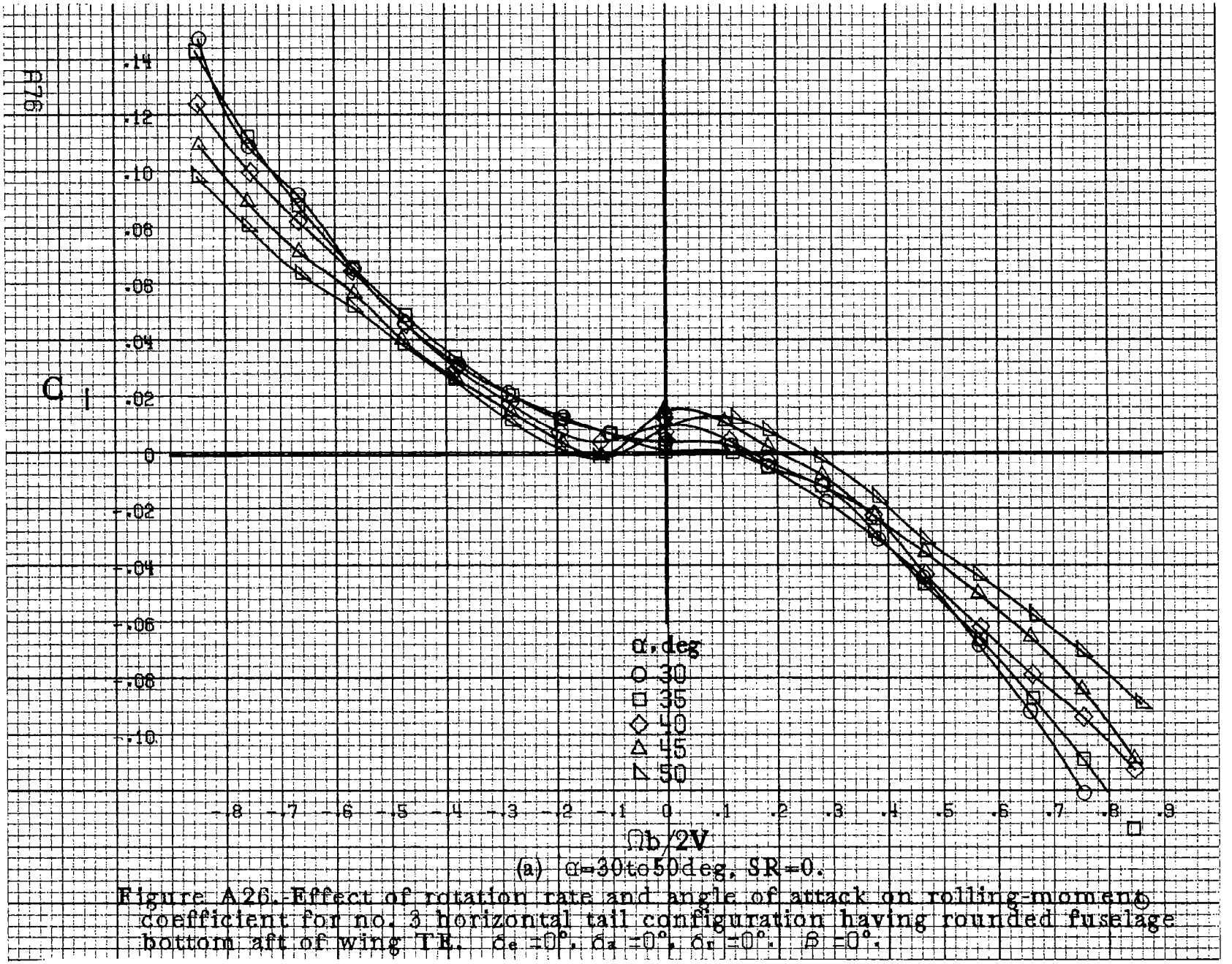

(a) α=30to50deg, SR=0.

Figure A26.-Effect of rotation rate and angle of attack on rolling-moment coefficient for no. 3 horizontal tail configuration having rounded fuselage bottom aft of wing TE. δ_e =0°, δ_a =0°, δ_r =0°. β =0°.

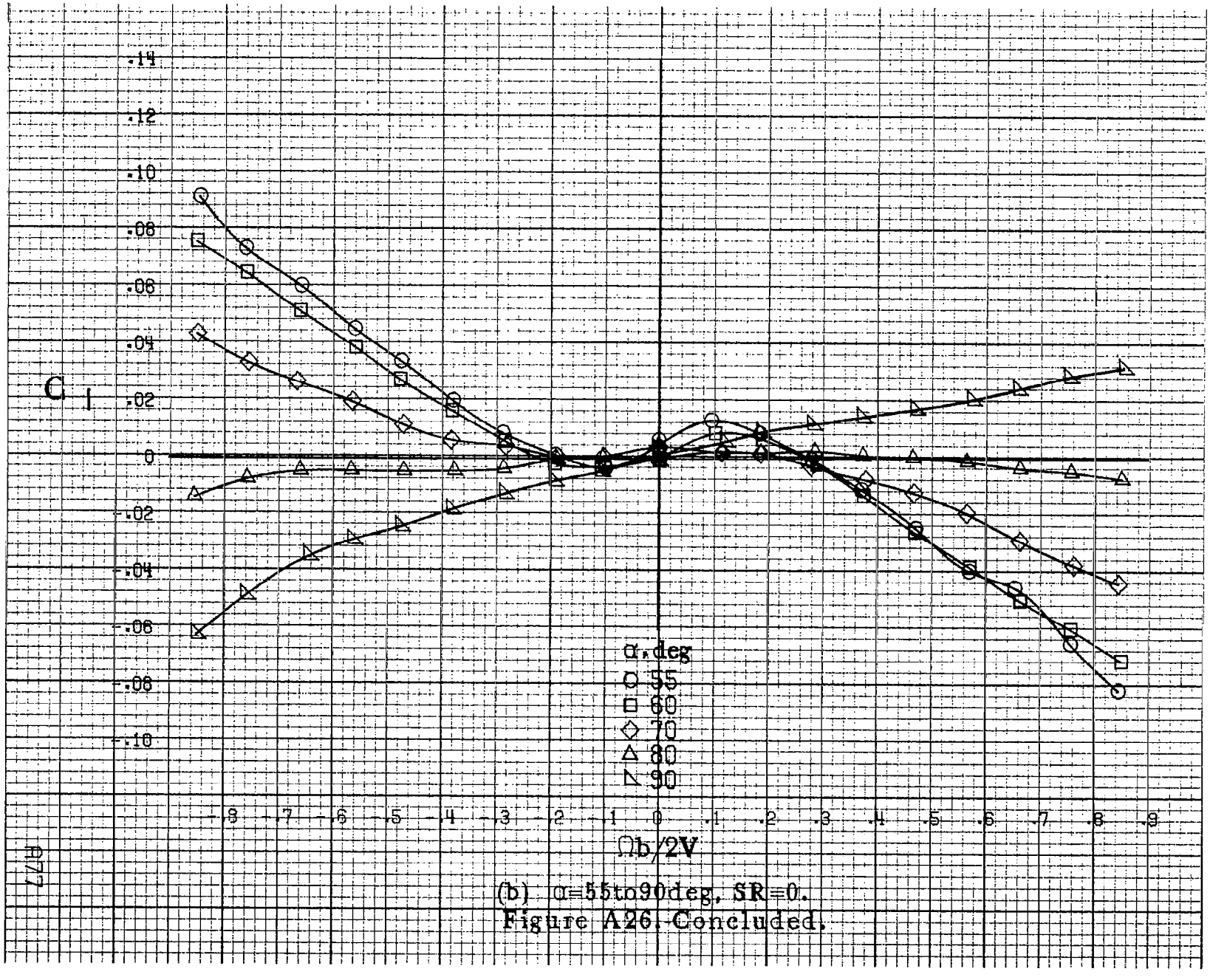

(b) α=55to90deg, SR=0.

Figure A26. Concluded.

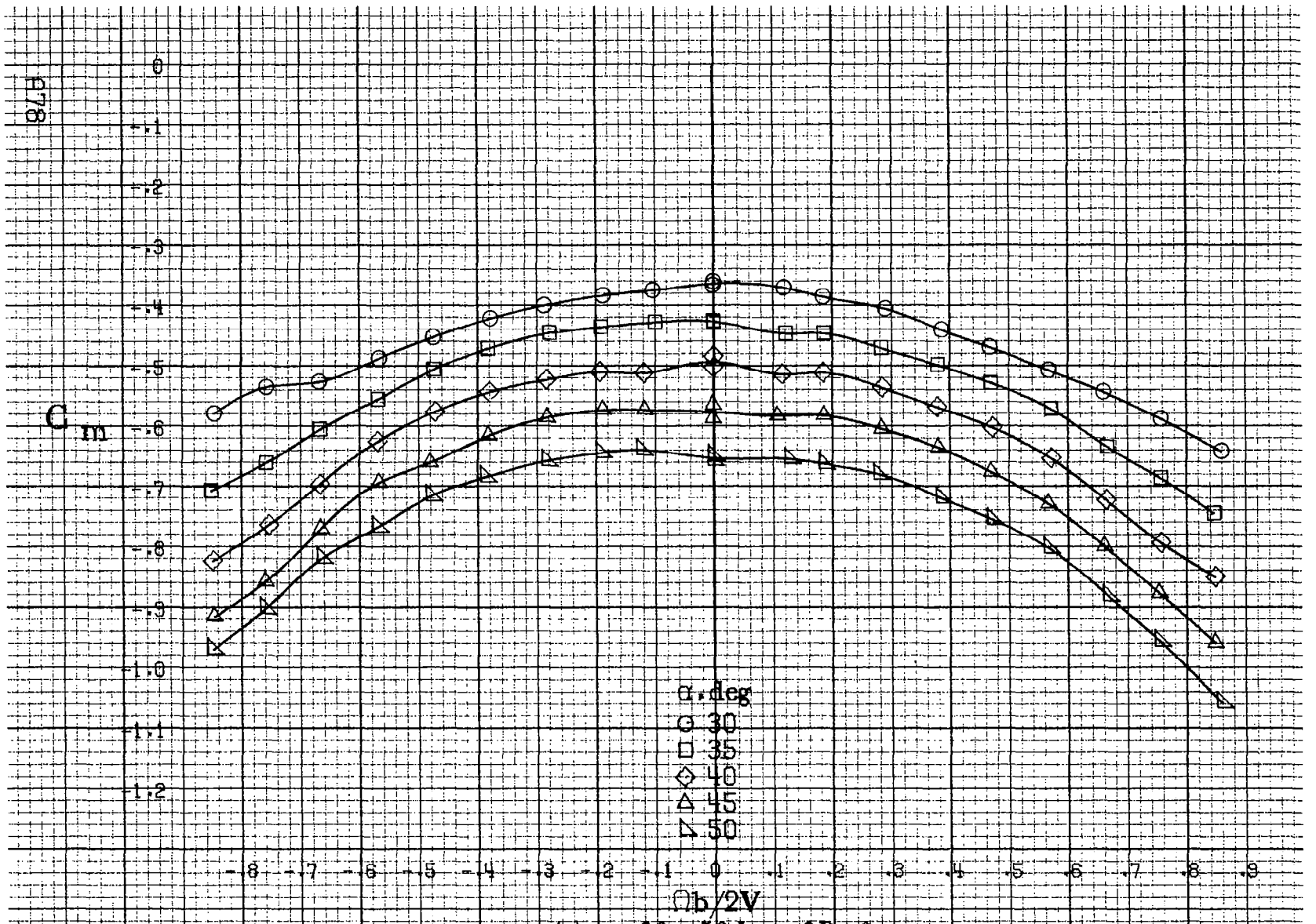

(a) α=30to50deg, SR=0.

Figure A27.-Effect of rotation rate and angle of attack on pitching-moment coefficient for no. 3 horizontal tail configuration having rounded fuselage bottom aft of wing TR. $\delta_e = 0°$, $\delta_a = 0°$, $\delta_r = 0°$, $\beta = 0°$.

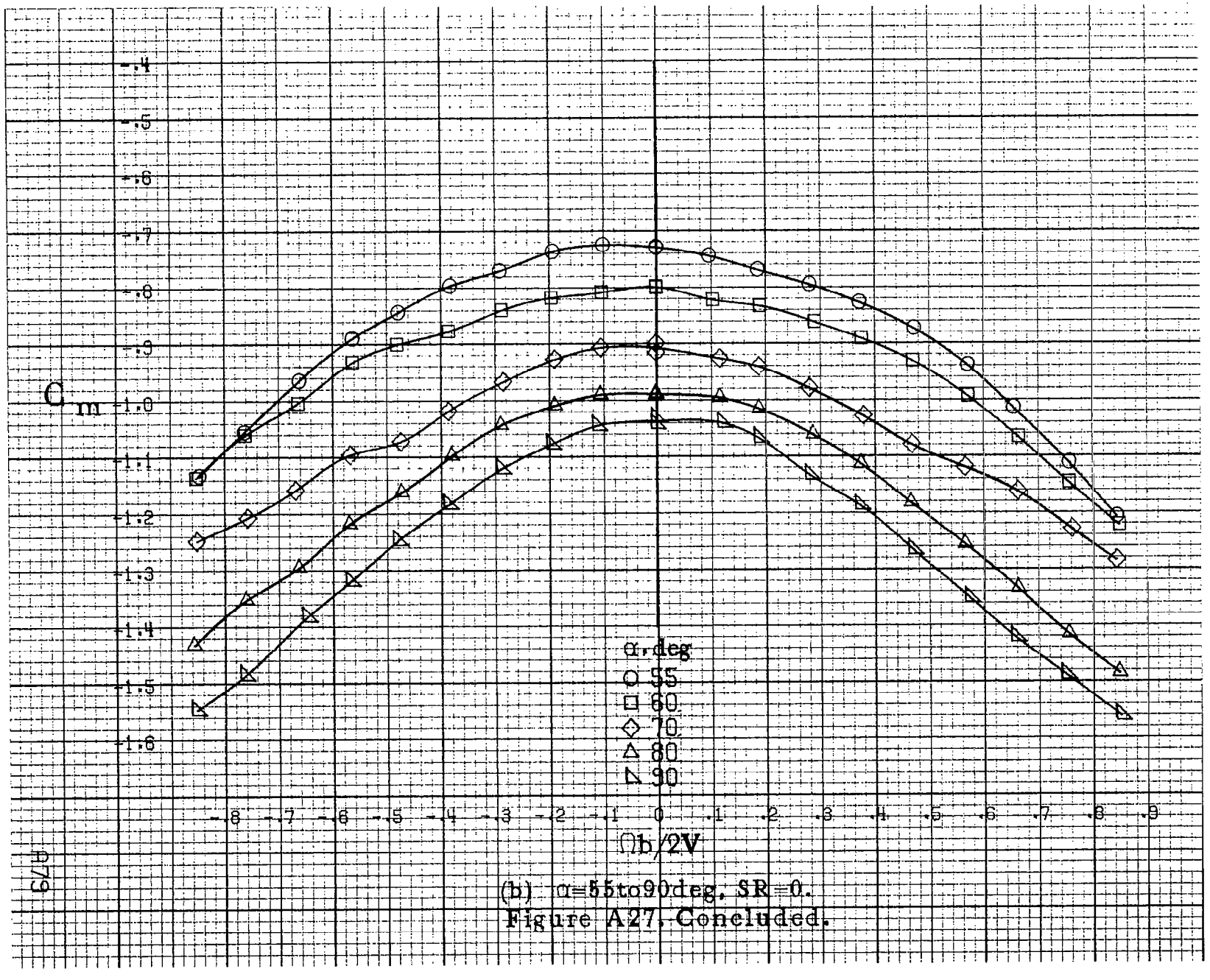

(b) α=55to90deg, SR=0.

Figure A27. Concluded.

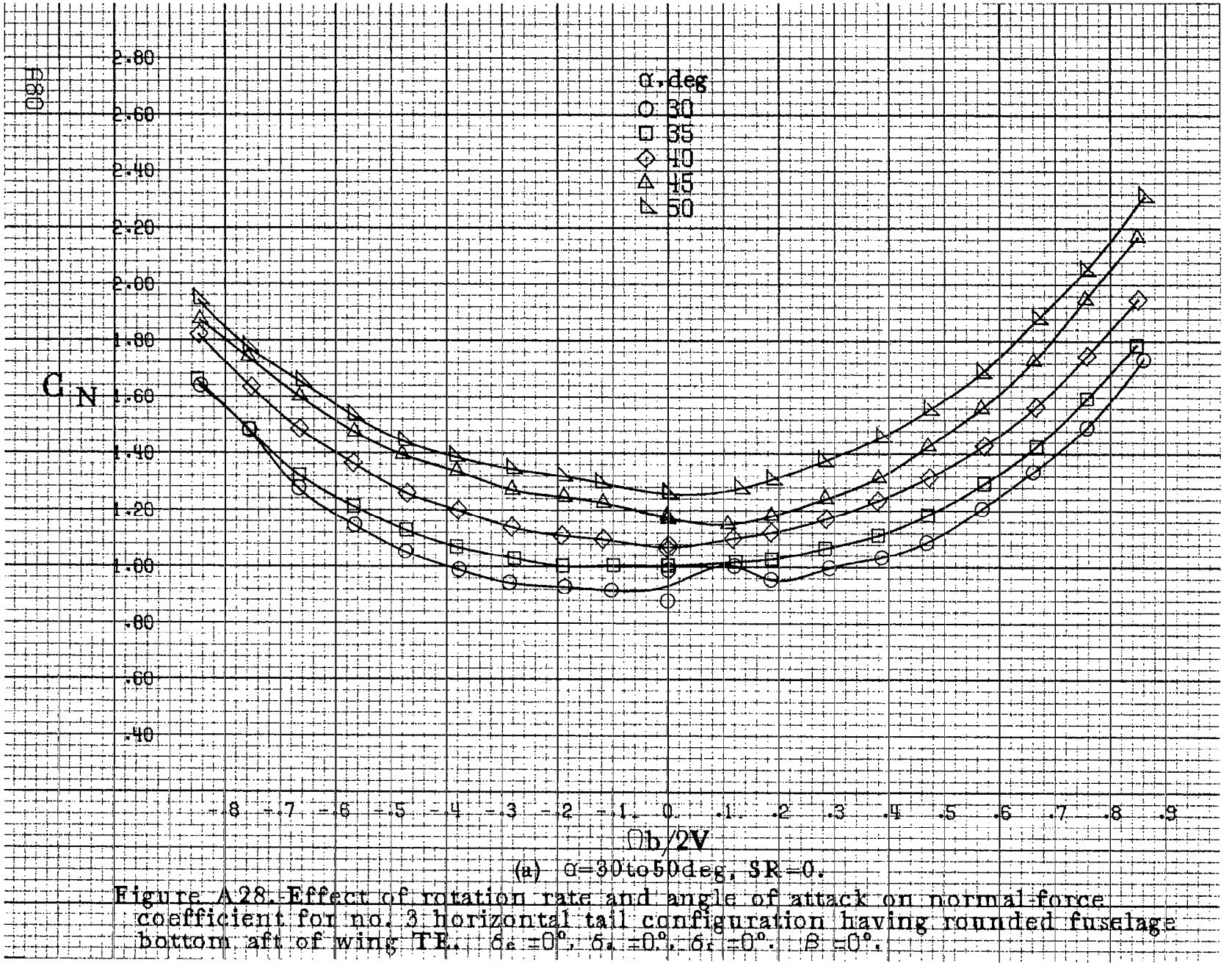

(a) α=30to50deg, SR=0.

Figure A28. Effect of rotation rate and angle of attack on normal-force coefficient for no. 3 horizontal tail configuration having rounded fuselage bottom aft of wing TE. $\delta_e = 0°$, $\delta_a = 0°$, $\delta_r = 0°$, $\beta = 0°$.

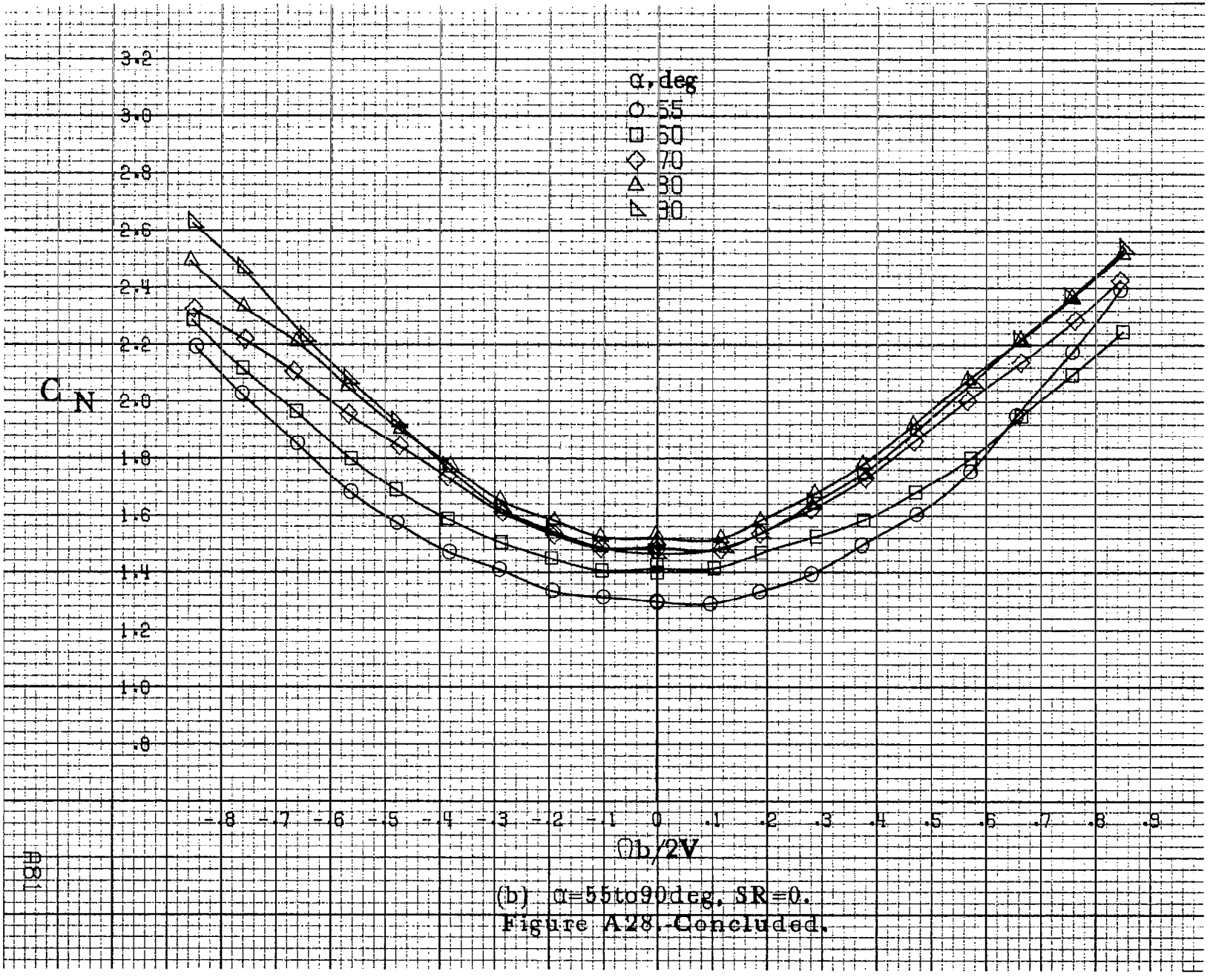

(b) α=55to90deg, SR=0.

Figure A28.-Concluded.

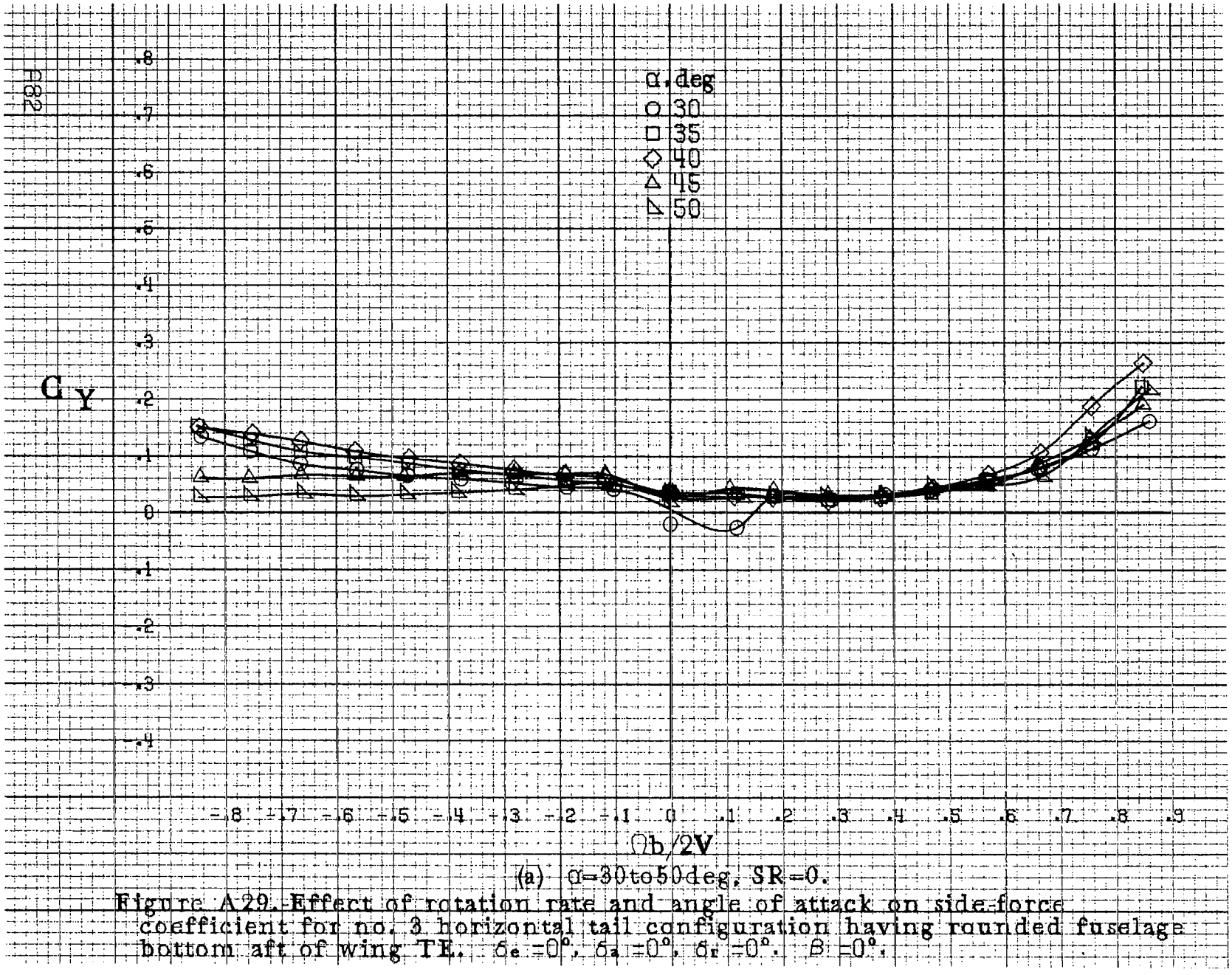

(a) α=30to50deg, SR=0.

Figure A29. Effect of rotation rate and angle of attack on side-force coefficient for no. 3 horizontal tail configuration having rounded fuselage bottom aft of wing TE. $\delta_e = 0°$, $\delta_a = 0°$, $\delta_r = 0°$, $\beta = 0°$.

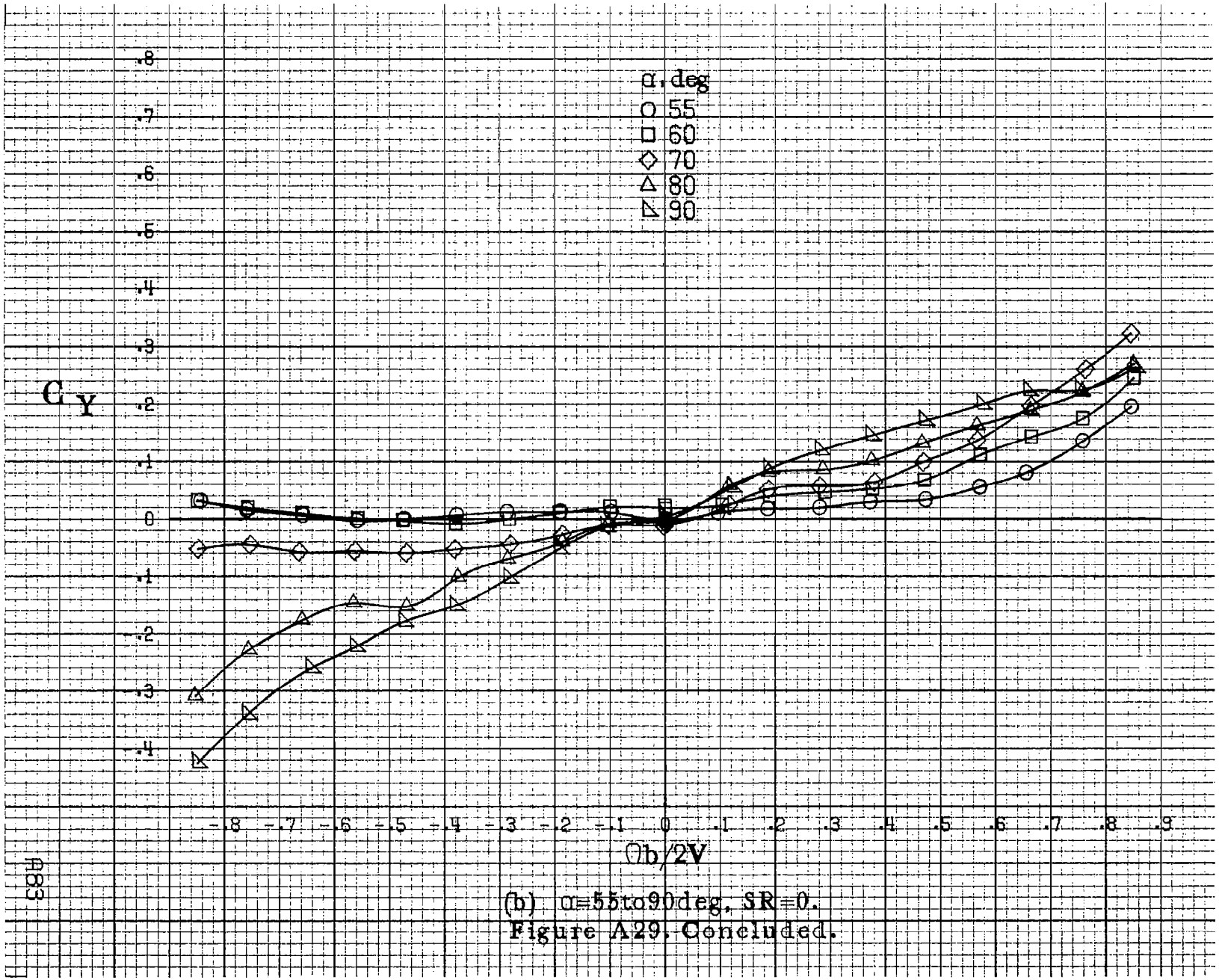

(b) α=55to90deg, SR=0.

Figure A29. Concluded.

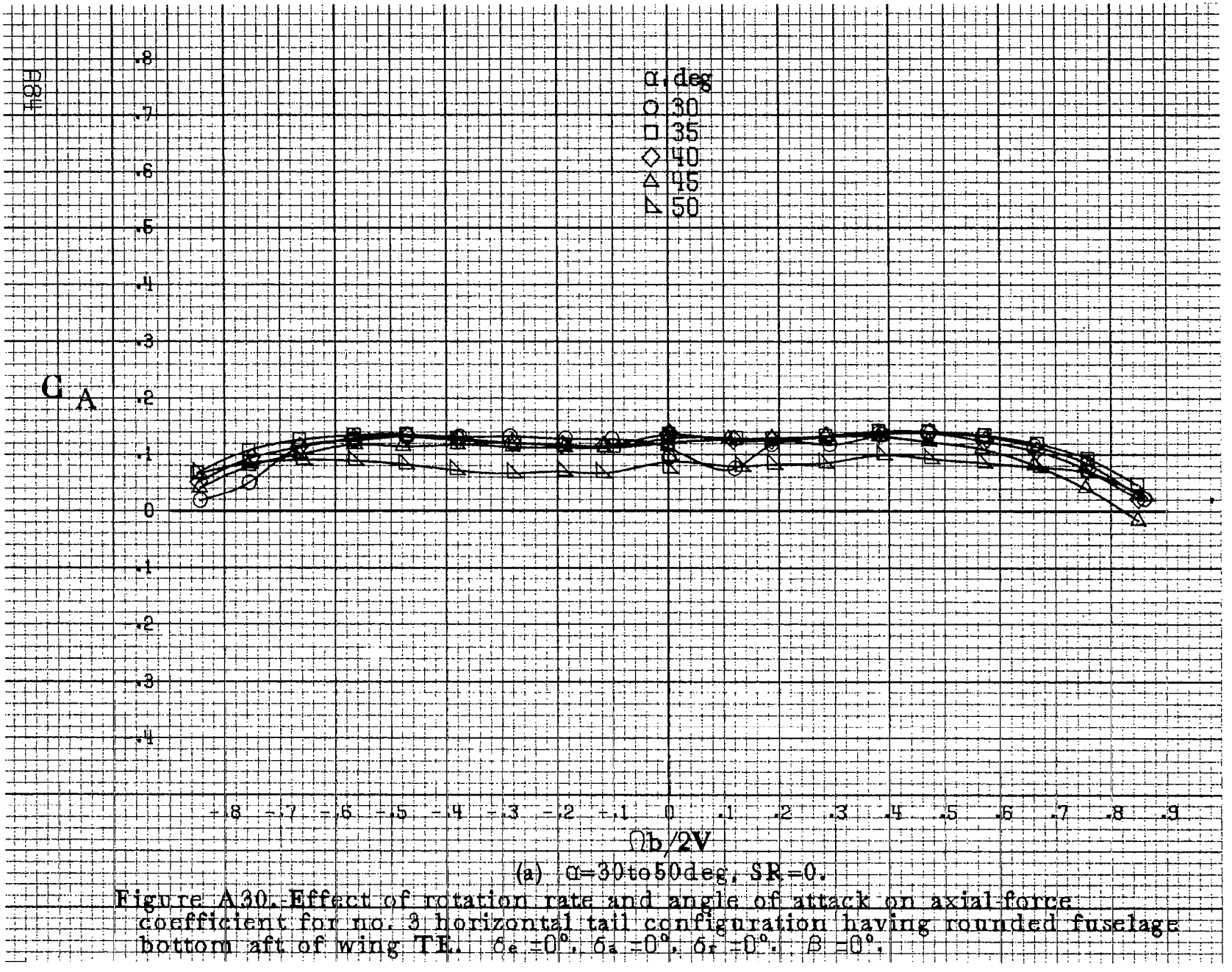

(a) α=30 to 50 deg, SR=0.

Figure A30. Effect of rotation rate and angle of attack on axial-force coefficient for no. 3 horizontal tail configuration having rounded fuselage bottom aft of wing TE. δ_e =0°, δ_a =0°, δ_r =0°, β =0°.

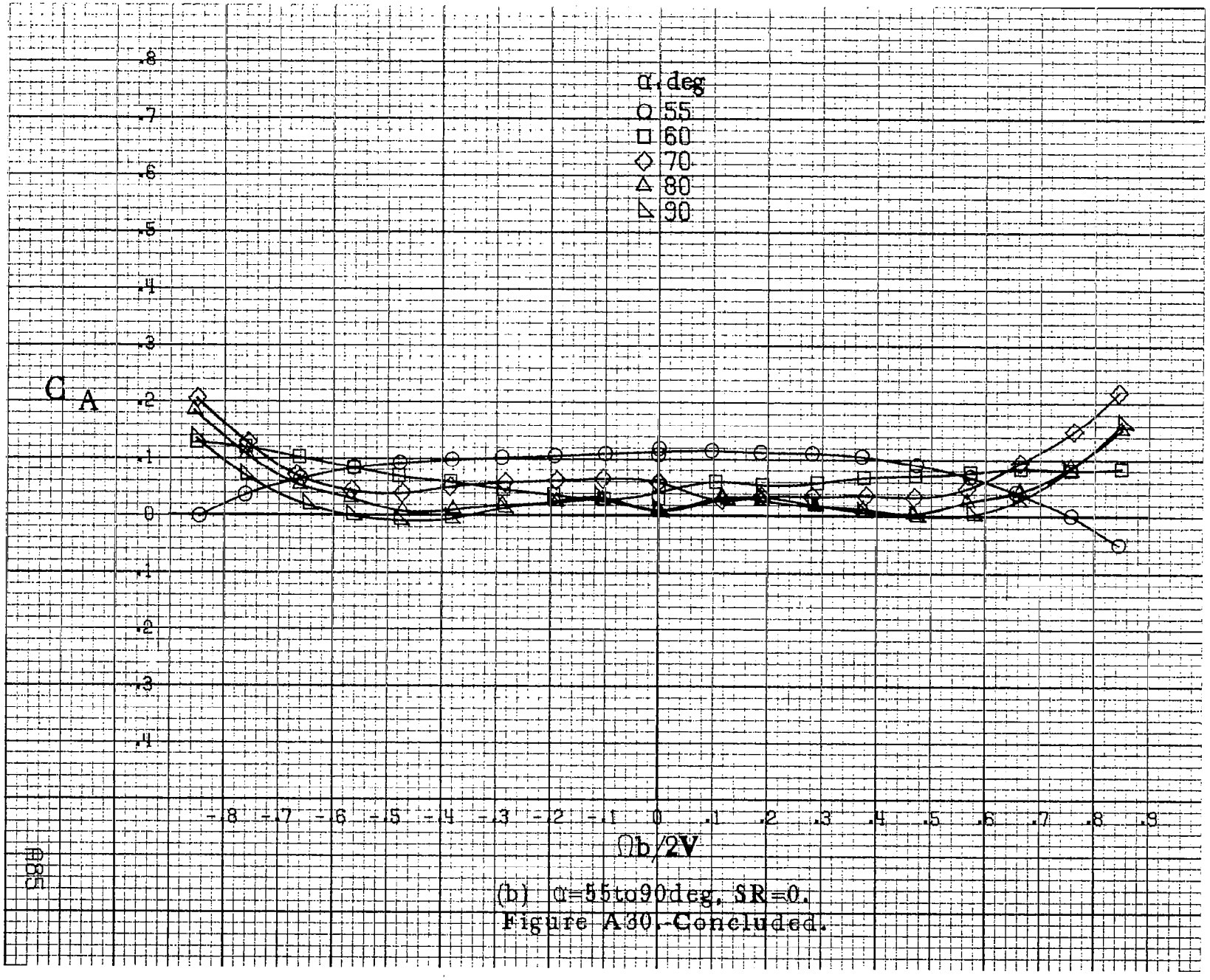

(b) α=55to90deg, SR=0.

Figure A30.-Concluded.

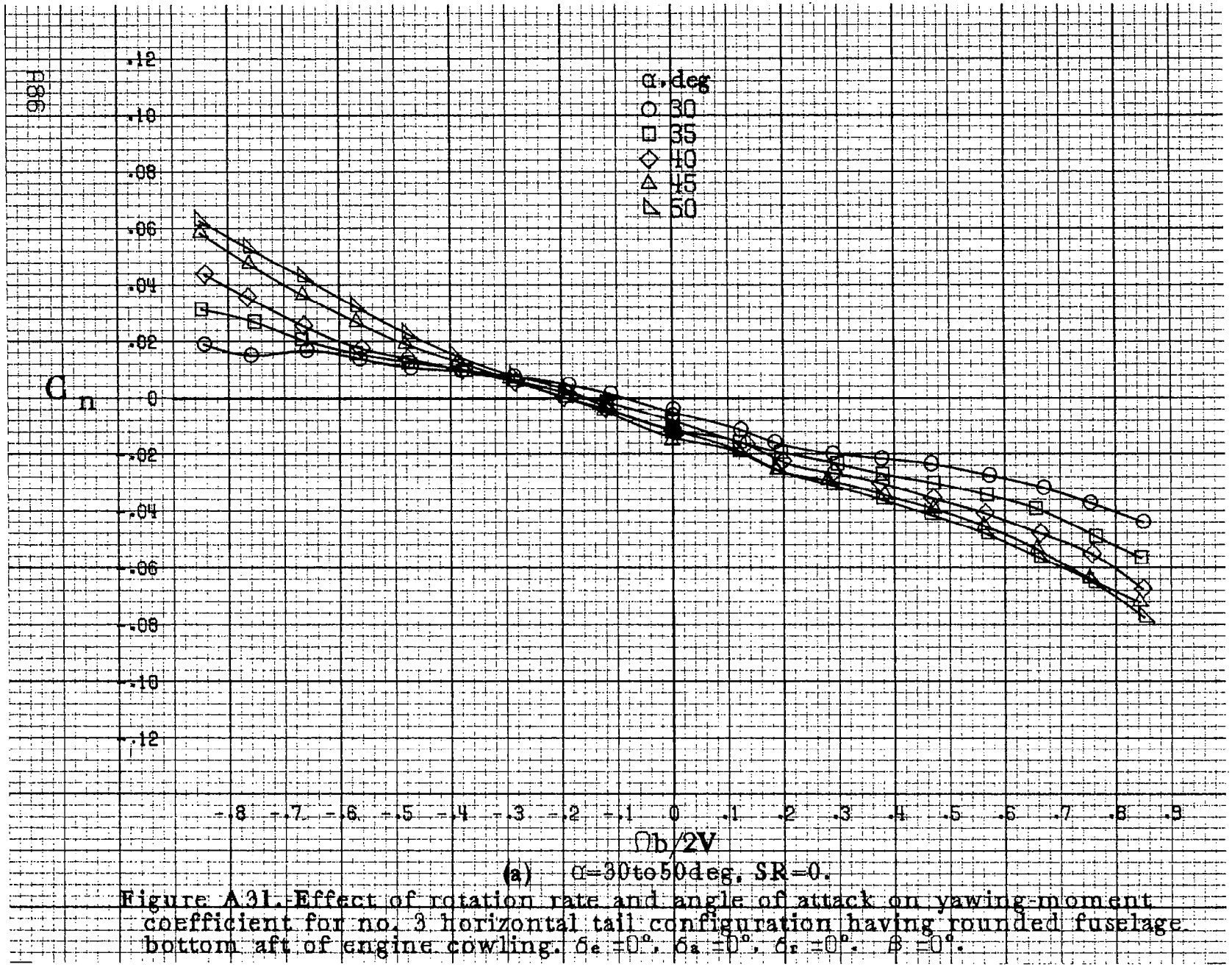

(a) α=30to50deg, SR=0.

Figure A31. Effect of rotation rate and angle of attack on yawing-moment coefficient for no. 3 horizontal tail configuration having rounded fuselage bottom aft of engine cowling. $\delta_e = 0°$, $\delta_a = 0°$, $\delta_r = 0°$, $\beta = 0°$.

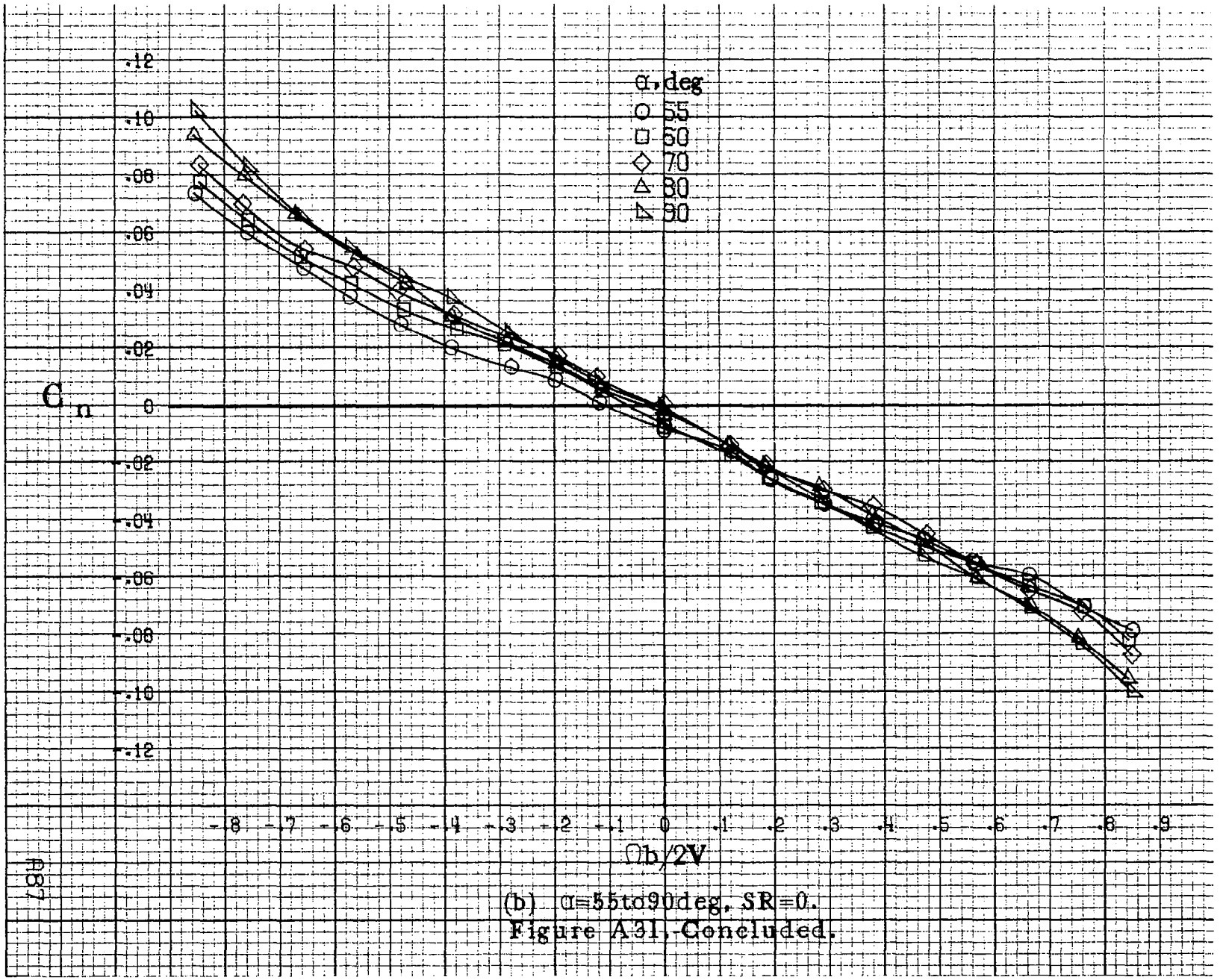

(b) $\alpha = 55$ to 90 deg, SR = 0.

Figure A31.- Concluded.

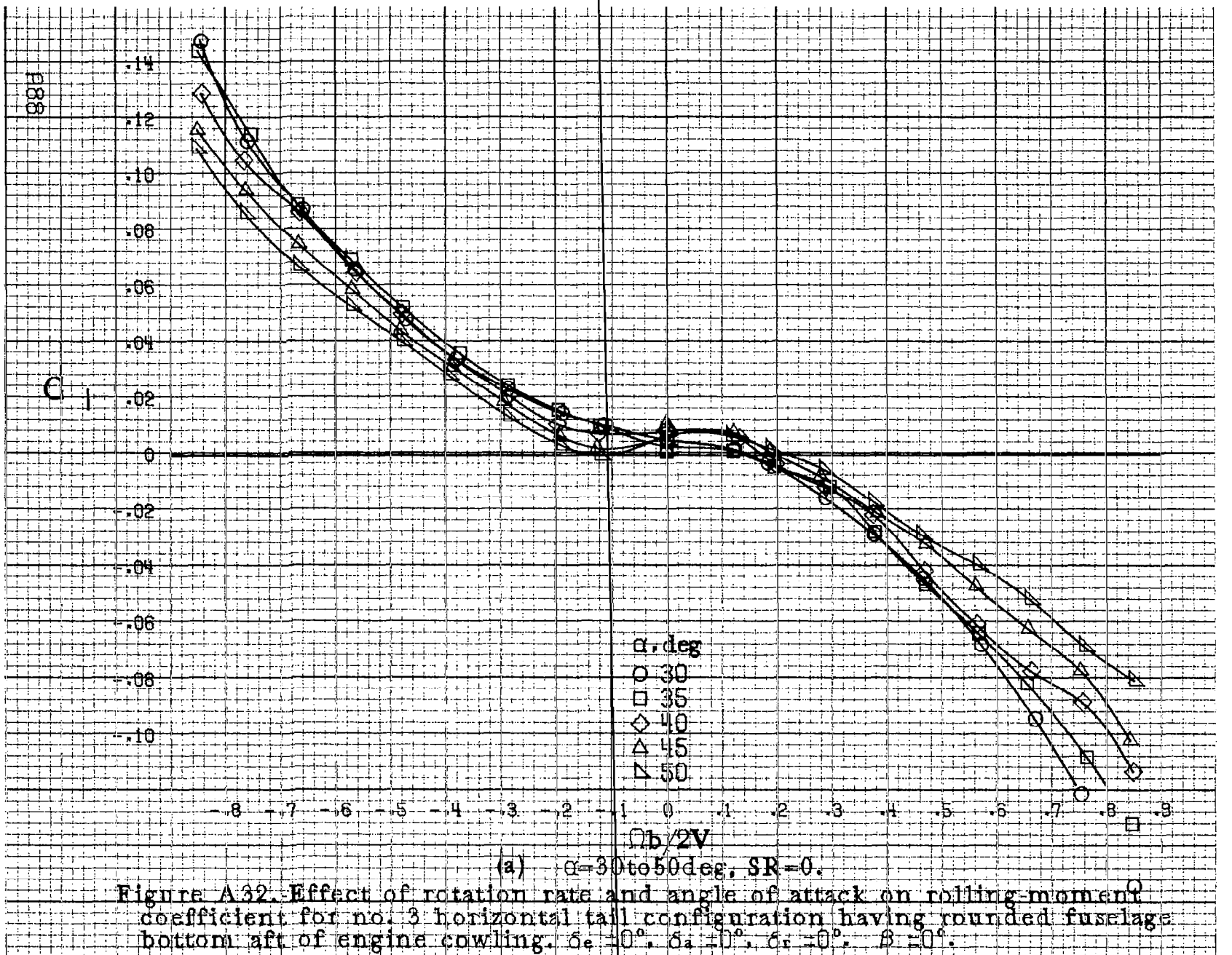

(a) α=30to50deg, SR=0.

Figure A32. Effect of rotation rate and angle of attack on rolling-moment coefficient for no. 3 horizontal tail configuration having rounded fuselage bottom aft of engine cowling. $\delta_e = 0°$, $\delta_a = 0°$, $\delta_r = 0°$, $\beta = 0°$.

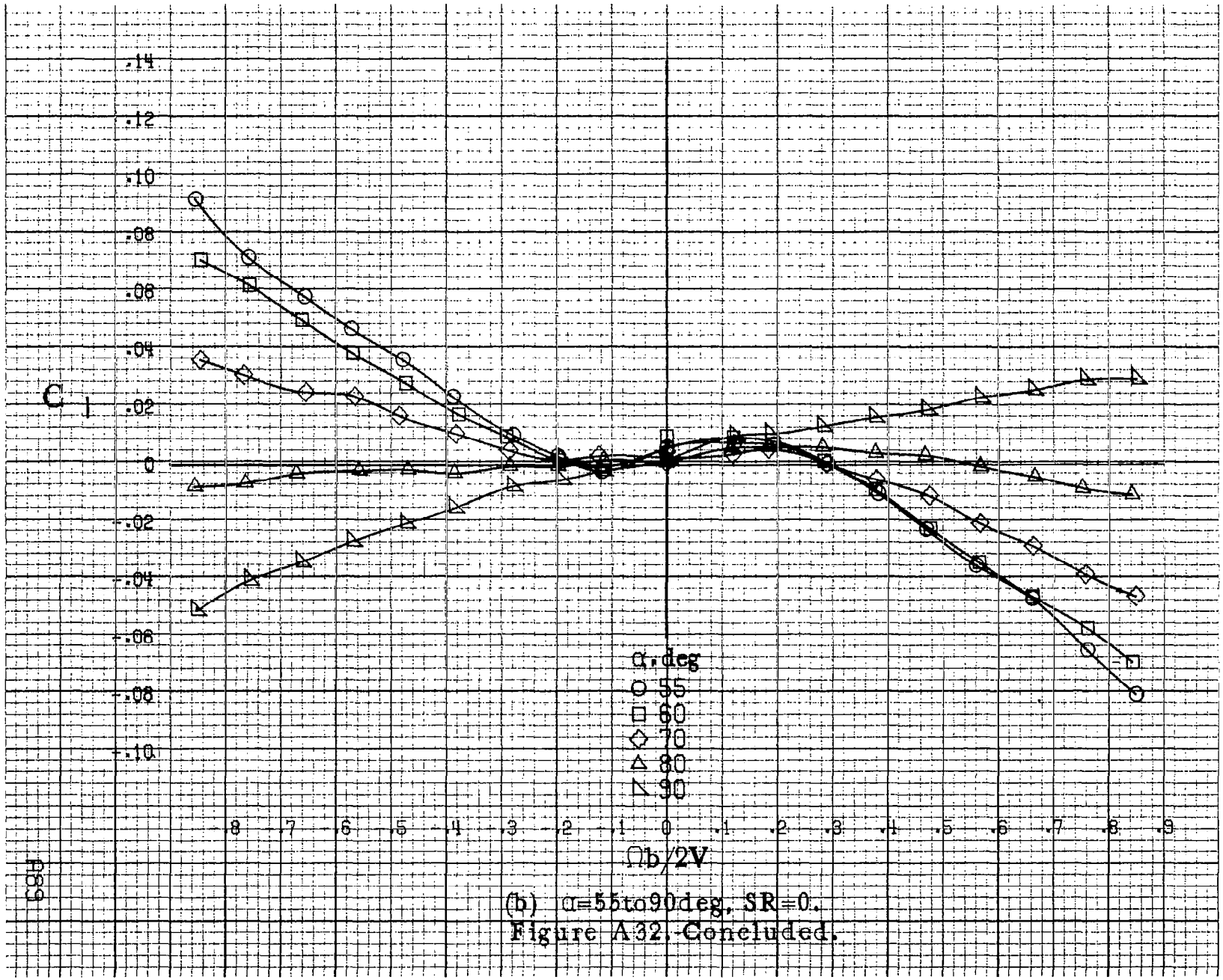

(b) α=55 to 90 deg, SR=0.

Figure A32.-Concluded.

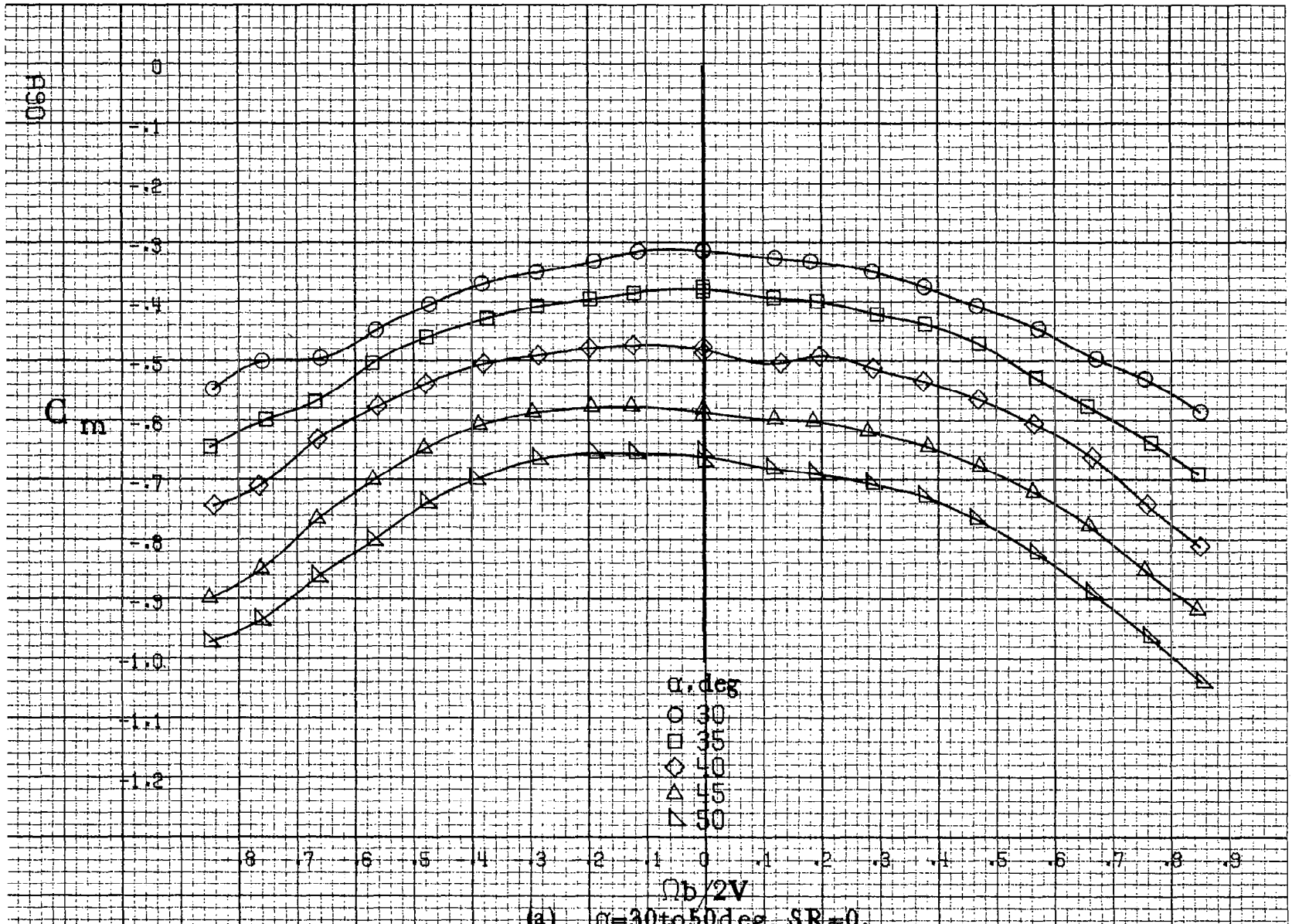

(a) α=30to50deg, SR=0.

Figure A33.-Effect of rotation rate and angle of attack on pitching-moment coefficient for no. 3 horizontal tail configuration having rounded fuselage bottom aft of engine cowling. $\delta_e = 0^\circ$, $\delta_a = 0^\circ$, $\delta_r = 0^\circ$, $\beta = 0^\circ$.

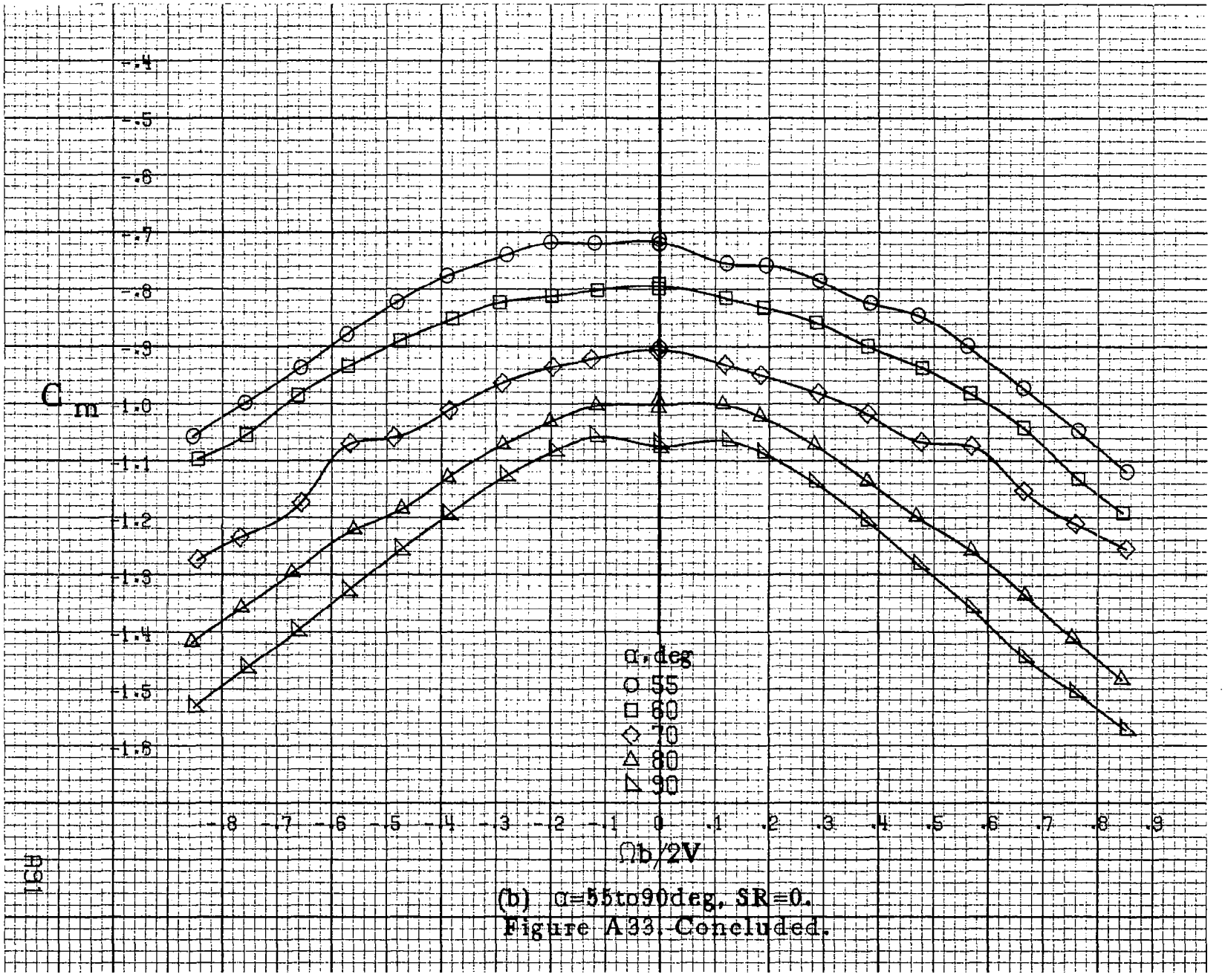

(b) α=55 to 90 deg, SR=0.

Figure A33.-Concluded.

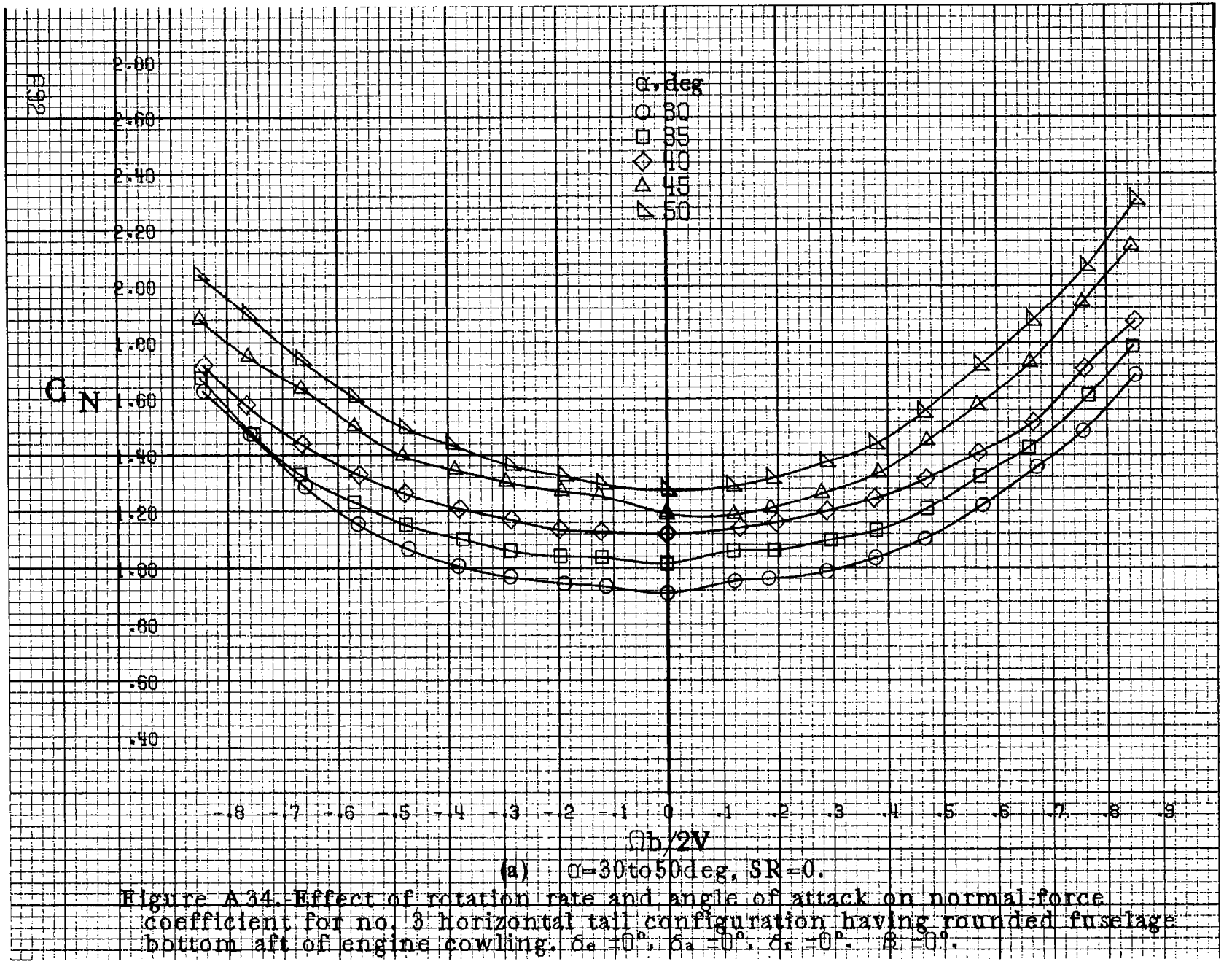

(a) α=30to50deg, SR=0.

Figure A34.-Effect of rotation rate and angle of attack on normal-force coefficient for no. 3 horizontal tail configuration having rounded fuselage bottom aft of engine cowling. $\delta_e = 0°$, $\delta_a = 0°$, $\delta_r = 0°$, $\beta = 0°$.

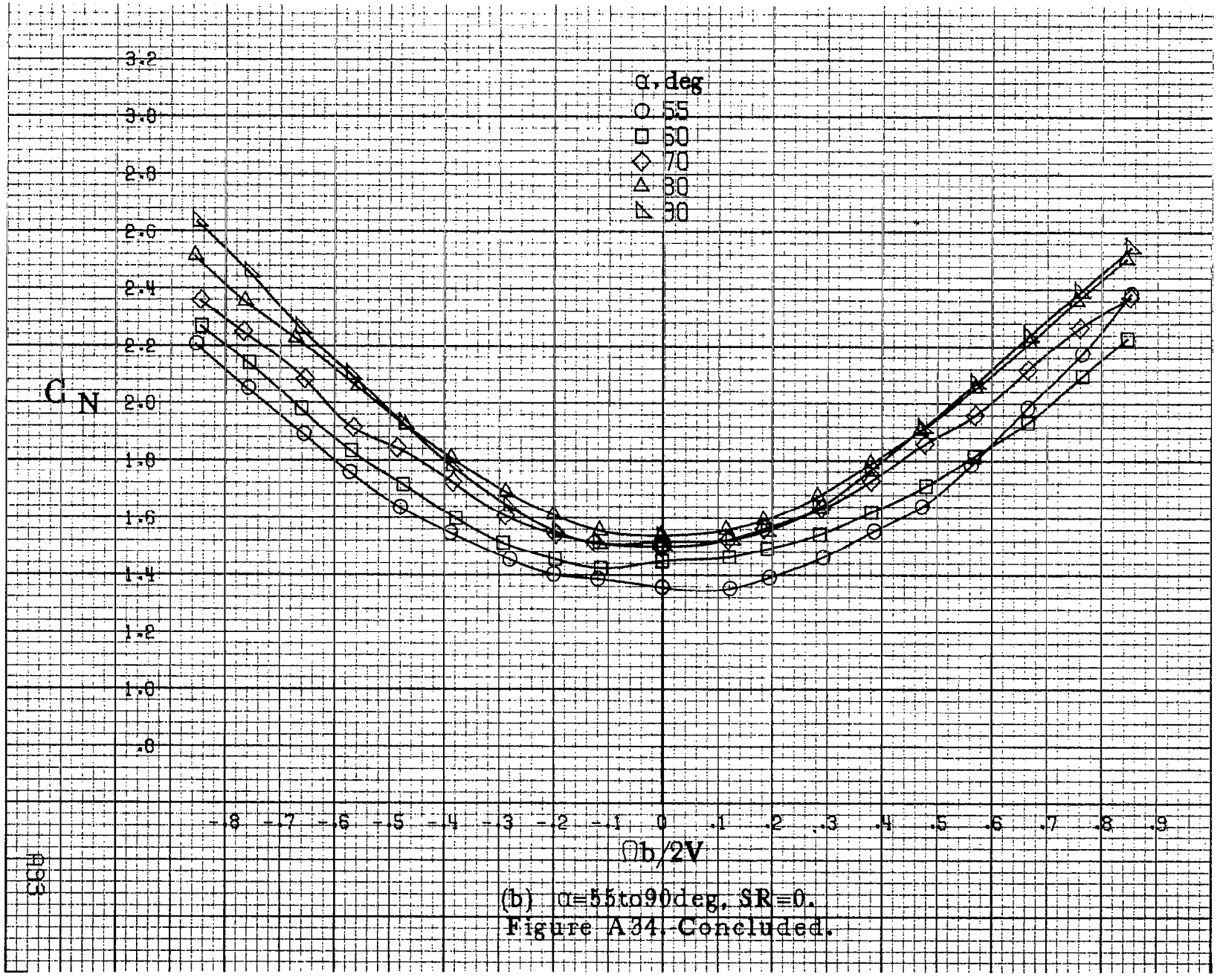

(b) α=55to90deg, SR=0.

Figure A34.-Concluded.

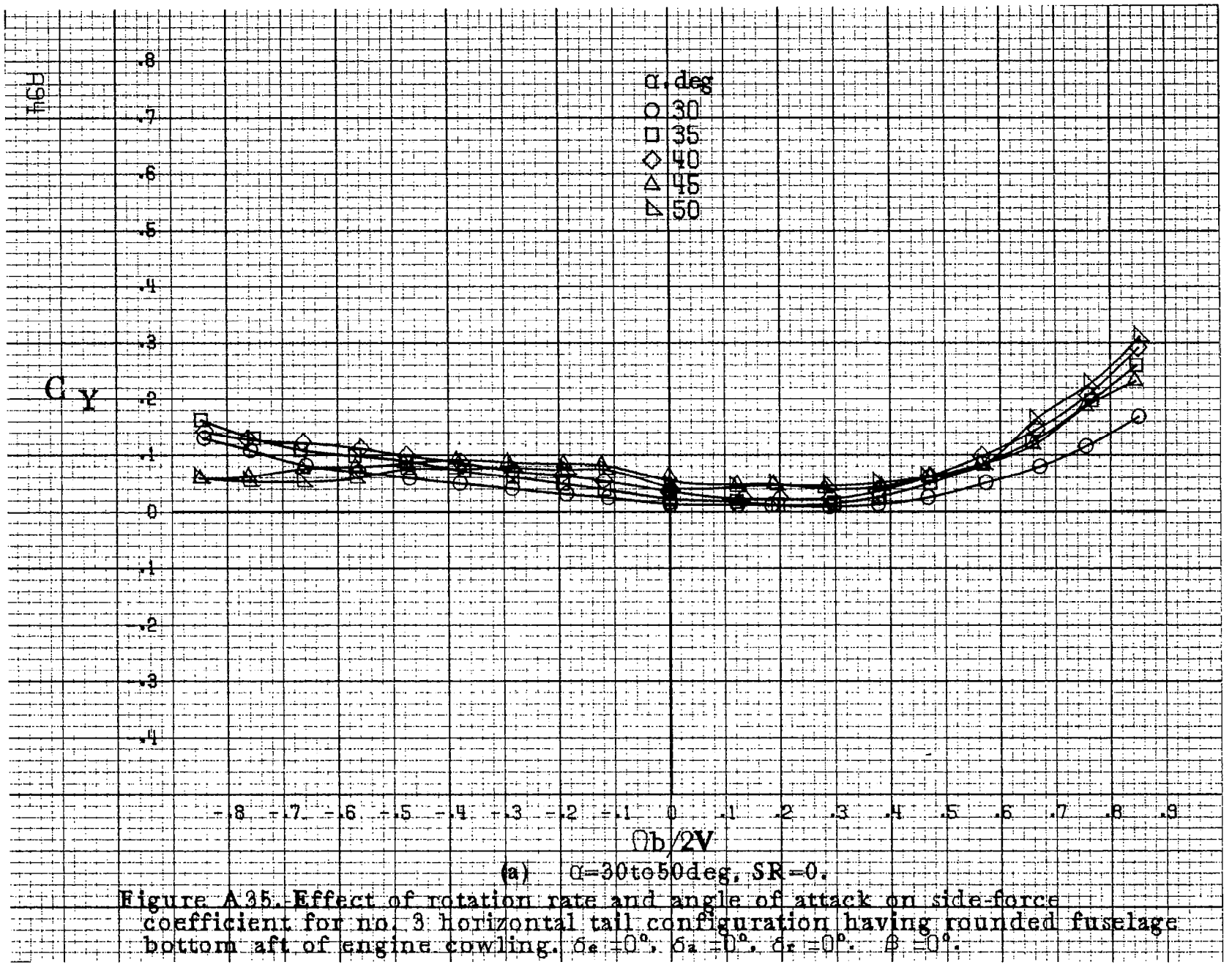

(a) α=30to50deg, SR=0.

Figure A35.-Effect of rotation rate and angle of attack on side-force coefficient for no. 3 horizontal tail configuration having rounded fuselage bottom aft of engine cowling. δ_e =0°, δ_a =0°, δ_r =0°, β =0°.

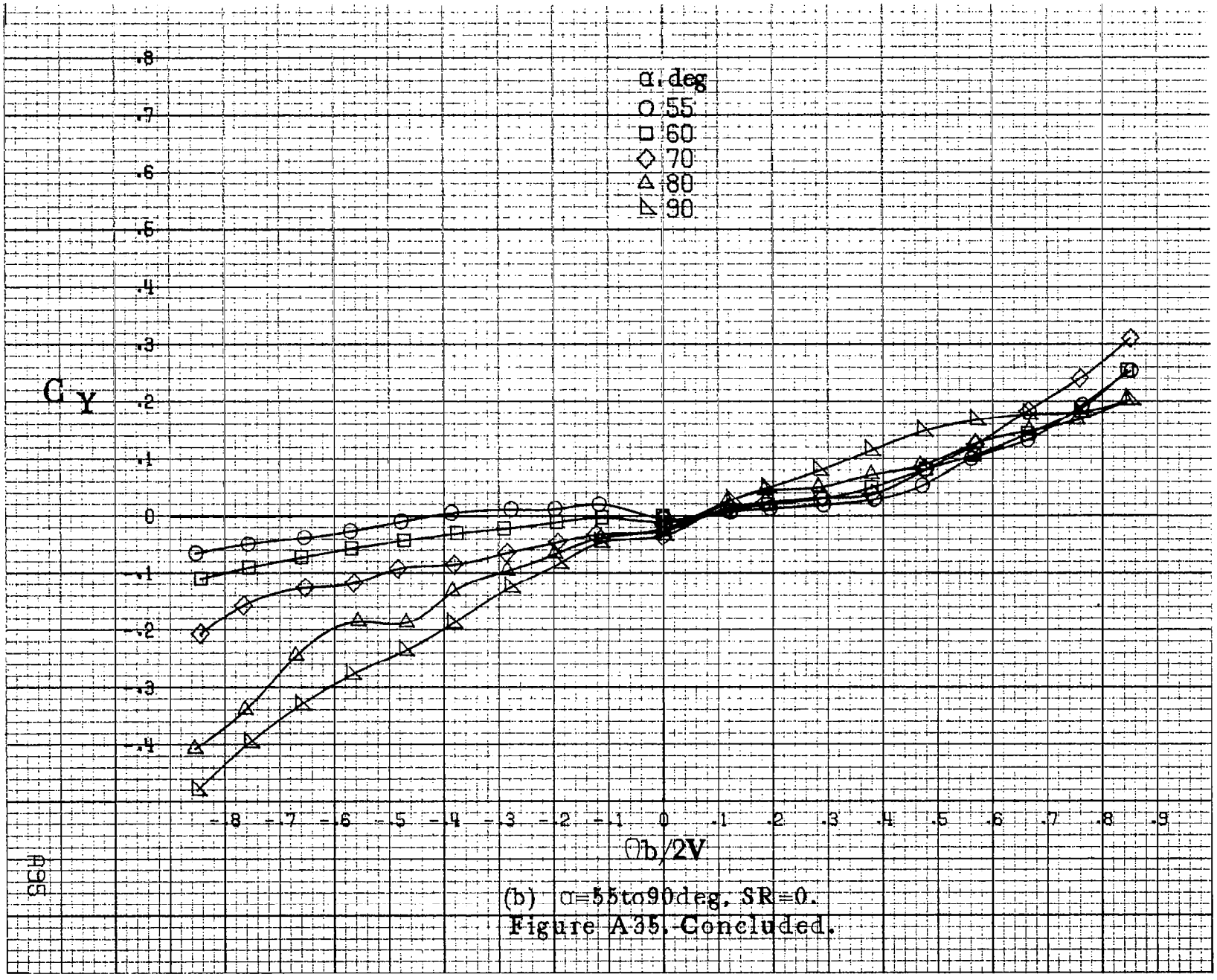

(b) $\alpha = 55$ to 90 deg, $SR = 0$.

Figure A35. Concluded.

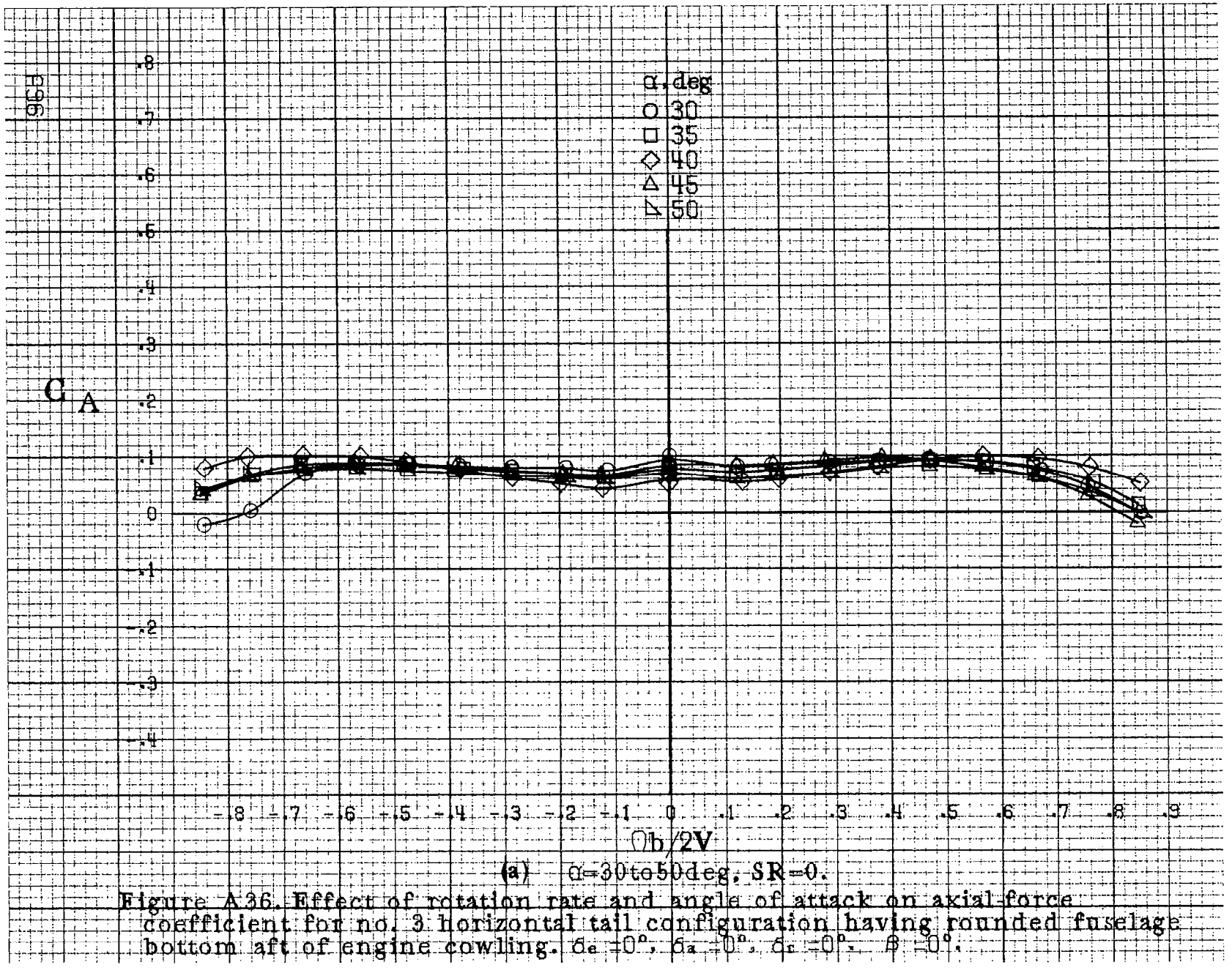

(a) α=30to50deg, SR=0.

Figure A36. Effect of rotation rate and angle of attack on axial-force coefficient for no. 3 horizontal tail configuration having rounded fuselage bottom aft of engine cowling. δ_e =0°, δ_a =0°, δ_r =0°, β =0°.

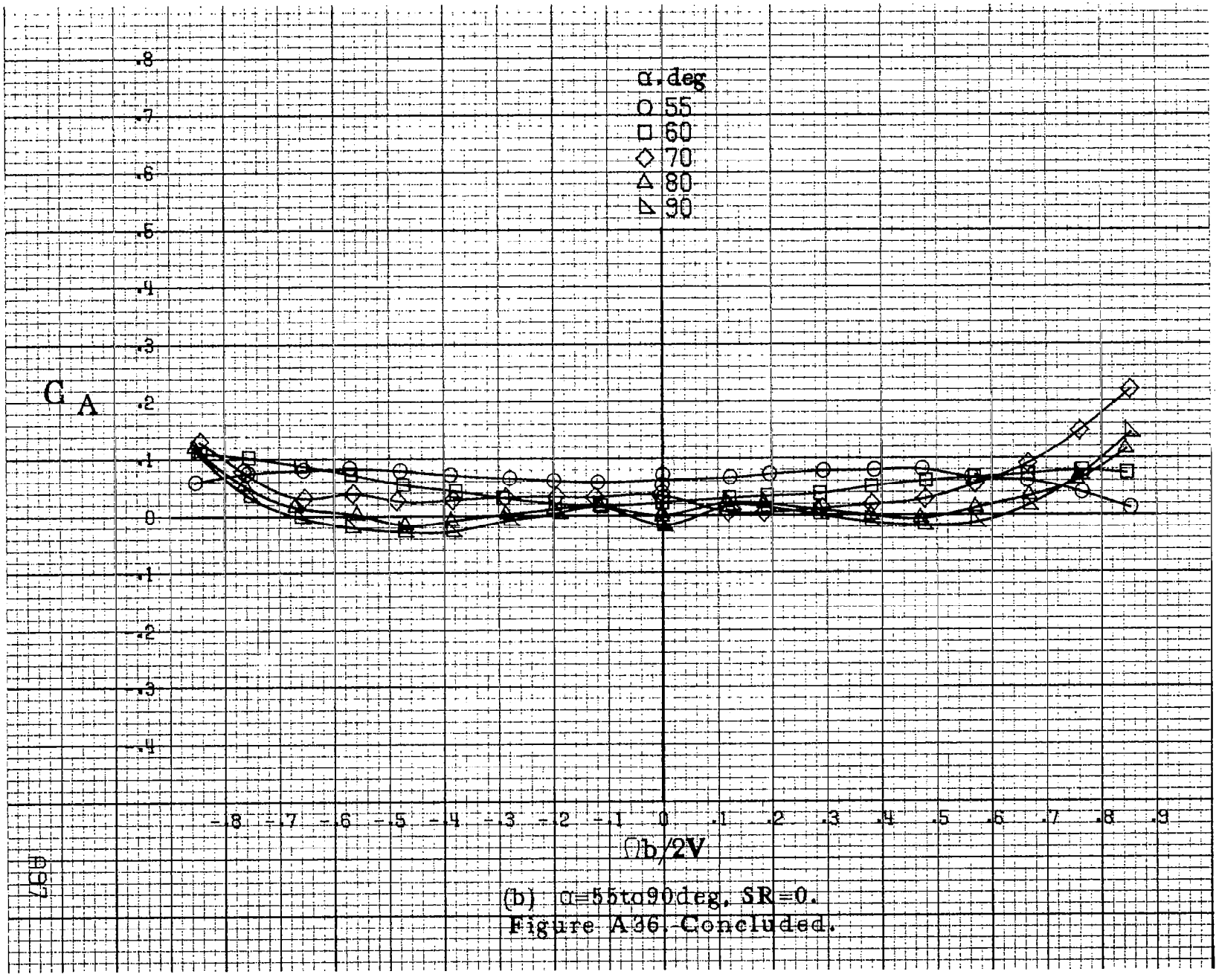

(b) α=55 to 90 deg, SR=0.

Figure A36. Concluded.

Figure A37. Lift coefficient as a function of angle of attack for various tail configurations.

1. Report No.	2. Government Accession No.	3. Recipient's Catalog No.
NASA CR-3101		

4. Title and Subtitle	5. Report Date
Rotary Balance Data for a Typical Single-Engine General Aviation Design for an Angle-of-Attack Range of 8° to 90° II - High-Wing Model A.	September 1979
	6. Performing Organization Code

7. Author(s)	8. Performing Organization Report No.
William Mulcay Robert Rose	

9. Performing Organization Name and Address	10. Work Unit No.
Bihrle Applied Research, Inc. 400 Jericho Turnpike Jericho, New York 11753	505-10-13-07
	11. Contract or Grant No.
	NAS1-14849, Task 31
	13. Type of Report and Period Covered
	Contractor Report
12. Sponsoring Agency Name and Address	14. Sponsoring Agency Code
National Aeronautics and Space Administration Washington, DC 20546	

15. Supplementary Notes

Langley Technical Monitor: James S. Bowman, Jr.

Topical report

16. Abstract

Aerodynamic characteristics obtained in a rotational flow environment utilizing a rotary balance located in the Langley spin tunnel are presented in plotted form for a 1/5-scale, single-engine, high-wing, general aviation airplane model. The configurations tested included various tail designs and fuselage shapes. Data are presented without analysis for an angle-of-attack range of 8° to 90° and clockwise and counter-clockwise rotations covering an $\frac{\Omega b}{2V}$ range from 0 to 0.85.

17. Key Words (Suggested by Author(s))	18. Distribution Statement
General Aviation Spinning Rotary balance High angle-of-attack wind tunnel data	Unclassified - Unlimited Subject Category 02

19. Security Classif. (of this report)	20. Security Classif. (of this page)	21. No. of Pages	22. Price*
Unclassified	Unclassified	114	$6.50

* For sale by the National Technical Information Service, Springfield, Virginia 22161

NASA-Langley, 1979